RADIATIVE KAON CAPTURE PROCESSES:

$K^-p \to Y\gamma$ and $K^-d \to \Lambda n\gamma$

by

RONALD LESTER WORKMAN

B.Sc., University of Victoria, 1981

M.Sc., University of British Columbia, 1984

A THESIS SUBMITTED IN PARTIAL FULFILLMENT OF

THE REQUIREMENTS FOR THE DEGREE OF

DOCTOR OF PHILOSOPHY

in

THE FACULTY OF GRADUATE STUDIES

Department of Physics

We accept this thesis as conforming

to the required standard

THE UNIVERSITY OF BRITISH COLUMBIA

October 1987

In presenting this thesis in partial fulfilment of the requirements for an advanced degree at the University of British Columbia, I agree that the Library shall make it freely available for reference and study. I further agree that permission for extensive copying of this thesis for scholarly purposes may be granted by the head of my department or by his or her representatives. It is understood that copying or publication of this thesis for financial gain shall not be allowed without my written permission.

Department of Physics

The University of British Columbia
1956 Main Mall
Vancouver, Canada
V6T 1Y3

Date Dec. 22, 1987

Abstract

The radiative capture reactions $K^-p \to \Lambda\gamma$, $K^-p \to \Sigma^0\gamma$ and $K^-d \to \Lambda n\gamma$ are investigated. Branching fractions are calculated for the K^-p reactions within a pole model alternatively utilizing both pseudoscalar and pseudovector coupling schemes. The photon spectrum has been calculated for the $K^-d \to \Lambda n\gamma$ within an impulse approximation model. The above calculations are particularly important as new and more precise data pertaining to the above reactions are expected from a recent Brookhaven experiment.

Both the pseudoscalar and pseudovector coupling schemes give branching fractions within the current experimental bounds. Sensitivity to the $\Lambda(1405)$ resonance is explored and improved constraints are determined for its contribution. A transition operator is also derived for use in the $K^-d \to \Lambda n\gamma$ calculation. Our methods and results are compared with those of other recent calculations of these reactions.

The $K^-d \to \Lambda n\gamma$ photon spectrum is also calculated in order to explore its sensitivity to the $\Lambda - n$ final state interaction. The high energy end of the photon spectrum is found to be sensitive to the choice of $\Lambda - n$ scattering parameters, yet relatively insensitive to the contributions from $\Sigma N \to \Lambda n$ conversion, the choice of deuteron wavefunctions and momentum dependence in the transition operator.

Contents

List of Tables

List of Figures

Acknowledgements

I would like to thank Dr. H.W. Fearing for his invaluable guidance and patience over the past four years. I would also like to thank Drs. D. Beder, D. Measday, B. Jennings, E. Truhlik and A. Gal for helpful suggestions and comments. Credit should also be given to Dr. J. Lowe for sending his Fortran code.

Finally, I would like to thank the Natural Sciences and Engineering Research Council and the University of British Columbia for financial assistance.

Chapter 1

INTRODUCTION AND HISTORICAL PERSPECTIVE

The kaon-nucleon and kaon-nucleus systems have provided a wealth of information on meson-nucleon interactions. Both the pion and kaon are spin-zero mesons with negative intrinsic parity. The kaon, however, introduces an additional strangeness quantum number, a quantity which is conserved in strong and electromagnetic interactions. The spectrum of near-threshold and sub-threshold resonances is also much richer in the kaon-nucleon system than in the analogous pion-nucleon system. The properties of these kaon-nucleon resonances have put strong constraints on the various models of meson-nucleon interactions.

In the following, we will study the reactions $K^-N \rightarrow Y\gamma$ and $K^-d \rightarrow \Lambda n\gamma$ in which a kaon with negligible energy is captured from an atomic s-state. This thesis has thus been divided into two parts. The first part describes the K^-N reactions. The $K^-p \rightarrow \Lambda\gamma$ and $K^-p \rightarrow \Sigma^0\gamma$ rates will be calculated from a set of Feynman diagrams, which will include, in addition to the usual Born terms, the most important resonant contributions in the s-,t- and u-channels. Both pseudoscalar (PS) and pseudovector (PV) coupling schemes will be employed. In addition, a two-component radiative kaon capture operator will be derived for use in the K^-d reaction. The second part of this thesis will then be an investigation of the photon spectrum from $K^-d \rightarrow \Lambda n\gamma$, calculated using the impulse approximation and the above mentioned radiative kaon

capture operator. Before describing our calculation in detail, however, we should first reflect on the importance of understanding these processes.

The $K^-d \to \Lambda n\gamma$ reaction is the strange analogue of $\pi^-d \to nn\gamma$. The latter, non-strange reaction has been utilized[1] in an accurate determination of the s-wave $n-n$ scattering length. Early theoretical calculations of $\pi^-d \to nn\gamma$, for at-rest pion capture, found[2] the high energy end of the photon spectrum to be sensitive to the final state $n-n$ interaction. This sensitivity is understood if one realizes that the high-energy limit of the photon spectrum corresponds to the geometry in which both neutrons are emitted anti-parallel to the photon and with zero relative momentum. An added bonus in this reaction is that, in the final state, the $\gamma - n$ interaction is negligible in comparison to the $n-n$ interaction. Thus, this calculation is relatively free of theoretical uncertainty when compared with calculations of reactions having three strongly interacting particles in the final state.

The use of $K^-d \to \Lambda n\gamma$ in a determination of $\Lambda - n$ scattering lengths is more beset by difficulty. Unlike the $\pi^-d \to nn\gamma$ reaction[2], the radiative K^-d capture is strongly suppressed[3] relative to final states containing three strongly interacting particles. This large background is a problem as existing kaon beams are not as refined as the pion beams at laboratories such as TRIUMF. Thus, sufficient statistics will be more difficult to obtain. In addition, background photons from the π^0 decay in the $K^-d \to \Lambda n\pi^0$ reaction may overwhelm a large part of the $K^-d \to \Lambda n\gamma$ photon spectrum. However, preliminary indications[4] suggest that these extraneous photons can be experimentally vetoed in the region of the photon spectrum most sensitive to the $\Lambda - n$ final state interaction.

These experimental difficulties have been confronted by an experimental group working at Brookhaven[3]. This group proposes to measure the photon spectrum from $K^-d \to \Lambda n\gamma$ as well as the branching ratios for $K^-p \to \Lambda\gamma$ and $K^-p \to \Sigma^0\gamma$, which we shall shortly discuss.

As the $K^-d \to \Lambda n\gamma$ reaction has not been studied theoretically in sufficient detail, we have begun this calculation in order to extract information from any forthcoming data. Apart from some early considerations[5] of $K^-d \to \Lambda n\gamma$ and $\gamma d \to \Lambda nK^+$, only two detailed calculations of the former reaction exist. The first[6] was carried out in analogy with the $\pi^-d \to nn\gamma$ calculation of reference 7. The radiative capture operator was taken to be momentum independent and of the form $\vec{\sigma}\cdot\vec{\epsilon}$. A Reid soft-core deuteron was used, and the influence of short range effects on the final state wave function was examined using the model of Picker, Redish and Stephenson[8]. The approximation of a frozen nucleus was made, and the kaonic wavefunction was assumed to be approximately constant over the range of strong interactions. From their investigation of the photon spectrum shape as a function of the scattering length combination $(a_s + 2a_t)/3$, it was found that the theoretical uncertainty in a determination of the above combination of singlet (a_s) and triplet (a_t) scattering lengths would be less than 0.2 fm. An interesting outcome of this calculation was the discovery of a region of the photon spectrum which was very sensitive to the $\Lambda - n$ final state interaction. This region extended from approximately 285 MeV to 293 MeV, the endpoint of the photon energy spectrum. Although this calculation was not published, it was in some ways more revealing than a calculation which appeared five years later[9].

This second calculation considered the capture reactions $K^-d \to YN\gamma$ for the YN states Λn, $\Sigma^0 n$ and $\Sigma^- p$, and allowed for conversion between the various YN states. Unfortunately, there were several inadequacies associated with this calculation. While relations were given for a full calculation of $K^-d \to YN\gamma$, only the Hulthen s-state deuteron was used in generating numerical results. More importantly, the calculated results concentrated on variations of the photon spectrum peak, which exists near 280 MeV, for different sets of scattering parameters describing the $K^-N \to Y\gamma$ and $YN \to Y'N'$ processes. As mentioned, the sensitive region is actually nearer to the endpoint of the spectrum.

In order to allow for conversion effects, explicit amplitudes of the form $F\vec{\sigma}\cdot\vec{\epsilon}$ are required for each of the reactions $K^-N \to Y\gamma$. The relative magnitudes of these amplitudes are sensitive[10] to the method of calculation. For this reason, the $K^-N \to Y\gamma$ amplitudes are interesting apart from their influence on the $K^-d \to \Lambda n\gamma$ interaction.

The $K^-p \to \Lambda\gamma$ and $K^-p \to \Sigma^0\gamma$ calculations are particularly interesting as they require knowledge of the poorly understood $\Lambda(1405)$ resonance. Two recent calculations of these processes, one in the cloudy bag model[11] (CBM) and the other in the non-relativistic quark model[12] (NRQM), indicate how widely opinions vary on the treatment and importance of this resonance in the $K^-p \to Y\gamma$ reactions.

In the CBM, the $\Lambda(1405)$ is incorporated implicitly through K^-N rescattering and is manifested mainly as a K^-N bound state. The lowest mass $\frac{1}{2}^-$ three-quark state is the $\Lambda(1630)$. Very different is the NRQM treatment. Here the dominant contribution to $K^-p \to Y\gamma$ is due to the $\Lambda(1405)$ which, in this model, is a 3-quark state and also the lowest mass $\frac{1}{2}^-$ resonance. Many diagrams, which are usually incorporated into a pole model calculation, have been neglected from the start in this treatment.

A recent pole model calculation of $K^-p \to \Lambda\gamma$ has also been performed[13]. In this calculation, experimental data[14] for the $(K^-p \to \Lambda\gamma)/(K^-p \to all)$ branching ratio were used to obtain a value for the $\Lambda(1405) \to \Lambda\gamma$ transition moment. Unfortunately, this calculation appears to contain some errors. It has also been criticized by both the CBM and NRQM papers[11,12] on other more fundamental grounds.

Our calculation of the $K^-p \to Y\gamma$ and $K^-d \to \Lambda n\gamma$ reactions will be compared in detail with previous calculations. First, however, we will indicate how our results were obtained. In Chapter 2 we describe the methods and conventions followed in our $K^-p \to Y\gamma$ rate calculation. In Chapter 3, the included set of Feynman diagrams is described, the invariant amplitude is constructed and the overall gauge invariance of our calculation is demonstrated. The two-component reduction of our amplitude, required for the $K^-d \to \Lambda n\gamma$ calculation, will also be performed here. Next, in Chapter 4, the

required coupling constants are determined. These couplings are then used to produce the $K^-p \to Y\gamma$ rate estimates of Chapter 5. Having obtained results, in Chapter 6 we confront the methods and predictions of the CBM[11], NRQM[12] and the previous pole model calculation of reference 13. In Chapter 7 we present the general formalism for our calculation of the $K^-d \to \Lambda n\gamma$ reaction within a simple impulse approximation model, neglecting any momentum dependence of the $K^-N \to Y\gamma$ transition operator. A general relation for the invariant amplitude will be given, including the effects of $\Sigma N \to \Lambda n$ conversion. The differential rate relation will also be presented here. In Chapter 8, we will indicate what additional complications arise when a momentum dependent transition operator is utilized. Having obtained the general relations required in our calculation of the $K^-d \to \Lambda n\gamma$ γ-spectrum, specific wavefunctions and parameters will be chosen in Chapter 9. In Chapter 10, we will present the numerical results of our γ-spectrum calculations. Here we will explore the sensitivities of our $K^-d \to \Lambda n\gamma$ γ-spectrum calculation to the various parameters chosen in the previous chapter. In Chapter 11, our results and methods will be compared to those of previous calculations. Finally, in Chapter 12, we will summarize the conclusions that may be drawn from our calculations of the $K^-p \to Y\gamma$ and $K^-d \to \Lambda n\gamma$ reactions. Appendix A addresses the problem of determining a sign for the $\Sigma^0 \to \Lambda$ transition moment. Appendix B describes in detail the methods we have used in order to evaluate the radial integrals arising in Chapters 7 and 8.

Chapter 2

THE $K^-p \to Y\gamma$ PRELIMINARIES

2.1 Introduction

The $K^-p \to \Lambda\gamma$ and $K^-p \to \Sigma^0\gamma$ reactions are attracting renewed interest due to a new Brookhaven experiment[3], which proposes to measure the branching ratios of these reactions with greatly improved accuracy. The $\Lambda\gamma$ reaction currently has an experimental branching fraction of $(2.8 \pm 0.8) \times 10^{-3}$[14] while there exists only an upper limit[15] of 4×10^{-3} for the $\Sigma^0\gamma$ branching fraction. Since the CBM[11] and NRQM[12] predict different structures for the sub-threshold $\Lambda(1405)$ resonance as well as different rates for the $K^-p \to Y\gamma$ reactions, these reactions provide an important test of the two models.

In addition to these quark model calculations, it is important to have a detailed pole model calculation, as Born approximation calculations of pion-photoproduction[16] have been successful in reproducing the threshold behavior of the $\gamma p \to n\pi^+$ and $\gamma n \to p\pi^-$ reactions. There, apart from small N^* contributions, the Born terms are sufficient to describe such processes. In the present calculation, however, the separation of Born from resonance effects is complicated by the presence of sub-threshold resonances. While this is indeed a problem, the threshold radiative kaon capture reactions are best suited for a determination of the $\Lambda(1405)$ coupling to $\Lambda\gamma$ and $\Sigma^0\gamma$. At higher energies, one must contend with a large number of other contributing resonances.

In order to extract the $\Lambda(1405)$ couplings, all other contributions to the amplitude

must be known or estimated to be small. This method of determining the $\Lambda(1405)$ radiative couplings was utilized recently by Burkhardt, Lowe and Rosenthal[13] for the $\Lambda\gamma$ reaction. In that calculation a PS coupling scheme was employed. In addition to the usual Born diagrams, the $\Sigma^0 \rightarrow \Lambda$ transition, as well as some N^* and K^* contributions, were included. The $\Lambda(1405)$ contribution was then parametrized and adjusted to fit the experimental $\Lambda\gamma$ branching fraction.

We have repeated the $K^-p \rightarrow \Lambda\gamma$ branching fraction calculation and have extended it to include PV strong couplings as well as the $K^-p \rightarrow \Sigma^0\gamma$ reaction. We have also considered the contribution of higher mass Y^* resonances in addition to the $\Lambda(1405)$. The N^* contribution has been given more careful consideration and, couplings have been derived from experimental information whenever possible.

Since the $\Lambda(1405)$ is just below the K^-p threshold and decays almost 100% of the time to $\Sigma\pi$, there exists no direct experimental information on its coupling to K^-p or $Y\gamma$. Thus, as in reference 13, the $\Lambda(1405)$ coupling is undetermined and adjusted to fit the data after all other contributions have been considered.

2.2 Rate Relations and Conventions

We consider the reaction in which a kaonic atom is formed prior to the strong K^-p interaction. Here the kaon energy is approximately zero and the strong capture is expected from an S-state[17]. Unfortunately, however, the principal quantum number of the state is not well known. It appears, though, that the kaonic wave function may be approximated by a constant over the range of strong interactions[17,18]. Thus, it may be removed from integrals involved in the rate calculation for $K^-p \rightarrow Y\gamma$. The decay rate for this process is then given by

$$\Gamma_{K^-p\rightarrow Y\gamma} = \mid \phi_K(0) \mid^2 \frac{m_Y k}{4\pi(m_K + m_p)m_K} \overline{\sum_{spins}} \mid M \mid^2, \tag{2.1}$$

wherein $\phi_K(0)$ is the kaonic wave function evaluated at the proton. The quantities m_Y, m_K, m_p and k are the hyperon, kaon and proton masses and the photon energy. The invariant amplitude, M, is given by the diagrams in figs. 1 and 2. $\overline{\Sigma}$ denotes a sum over final and average over initial spins.

In order to obtain branching ratios, we also require the total rate for all K^-p processes. We will use the pseudopotential method employed by Burkhardt et al.[13] in order to calculate this rate. The total rate is then given by

$$\Gamma_{K^-p\rightarrow all} = 2W_p \mid \phi_K(0) \mid^2, \tag{2.2}$$

wherein W_p is the imaginary part of the K^-p pseudopotential and has the value[13] (560 ± 135) MeV fm^3. One must assume, as seems reasonable, that $\mid \phi_K(0) \mid^2$ averaged over the states from which capture occurs is the same for the $K^-p \rightarrow all$ processes as for $K^-p \rightarrow Y\gamma$, so that it cancels in the branching ratio. It should be emphasized that all branching ratio results we obtain, except the ratio $K^-p \rightarrow \Lambda\gamma / K^-p \rightarrow \Sigma^0\gamma$, scale inversely with W_p and will be uncertain by an amount corresponding to the uncertainty in W_p.

In the following, we shall use p_p, p_K and p_Y to denote the proton, kaon and lambda or sigma hyperon 4-momentum. The corresponding 3-vector will always be represented

by an arrow over the 4-vector symbol. In addition, the unit vector in the direction of a 3-vector $\vec{s}$ will be represented by $\hat{s}$.

In the kaon-proton center-of-mass, we have the following simple energy and momentum conservation relations

$$m_p + m_K = E_\Lambda + k, \tag{2.3}$$

and

$$\vec{p}_\Lambda + \vec{k} = 0, \tag{2.4}$$

wherein $E_\Lambda = \sqrt{(\vec{p}_\Lambda)^2 + m_\Lambda^2}$. The Mandlestam variables for general momentum are given by the relations

$$s = (p_p + p_K)^2, \tag{2.5}$$

$$t = (p_K - k)^2, \tag{2.6}$$

$$u = (p_p - k)^2. \tag{2.7}$$

In the particular case of at-rest kaon capture, these reduce to the relations

$$s = (m_p + m_K)^2, \tag{2.8}$$

$$t = m_K^2 - 2m_K k, \tag{2.9}$$

$$u = m_p^2 - 2m_p k, \tag{2.10}$$

which we shall use often. The metric and γ-matrix conventions of Bjorken and Drell[19] have been followed throughout.

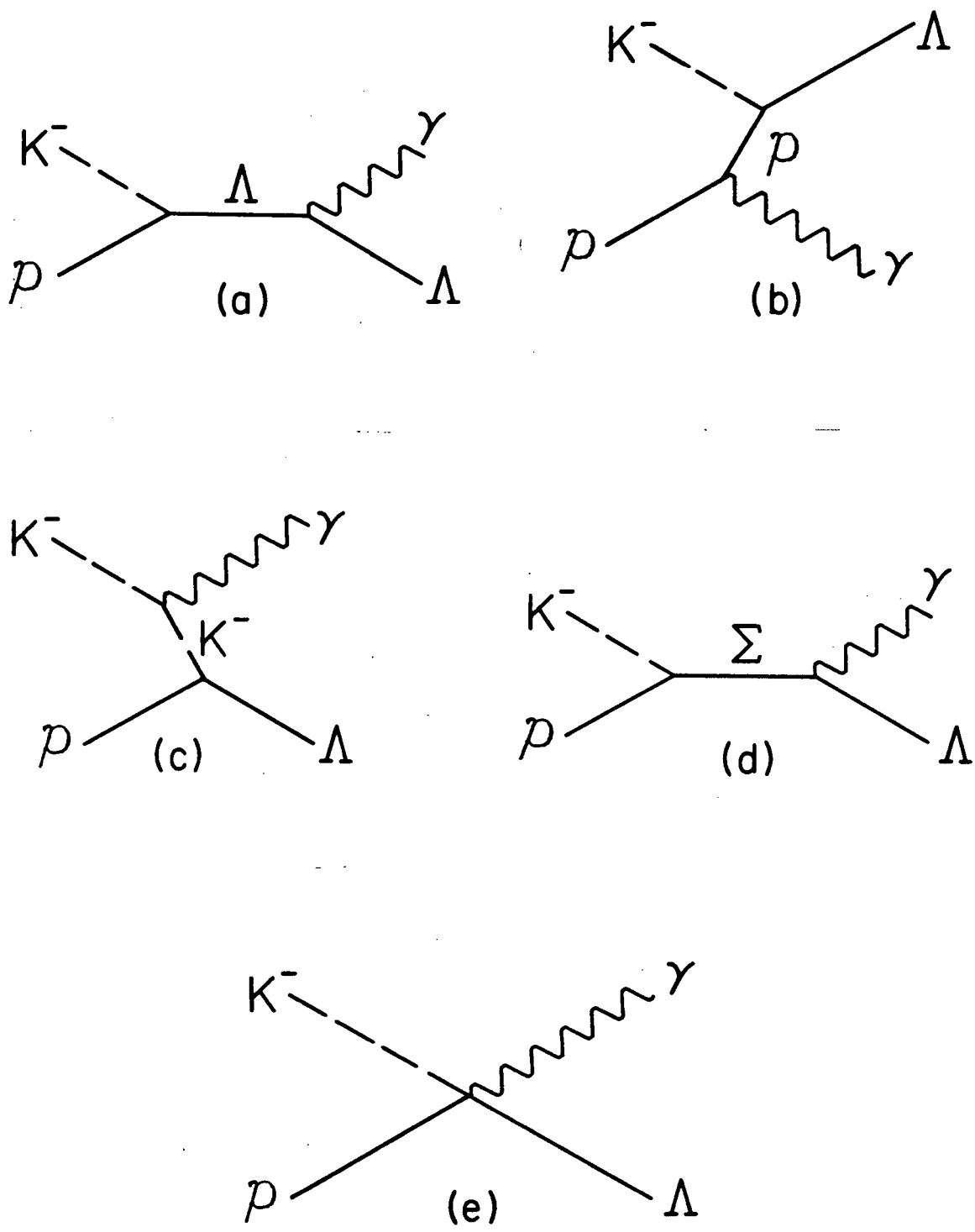

Figure 2.1: Non-resonant diagrams for $K^- p \to \Lambda\gamma$

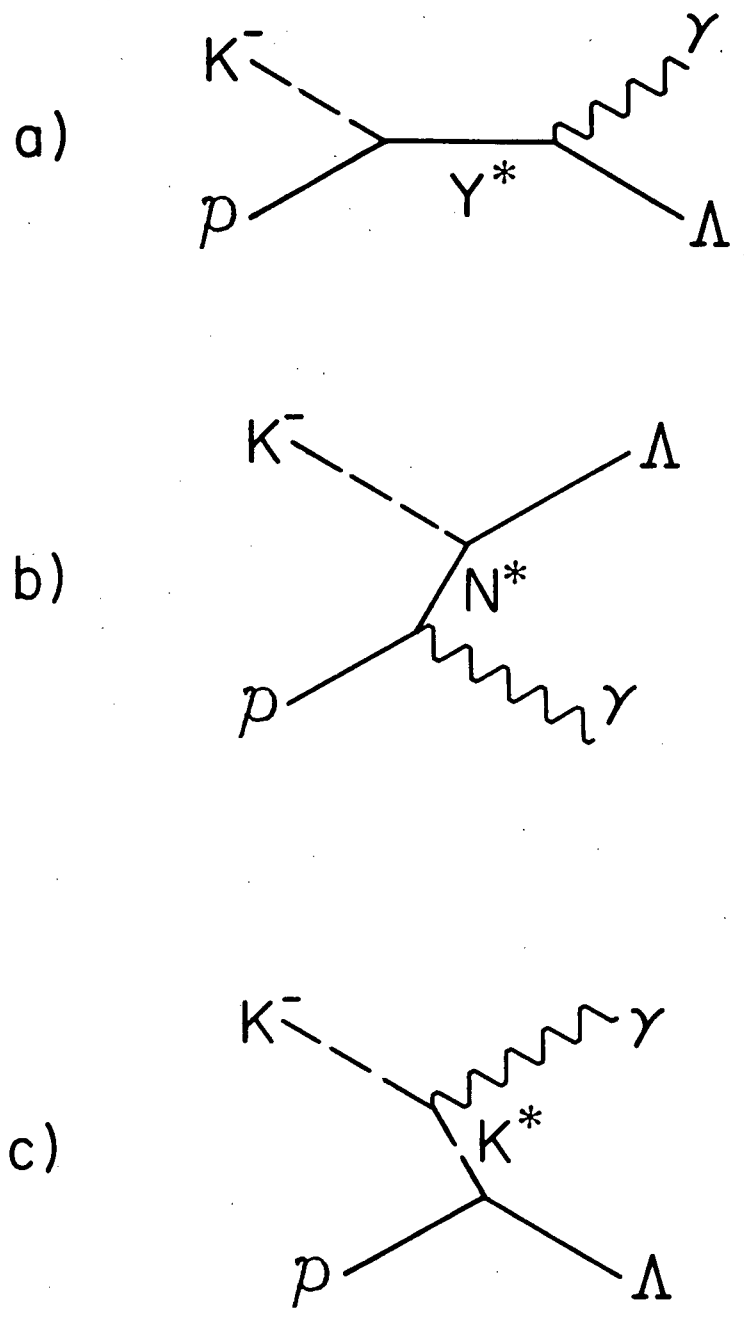

Figure 2.2: Resonant diagrams for $K^- p \to \Lambda\gamma$

Chapter 3

THE INVARIANT AMPLITUDE

3.1 Construction of the Amplitude

In Chapter 2 we found that the poorly known kaonic wavefunction could be eliminated from our calculation, if we restricted our attention to branching ratios. Thus, apart from the pseudopotential input to the total rate calculation, all of the model dependence in our calculation is contained in M, the invariant amplitude, which we shall now construct.

We describe first the pseudoscalar(PS) $K^- p \to \Lambda\gamma$ calculation. To construct the amplitude we start with the simple Born terms involving the intermediate radiating p, Λ and K graphs as well as the $\Sigma^0 \to \Lambda$ transition graph, as given in fig. 1(a-d). In addition to these graphs, we considered all $J^P = \frac{1}{2}^{\pm}$ s-wave Y^* resonances below 2 GeV. Of the possible u-channel N^* resonances, we retained only those which had an appreciable branching fraction to the $p\gamma$ and ΛK final states. The t-channel $K^*(892)$ contribution of fig. 2(c) was also included.

The form of the amplitude, M, required in equation (2.1), is given below. Equation (3.1) contains terms which are representative of each exchange considered above, using PS couplings.

$$M = \sum_{i=1}^{6} M_i, \tag{3.1}$$

wherein

$$M_1 = g_{Kp\Lambda} \frac{e\kappa_\Lambda}{2m_p} \overline{u}_\Lambda \epsilon \cdot \gamma k \cdot \gamma \frac{[(p_\Lambda + k) \cdot \gamma + m_\Lambda]}{s - m_\Lambda^2} \gamma_5 u_p$$

$$+ \quad g_{Kp\Lambda} e\overline{u}_\Lambda \gamma_5 \frac{[(p_p - k)\cdot\gamma + m_p]}{u - m_p^2} \left\{ \epsilon\cdot\gamma + \frac{\kappa_p}{2m_p} \epsilon\cdot\gamma k\cdot\gamma \right\} u_p$$

$$- \quad 2g_{Kp\Lambda} e\overline{u}_\Lambda \gamma_5 \frac{p_K\cdot\epsilon}{t - m_k^2} u_p, \tag{3.2}$$

$$M_2 = g_{Kp\Sigma} \frac{e\kappa_{\Sigma\Lambda}}{2m_p} \overline{u}_\Lambda \epsilon\cdot\gamma k\cdot\gamma \frac{[(p_\Lambda + k)\cdot\gamma + m_\Sigma]}{s - m_\Sigma^2} \gamma_5 u_p, \tag{3.3}$$

$$M_3 = g_{Kp\Lambda(1405)} \frac{e\kappa_{\Lambda(1405)\Lambda}}{2m_p} \overline{u}_\Lambda \epsilon\cdot\gamma k\cdot\gamma\gamma_5 \frac{[(p_\Lambda + k)\cdot\gamma + m_{\Lambda(1405)}]}{s - m_{\Lambda(1405)}^2 + i m_{\Lambda(1405)}\Gamma} u_p, \tag{3.4}$$

$$M_4 = g_{KN(+)\Lambda} \frac{e\kappa_{N(+)p}}{2m_p} \overline{u}_\Lambda \gamma_5 \frac{[(p_p - k)\cdot\gamma + m_{N(+)}]}{u - m_{N(+)}^2 + i m_{N(+)}\Gamma} \epsilon\cdot\gamma k\cdot\gamma u_p, \tag{3.5}$$

$$M_5 = g_{KN(-)\Lambda} \frac{e\kappa_{N(-)p}}{2m_p} \overline{u}_\Lambda \frac{[(p_p - k)\cdot\gamma + m_{N(-)}]}{u - m_{N(-)}^2 + i m_{N(-)}\Gamma} \epsilon\cdot\gamma k\cdot\gamma\gamma_5 u_p, \tag{3.6}$$

$$M_6 = \overline{u}_\Lambda [g^V_{K^*p\Lambda}\gamma^\alpha + g^T_{K^*p\Lambda}(p_\Lambda - p_p)\cdot\gamma\gamma^\alpha] \left\{ -g_{\alpha\mu} + \frac{(p_\Lambda - p_p)_\alpha (p_\Lambda - p_p)_\mu}{m_{K^*}^2} \right\}$$

$$\cdot \frac{\kappa_{K^*K}}{2m_p(t - m_{K^*}^2 + i m_{K^*}\Gamma)} i\varepsilon^{\mu\nu\rho\sigma} \epsilon_\nu k_\rho (p_\Lambda - p_p)_\sigma u_p. \tag{3.7}$$

In the above, $N^{(\pm)}$ refers to N^* resonances with $J^P = \frac{1}{2}^\pm$. Equation (3.2) gives the p, Λ and K contributions, while equations (3.3) and (3.4) are due to the $\Sigma(1192)\frac{1}{2}^+$ and the $\Lambda(1405)\frac{1}{2}^-$. Finally, equations (3.5), (3.6) and (3.7) give the N^+, N^- and $K^*(892)$ contributions, respectively. The form of M for higher Y^* s-channel $J^P = \frac{1}{2}^\pm$ resonances can be easily obtained from equations (3.3) and (3.4). The quantities Γ, g and κ are respectively the width, strong coupling constant and anomalous magnetic or transition moment associated with each particle exchange. Note that, although the third (kaon radiation) term in equation (3.2) is required in general for gauge invariance, it does not contribute for at-rest capture reactions calculated in the transverse gauge. The dominant contribution to M, in the transverse gauge and in the the absence of resonances, is due to the second (proton radiation) term, as should be recalled from pion-photoproduction[20].

In order to calculate the PV form of M, we have used the following substitution for the coupling at the strong vertex

$$g_{KNY}\gamma_5 \rightarrow \tilde{g}_{KNY}q\cdot\gamma\gamma_5. \tag{3.8}$$

The on-shell equivalence

$$\overline{u}_Y g_{KNY}\gamma_5 u_N = \overline{u}_Y \tilde{g}_{KNY} q\cdot\gamma\gamma_5 u_N \quad ; \quad q = p_Y - p_N, \tag{3.9}$$

is used to relate $\tilde{g}_{KNY}$ to g_{KNY}, and gives $\tilde{g}_{KNY} = g_{KNY}/(m_Y + m_N)$, which is appropriate when the N and Y have the same parity. In those cases where N and Y have opposite parities, $\gamma_5 \rightarrow 1$ in equations (3.8) and (3.9) and, $\tilde{g}_{KNY} = g_{KNY}/(m_Y - m_N)$. The K^*NY coupling was left unchanged. In addition to the above change, to ensure gauge invariance in the PV case, we must add to the amplitude in equation (3.1) the following contact term corresponding to fig. 1(e):

$$M_{Contact} = \tilde{g}_{Kp\Lambda} e\overline{u}_\Lambda \epsilon\cdot\gamma\gamma_5 u_p. \tag{3.10}$$

In the transverse gauge this is the dominant non-resonant contribution to M for the PV case. Once again, this is expected from pion-photoproduction[20].

The $K^-p \rightarrow \Sigma^0\gamma$ amplitudes have the same basic form as described for $K^-p \rightarrow \Lambda\gamma$. Differences arise from the choice of appropriate couplings at the strong and electromagnetic vertices, corresponding to a $\Sigma^0\gamma$ final state which affects the momenta, propagators and phase space. The set of intermediate resonances considered for the $\Lambda\gamma$ final state is also considered for $K^-p \rightarrow \Sigma^0\gamma$, though now of course it is the $\Lambda \rightarrow \Sigma^0$ transition which enters, rather than $\Sigma^0 \rightarrow \Lambda$.

The numerical branching ratios of Chapter 5 are a result of two independent numerical evaluations of equations (2.1) and (2.2). The amplitude M in equation (3.1) was converted into a matrix equation using the γ-matrix representations given in Bjorken and Drell[19]. Once in a matrix form, the amplitudes were obtained by explicit numerical evaluations of the matrix products. Checks were also made by hand wherever feasible.

The requirement of gauge invariance is clearly satisfied by the invariant amplitude. The PS and PV Born terms are gauge-invariant sets of diagrams. Since the N^* and Y^* diagrams involve only magnetic couplings, they are individually gauge invariant. The K^* diagram is also individually gauge invariant, as the corresponding amplitude is proportional to a term in which both ϵ^μ and k^μ are contracted with the totally antisymmetric tensor.

3.2 The Two-Component Reduction

In this section the invariant amplitude of equation (3.1) will be reduced to a two-component form. This form of the amplitude will later be utilized in an impulse approximation calculation of the $K^- d \to \Lambda n \gamma$ process. Furthermore, in a two-component form, the requirement of gauge invariance can be checked more easily. The relative size of the various contributions to our amplitude will also be obvious.

First we will write the amplitude of equation (3.1) in the form

$$M = e\overline{u}_\Lambda (A \cdot \epsilon + B\epsilon \cdot \gamma + C \cdot \epsilon k \cdot \gamma + D\epsilon \cdot \gamma k \cdot \gamma)\gamma_5 u_p. \tag{3.11}$$

By reducing the $K^- p \to \Lambda\gamma$ Born plus $\Sigma^0 \to \Lambda$ plus $\Lambda(1405)$ amplitudes, we find for the terms in equation (3.11)

$$A \cdot \epsilon = g_{Kp\Lambda} \left\{ \frac{2p_p \cdot \epsilon}{u - m_p^2} - \frac{2p_K \cdot \epsilon}{t - m_K^2} \right\}, \tag{3.12}$$

$$\begin{aligned} B = {} & g_{Kp\Lambda} \left\{ \left(\frac{\kappa_\Lambda}{m_p} \right) \frac{p_\Lambda \cdot k}{s - m_\Lambda^2} + \left(\frac{\kappa_p}{m_p} \right) \frac{p_p \cdot k}{u - m_p^2} \right\} \\ & + g_{Kp\Sigma} \left(\frac{\kappa_{\Sigma\Lambda}}{m_p} \right) \frac{p_\Lambda \cdot k}{s - m_\Sigma^2} - g_{Kp\Lambda(1405)} \left(\frac{\kappa_{\Lambda(1405)\Lambda}}{m_p} \right) \frac{p_\Lambda \cdot k}{s - m_{\Lambda(1405)}^2}, \end{aligned} \tag{3.13}$$

$$\begin{aligned} C \cdot \epsilon = {} & -g_{Kp\Lambda} \left\{ \left(\frac{\kappa_p}{m_p} \right) \frac{p_p \cdot \epsilon}{u - m_p^2} + \left(\frac{\kappa_\Lambda}{m_p} \right) \frac{p_\Lambda \cdot \epsilon}{s - m_\Lambda^2} \right\} \\ & - g_{Kp\Sigma} \left(\frac{\kappa_{\Sigma\Lambda}}{m_p} \right) \frac{p_\Lambda \cdot \epsilon}{s - m_\Sigma^2} + g_{Kp\Lambda(1405)} \left(\frac{\kappa_{\Lambda(1405)\Lambda}}{m_p} \right) \frac{p_\Lambda \cdot \epsilon}{s - m_{\Lambda(1405)}^2}, \end{aligned} \tag{3.14}$$

$$\begin{aligned} D = {} & g_{Kp\Lambda} \left\{ \left(\frac{m_\Lambda}{m_p} \right) \frac{\kappa_\Lambda}{s - m_\Lambda^2} + \frac{(1 + \kappa_p)}{u - m_p^2} \right\} \\ & + g_{Kp\Sigma} \left(\frac{\kappa_{\Sigma\Lambda}}{2m_p} \right) \frac{(m_\Lambda + m_\Sigma)}{s - m_\Sigma^2} + g_{Kp\Lambda(1405)} \left(\frac{\kappa_{\Lambda(1405)\Lambda}}{2m_p} \right) \frac{(m_{\Lambda(1405)} - m_\Lambda)}{s - m_{\Lambda(1405)}^2}, \end{aligned} \tag{3.15}$$

wherein, curly brackets isolate contributions from the Born terms, and the replacement $m_{\Lambda(1405)} \to m_{\Lambda(1405)} - i\Gamma/2$ is implicit. From the form of equation (3.11) and gauge invariance, we find the relations

$$k \cdot A = 0, \tag{3.16}$$

and

$$B + k \cdot C = 0. \tag{3.17}$$

The term in equation (3.11) proportional to D is gauge invariant by itself and thus gauge invariance does not constrain it. A two-component form for equation (3.11) results if one uses the following relations, valid in the transverse gauge:

$$\overline{u}_\Lambda \gamma_5 u_p = \sqrt{\frac{E_\Lambda + m_\Lambda}{2m_\Lambda}} \sqrt{\frac{E_p + m_p}{2m_p}} \chi_\Lambda^\dagger \left\{ \frac{\vec{\sigma} \cdot \vec{p_p}}{E_p + m_p} - \frac{\vec{\sigma} \cdot \vec{p_\Lambda}}{E_\Lambda + m_\Lambda} \right\} \chi_p, \tag{3.18}$$

$$\overline{u}_\Lambda \epsilon \cdot \gamma \gamma_5 u_p = \sqrt{\frac{E_\Lambda + m_\Lambda}{2m_\Lambda}} \sqrt{\frac{E_p + m_p}{2m_p}} \chi_\Lambda^\dagger \left\{ -\vec{\sigma} \cdot \vec{\epsilon} - \frac{\vec{\sigma} \cdot \vec{p}_\Lambda}{E_\Lambda + m_\Lambda} \vec{\sigma} \cdot \vec{\epsilon} \frac{\vec{\sigma} \cdot \vec{p_p}}{E_p + m_p} \right\} \chi_p, \tag{3.19}$$

$$\overline{u}_\Lambda k \cdot \gamma \gamma_5 u_p = \sqrt{\frac{E_\Lambda + m_\Lambda}{2m_\Lambda}} \sqrt{\frac{E_p + m_p}{2m_p}} \cdot$$

$$\cdot \chi_\Lambda^\dagger \left\{ -\vec{\sigma} \cdot \vec{k} + k \left(\frac{\vec{\sigma} \cdot \vec{p}_\Lambda}{E_\Lambda + m_\Lambda} + \frac{\vec{\sigma} \cdot \vec{p_p}}{E_p + m_p} \right) - \frac{\vec{\sigma} \cdot \vec{p}_\Lambda}{E_\Lambda + m_\Lambda} \vec{\sigma} \cdot \vec{k} \frac{\vec{\sigma} \cdot \vec{p_p}}{E_p + m_p} \right\} \chi_p, \tag{3.20}$$

$$\overline{u}_\Lambda \epsilon \cdot \gamma k \cdot \gamma \gamma_5 u_p = \sqrt{\frac{E_\Lambda + m_\Lambda}{2m_\Lambda}} \sqrt{\frac{E_p + m_p}{2m_p}} \cdot$$

$$\cdot \chi_\Lambda^\dagger \left\{ k \vec{\sigma} \cdot \vec{\epsilon} + i \frac{\vec{\sigma} \cdot \vec{p}_\Lambda}{E_\Lambda + m_\Lambda} \vec{\sigma} \cdot \vec{\epsilon} \times \vec{k} - i \vec{\sigma} \cdot \vec{\epsilon} \times \vec{k} \frac{\vec{\sigma} \cdot \vec{p_p}}{E_p + m_p} - \frac{\vec{\sigma} \cdot \vec{p}_\Lambda}{E_\Lambda + m_\Lambda} k \vec{\sigma} \cdot \vec{\epsilon} \frac{\vec{\sigma} \cdot \vec{p_p}}{E_p + m_p} \right\} \chi_p, \tag{3.21}$$

wherein χ represents a two-component spinor.

The further imposition of the energy and momentum constraints given in equations (2.3) and (2.4), corresponding to an at-rest kaon capture process, significantly reduces the number of contributing terms. Both the $A \cdot \epsilon$ and $C \cdot \epsilon$ terms give zero contribution for an at-rest capture in the transverse gauge. In this simple case, the amplitude in equation (3.11) can be written in the form

$$M = \frac{e \tilde{F}_1^{PS}}{2m_p} \chi_\Lambda^\dagger \vec{\sigma} \cdot \vec{\epsilon} \chi_p, \tag{3.22}$$

where $\tilde{F}^{PS}$ is the momentum dependent factor corresponding to a PS set of diagrams. For the Born plus $\Sigma^0 \to \Lambda$ transition contribution, given in equations (3.2) and (3.3), we have the following result

$$\begin{aligned}\tilde{F}_1^{PS} &= -g_{Kp\Lambda}\left\{1+\kappa_\Lambda\left(1-\frac{m_\Lambda}{m_K+m_p}\right)-\left(\frac{k}{E_\Lambda+m_\Lambda}\right)\left(\kappa_\Lambda\frac{m_\Lambda}{m_K+m_p}-(1+\kappa_p)\right)\right\} \\ &+ g_{Kp\Sigma}\kappa_{\Sigma\Lambda}\frac{k}{s-m_\Sigma^2}\left\{(m_\Sigma+m_\Lambda)\left(1+\frac{k}{E_\Lambda+m_\Lambda}\right)-2(m_K+m_p)\right\}. \qquad (3.23)\end{aligned}$$

The term proportional to $g_{Kp\Lambda}$ in equation (3.23) contains the contribution from M_1, while the term proportional to $g_{Kp\Sigma}$ contains the contribution from M_2. This reduction shows clearly the relative importance of these diagrams. Note that the $O(k/m)$ terms in equation (3.23) are much larger than the analogous terms from pion photoproduction and cannot be neglected.

The PV amplitude can also be reduced to the form of equation (3.22). This is accomplished most easily by reducing the $q\cdot\gamma$ factor of equation (3.8) using the Dirac equation. In this way, the following expression, appearing in the PV Born amplitude

$$\overline{u}_\Lambda\frac{p_K\cdot\gamma}{m_p+m_\Lambda}\gamma_5\frac{(p_p-k)\cdot\gamma+m_p}{u-m_p^2}, \qquad (3.24)$$

can be reduced to the form

$$\overline{u}_\Lambda\gamma_5\left\{\frac{1}{m_p+m_\Lambda}+\frac{(p_p-k)\cdot\gamma+m_p}{u-m_p^2}\right\}. \qquad (3.25)$$

Similarly, the PV expression

$$\frac{(p_\Lambda+k)\cdot\gamma+m_\Lambda}{s-m_\Lambda^2}\frac{p_K\cdot\gamma}{m_p+m_\Lambda}\gamma_5 u_p, \qquad (3.26)$$

is equivalent to

$$\left\{\frac{1}{m_p+m_\Lambda}+\frac{(p_\Lambda+k)\cdot\gamma+m_\Lambda}{s-m_\Lambda^2}\right\}\gamma_5 u_p. \qquad (3.27)$$

Using the above relations, one finds that the PS and PV prescriptions give two-component results differing only by a small term:

$$\tilde{F}_1^{PV}=\tilde{F}_1^{PS}+k\left(\frac{g_{Kp\Lambda}}{m_\Lambda+m_p}(\kappa_\Lambda+\kappa_p)+\frac{g_{Kp\Sigma}}{m_\Sigma+m_p}\kappa_{\Sigma\Lambda}\right)\left(1+\frac{k}{E_\Lambda+m_\Lambda}\right). \qquad (3.28)$$

The Born contribution to $\tilde{F}_1^{PS}$ can be simplified to

$$\tilde{F}_1^{PS}(Born) = -g_{Kp\Lambda}\left\{1 + \frac{k}{E_\Lambda + m_\Lambda}(1 + \kappa_p + \kappa_\Lambda)\right\}, \tag{3.29}$$

by regrouping terms in the first line of equation (3.23). In this form, we can easily compare the amplitude with the analogous pion-photoproduction amplitude for $\gamma n \to p\pi^-$. Dressler[20] has derived explicit PS and PV two-component expressions which, when written in the notation of equation (3.22),

$$\tilde{F}^{PS}(\gamma n \to p\pi^-) = -g_{\pi pn}\left\{\left(1 + \frac{k}{2m_p}\right) + \frac{m_\pi}{2m_p}(\kappa_p + \kappa_n)\right\}, \tag{3.30}$$

$$\tilde{F}^{PV}(\gamma n \to p\pi^-) = -g_{\pi pn}\left(1 + \frac{k}{2m_p}\right), \tag{3.31}$$

compare favorably with our expressions (3.28) and (3.29).

Comparing equations (3.28) to (3.31), we can easily see why PS $O(k/m)$ effects are larger for $K^-p \to \Lambda\gamma$ than for the analogous $\pi^-p \to n\gamma$ reaction. Apart from a larger photon momentum in the $K^-p \to \Lambda\gamma$ reaction, the proton and neutron anomalous magnetic moment contributions nearly cancel in equation (3.30), while the sum of proton and lambda contributions in equation (3.29) does not. By the same argument, Born PS and PV calculations will differ more for $K^-p \to \Lambda\gamma$ than for $\pi^-p \to n\gamma$.

Two-component reductions of the $K^-p \to \Sigma^0\gamma$ and $K^-n \to \Sigma^-\gamma$ amplitudes will also be required in the $K^-d \to \Lambda n\gamma$ impulse approximation calculation of Chapter 7.

For the PS Born plus $\Lambda \to \Sigma^0$ transition $K^-p \to \Sigma^0\gamma$ amplitude, a reduction to the form of equation (3.22) results in the momentum dependent factor

$$\begin{aligned}\tilde{F}_2^{PS} &= -g_{Kp\Sigma}\left\{1 + \kappa_\Sigma\left(1 - \frac{m_\Sigma}{m_K + m_p}\right) - \left(\frac{k}{E_\Sigma + m_\Sigma}\right)\left(\kappa_\Sigma\frac{m_\Sigma}{m_K + m_p} - (1 + \kappa_p)\right)\right\} \\ &+ g_{Kp\Sigma}\kappa_{\Sigma\Lambda}\frac{k}{s - m_\Lambda^2}\left\{(m_\Sigma + m_\Lambda)\left(1 + \frac{k}{E_\Sigma + m_\Sigma}\right) - 2(m_K + m_p)\right\},\end{aligned} \tag{3.32}$$

which can be obtained by simply making the replacement $\Lambda \leftrightarrow \Sigma$ in equation (3.23). A simplified relation for $\tilde{F}_2^{PS}(Born)$ is also obtained by making the replacement $\Lambda \to \Sigma$

in equation (3.29). As κ_{Σ^0} and κ_Λ have opposite signs, the difference between Born PS and PV calculations will be greater for $\Sigma^0\gamma$ than $\Lambda\gamma$.

The $K^-n \to \Sigma^-\gamma$ PS Born amplitude is constructed as was the $K^-p \to \Lambda\gamma$ amplitude described in Section 3.1. Diagrams involving the intermediate radiating n, Σ^- and K are summed to give the total Born amplitude:

$$\begin{aligned} M(K^-n \to \Sigma^-\gamma) &= g_{Kn\Sigma} e\overline{u}_\Sigma \left(-\epsilon\cdot\gamma + \frac{\kappa_{\Sigma^-}}{2m_p}\epsilon\cdot\gamma k\cdot\gamma\right)\frac{(p_{\Sigma^-}+k)\cdot\gamma + m_\Sigma}{s-m_\Sigma^2}\gamma_5 u_n \\ &+ g_{Kn\Sigma} e\overline{u}_\Sigma\gamma_5 \frac{(p_n-k)\cdot\gamma + m_n}{u-m_n^2}\frac{\kappa_n}{2m_p}\epsilon\cdot\gamma k\cdot\gamma u_n \\ &- 2g_{Kn\Sigma} e\overline{u}_\Sigma\gamma_5\frac{p_K\cdot\epsilon}{t-m_K^2}u_n. \end{aligned} \tag{3.33}$$

Once again, reducing $M(K^-n \to \Sigma^-\gamma)$ to the form of equation (3.22) we find

$$\begin{aligned} \tilde{F}_3^{PS} &= -g_{Kn\Sigma}\left\{\frac{m_p}{m_K+m_n} + \kappa_{\Sigma^-}\left(1-\frac{m_\Sigma}{m_K+m_n}\right)\right\} \\ &+ g_{Kn\Sigma}\frac{k}{E_\Sigma+m_\Sigma}\left(\kappa_{\Sigma^-}\frac{m_\Sigma}{m_K+m_n} - \frac{m_p}{m_K+m_p} - \kappa_n\right), \end{aligned} \tag{3.34}$$

where, in equations (3.33) and (3.34), m_Σ is the Σ^- mass. The coupling constants $g_{Kp\Sigma}$ and $g_{Kn\Sigma}$ are related by isospin, which we use to find[21] $g_{Kn\Sigma}$ equal to $\sqrt{2}g_{Kp\Sigma}$. In Chapter 7, the operator $F_i^{PS}\vec{\sigma}\cdot\vec{\epsilon}$ will act between the deuteron and YN final state spin wavefunctions, where the factor F_i^{PS} is equal to $(e/2m_p)\tilde{F}_i^{PS}$.

3.3 The Momentum Dependent Transition Operator

In Chapter 8, an impulse approximation calculation, utilizing a momentum dependent $K^-p \rightarrow \Lambda\gamma$ transition operator, will be performed for the $K^-d \rightarrow \Lambda n\gamma$ reaction. Here we will construct the operator to be used.

The following derivation is similar to the two-component reduction of Section 3.2. However, we will now retain the proton momentum in order to account for its motion in the deuteron. As the kaon is captured from an atomic state with negligible momentum, in the deuteron rest frame, the following momentum conservation relation holds for the capture process:

$$\vec{p}_p = \vec{p}_\Lambda + \vec{k}. \tag{3.35}$$

We then have the following relations for the Mandlestam variables:

$$s = m_K^2 + m_p^2 + 2m_K E_p, \tag{3.36}$$

$$t = m_K^2 - 2m_K k, \tag{3.37}$$

$$u = m_p^2 - 2(E_p k - \vec{p}_p \cdot \vec{k}). \tag{3.38}$$

As the proton's fermi momentum distribution is peaked below 100 MeV, E_p can be replaced with m_p to a good approximation in equations (3.36) and (3.38). Thus, s and t are equivalent to their at-rest capture values. The propagator $(u - m_p^2)^{-1}$ is modified and can be approximated using

$$\frac{1}{u - m_p^2} \approx \frac{-1}{2m_p k}\left(1 + \frac{\vec{p}_p \cdot \hat{k}}{m_p}\right), \tag{3.39}$$

where the $\vec{p}_p$ term is a small correction to the at-rest capture propagator.

In practice, the momenta appearing in our transition operator will be converted to gradient operators for the coordinate space impulse approximation calculation. From

equation (3.35) it is clear that we may eliminate the lambda momentum in favor of the proton and photon momenta. This we will do in order to restrict the required derivatives to the photon and deuteron wavefunctions.

It is convenient to first eliminate the explicit dependence on p_Λ in the Born (M_1) plus $\Sigma^0 \to \Lambda$ (M_2) plus $\Lambda(1405)$ (M_3) amplitudes of equation (3.1):

$$\begin{aligned} M_1 &= g_{Kp\Lambda}\frac{e\kappa_\Lambda}{2m_p}\overline{u}_\Lambda \epsilon\cdot\gamma k\cdot\gamma\frac{[m_\Lambda - m_p + m_K\gamma_0]}{s-m_\Lambda^2}\gamma_5 u_p \\ &+ g_{Kp\Lambda}e\overline{u}_\Lambda\gamma_5\frac{[(p_p-k)\cdot\gamma + m_p]}{u-m_p^2}\left\{\epsilon\cdot\gamma + \frac{\kappa_p}{2m_p}\epsilon\cdot\gamma k\cdot\gamma\right\}u_p \\ &- 2g_{Kp\Lambda}e\overline{u}_\Lambda\gamma_5\frac{p_K\cdot\epsilon}{t-m_k^2}u_p, \end{aligned} \tag{3.40}$$

$$M_2 = g_{Kp\Sigma}\frac{e\kappa_{\Sigma\Lambda}}{2m_p}\overline{u}_\Lambda\epsilon\cdot\gamma k\cdot\gamma\frac{[m_\Sigma - m_p + m_K\gamma_0]}{s-m_\Sigma^2}\gamma_5 u_p, \tag{3.41}$$

$$M_3 = g_{Kp\Lambda(1405)}\frac{e\kappa_{\Lambda(1405)\Lambda}}{2m_p}\overline{u}_\Lambda\epsilon\cdot\gamma k\cdot\gamma\gamma_5\frac{[m_{\Lambda(1405)} + m_p + m_K\gamma_0]}{s-m_{\Lambda(1405)}^2}u_p, \tag{3.42}$$

where as in Section 3.2, the $\Lambda(1405)$ mass is complex, and the third (kaon radiation) amplitude in M_1 again gives zero contribution.

We will retain terms of $O(p_p/m)$ and $O(k/m)$ relative to the leading order term in our two-component amplitude. To this order, the following truncations are sufficient:

$$\overline{u}_\Lambda\gamma_5 u_p \approx \chi_\Lambda^\dagger\frac{\vec{\sigma}\cdot\vec{k}}{2m_\Lambda}\chi_p, \tag{3.43}$$

$$\overline{u}_\Lambda\epsilon\cdot\gamma\gamma_5 u_p \approx -\chi_\Lambda^\dagger\vec{\sigma}\cdot\vec{\epsilon}\chi_p, \tag{3.44}$$

$$\overline{u}_\Lambda k\cdot\gamma\gamma_5 u_p \approx -\chi_\Lambda^\dagger\vec{\sigma}\cdot\vec{k}\chi_p, \tag{3.45}$$

$$\overline{u}_\Lambda\epsilon\cdot\gamma k\cdot\gamma\gamma_5 u_p \approx \chi_\Lambda^\dagger k\vec{\sigma}\cdot\vec{\epsilon}\left(1+\frac{k}{2m_\Lambda}\right)\chi_p, \tag{3.46}$$

when combined with the factors, defined in equation (3.11),

$$A \cdot \epsilon \approx g_{Kp\Lambda} \frac{\vec{p}_p \cdot \vec{\epsilon}}{m_p k} \left(1 + \frac{\vec{p}_p \cdot \hat{k}}{m_p}\right), \tag{3.47}$$

$$B \approx -g_{Kp\Lambda} \left(\frac{\kappa_p}{2m_p}\right), \tag{3.48}$$

$$C \cdot \epsilon \approx -g_{Kp\Lambda} \left(\frac{\kappa_p}{m_p}\right) \frac{\vec{p}_p \cdot \vec{\epsilon}}{2m_p k} \left(1 + \frac{\vec{p}_p \cdot \hat{k}}{m_p}\right), \tag{3.49}$$

$$D \approx -g_{Kp\Lambda} \frac{(1+\kappa_p)}{2m_p k} \left(1 + \frac{\vec{p}_p \cdot \hat{k}}{m_p}\right) - g_{Kp\Lambda} \left(\frac{\kappa_\Lambda}{2m_p}\right) \frac{1}{(m_K + m_p) + m_\Lambda}$$

$$-g_{Kp\Sigma} \left(\frac{\kappa_{\Sigma\Lambda}}{2m_p}\right) \frac{1}{(m_K + m_p) + m_\Sigma} + g_{Kp\Lambda(1405)} \left(\frac{\kappa_{\Lambda(1405)\Lambda}}{2m_p}\right) \frac{1}{(m_K + m_p) - m_{\Lambda(1405)}}. \tag{3.50}$$

Combining terms, we have the following transition operator:

$$\hat{T} = -\frac{e g_{Kp\Lambda}}{2m_p} \left\{1 + \frac{k}{2m_\Lambda}(1 + \kappa_p + \kappa_\Lambda)\right\} \vec{\sigma} \cdot \vec{\epsilon}$$

$$-\frac{e g_{Kp\Lambda}}{2m_p}(1+\kappa_p) \left\{\frac{\vec{p}_p \cdot \hat{k}}{m_p} \vec{\sigma} \cdot \vec{\epsilon} - \frac{\vec{p}_p \cdot \vec{\epsilon}}{m_p} \vec{\sigma} \cdot \hat{k}\right\}$$

$$-\frac{k}{2m_\Lambda} \left\{\frac{e g_{Kp\Sigma}}{2m_p} \left(\frac{2m_\Lambda}{\sqrt{s} + m_\Sigma}\right) \kappa_{\Sigma\Lambda} - \frac{e g_{Kp\Lambda(1405)}}{2m_p} \left(\frac{2m_\Lambda}{\sqrt{s} - m_{\Lambda(1405)}}\right) \kappa_{\Lambda(1405)\Lambda}\right\} \vec{\sigma} \cdot \vec{\epsilon}, \tag{3.51}$$

which depends on the two momentum scales, $\vec{k}$ and $\vec{p_p}$. The terms involving $\vec{p}_p$ have been simplified through the neglect of pieces proportional to $(1 - m_p/m_\Lambda)$. The approximations made in deriving equation (3.51) will be justified in Chapter 10, where the effect of these momentum dependent terms is calculated.

Having gained some insight into the structure of M, we next proceed to a discussion of the coupling constants used in our numerical calculations.

Chapter 4

DETERMINATION OF COUPLING CONSTANTS

In order to evaluate numerically the amplitude in equation (3.1), we require several strong coupling constants as well as magnetic and transition moments for the electromagnetic vertices. Since our results are sensitive to the choice of these couplings, this chapter will give a detailed outline of the methods we employed in their determination. The values used in our numerical calculation are given in Table 4.1.

The most important of these parameters are those which determine the Born plus $\Sigma^0 \to \Lambda$ transition terms of fig. 1, but fortunately these are for the most part fairly well determined. However, two comments should be made about the values in Table 4.1. First, one should note that only the magnitude of $\kappa_{\Sigma\Lambda}$ is experimentally known. Thus, we have chosen a sign from the SU(3) prediction[21]:

$$\kappa_{\Sigma\Lambda} = -\frac{\sqrt{3}}{2}\kappa_n \approx +1.7, \tag{4.1}$$

which is in good agreement with the experimental magnitude. As this choice is not universally agreed upon, the $\kappa_{\Sigma\Lambda}$ sign is discussed in Appendix A. The magnitude of $\kappa_{\Sigma\Lambda}$ is taken from the most recent experimental determination[22].

In addition, since the Σ^0 magnetic moment is not experimentally determined, we have used the isospin relation[21]

$$\kappa_{\Sigma^0} = \frac{1}{2}(\mu_{\Sigma^-} + \mu_{\Sigma^+}), \tag{4.2}$$

to estimate its value. Experimental values for the total magnetic moments, $\mu_{\Sigma^\pm}$, have been taken from the most recent particle data compilation[23].

For the strong $Kp\Lambda$ coupling, we have taken the recent dispersion relation determination of Martin[24]. In addition, we have taken Antolin's very recent value[25] for the $Kp\Sigma$ coupling, which is based on an analysis of charge exchange data and is consistent with the earlier estimate given by Martin. The relative sign of the $g_{Kp\Lambda}$ and $g_{Kp\Sigma}$ couplings is determined by the SU(6) expectation.

The radiative $K^* \rightarrow K\gamma$ coupling can be estimated from the K^* total width and branching fraction to $K\gamma$[23]. Using our form of the $K^*K\gamma$ vertex factor, as given in equation (3.7), the radiative width and coupling constant κ_{K^*K} are related up to a sign by

$$\Gamma_{K^*\rightarrow K\gamma} = \frac{\alpha}{24}\left(\frac{\kappa_{K^*K}}{2m_p}\right)^2 m_{K^*}^3 \left\{1-\left(\frac{m_K}{m_{K^*}}\right)^2\right\}^3, \tag{4.3}$$

wherein α is the fine structure constant. The strong $K^*\Lambda N$ and $K^*\Sigma N$ couplings are not well known. Thus SU(3) relations have been employed in order to relate these couplings to the better known ρNN couplings. The relations are[26]

$$g^{V(T)}_{K^*\Lambda N} = -\frac{\sqrt{3}}{3}(1+2\alpha_{e(m)})g^{V(T)}_{\rho NN}, \tag{4.4}$$

and

$$g^{V(T)}_{K^*\Sigma N} = (1-2\alpha_{e(m)})g^{V(T)}_{\rho NN}, \tag{4.5}$$

wherein α_e and α_m are independent constants appropriate for the vector and tensor couplings respectively. We have used the dispersion relation results[27] of Pietarinen for the ρNN couplings. Using Pietarinen's values

$$g^V_{\rho NN} = 2.6 \qquad g^T_{\rho NN} = 16.0, \tag{4.6}$$

and the static SU(6) values[28,29] of 1 and $\frac{2}{5}$ for α_e and α_m respectively, we find $K^*\Lambda N$ and $K^*\Sigma N$ couplings

$$g^V_{K^*\Lambda N} = -4.5 \qquad g^T_{K^*\Lambda N} = -16.7, \tag{4.7}$$

$$g^V_{K^*\Sigma N} = -2.6 \qquad g^T_{K^*\Sigma N} = 3.2, \tag{4.8}$$

which are in basic agreement with Nagels' fitted values[29]. The tensor $K^*\Sigma N$ coupling shows the poorest agreement with Nagels' value. However, we shall find that this discrepancy does not appreciably affect our final result. The relative sign of the KYN and K^*YN couplings was chosen to conform with Nagels' value.

The largest $J^P = \frac{1}{2}^-$ resonant s-channel contributions, apart from that due to the $\Lambda(1405)$, are due to the $\Lambda(1670)\frac{1}{2}^-$, $\Lambda(1800)\frac{1}{2}^-$ and $\Sigma(1750)\frac{1}{2}^-$. Strong couplings have been estimated from the full widths and branching fractions of these resonances, using relations of the form

$$\Gamma_{B(\frac{1}{2}^-)\to B'(\frac{1}{2}^+)M(0^-)} = \frac{g^2_{BB'M}}{8\pi}\frac{(m_B + m_{B'})^2 - m_M^2}{m_B^2}Q, \tag{4.9}$$

wherein Q is the decay 3-momentum of the outgoing kaon. Since there are no photon decays listed for these resonances in the most recent particle data compilation[23], we have used the NRQM results as guidance. From the decay widths, generated using amplitudes from the Isgur/Karl model[30], tabulated in Table II of reference 12, we have calculated transition moments using

$$\Gamma_{B(\frac{1}{2})\to B'(\frac{1}{2})\gamma} = \frac{\alpha k^3}{m_p^2}\kappa^2_{BB'}. \tag{4.10}$$

The $\Lambda(1600)\frac{1}{2}^+$, $\Lambda(1800)\frac{1}{2}^+$ and $\Sigma(1660)\frac{1}{2}^+$ can also contribute in the s-channel. However, as we have neither experimental nor NRQM estimates of their photon decay widths, they have not been included. The effect of this omission is considered in the next chapter.

There are two N^* resonances with significant decay fractions to $p\gamma$ and ΛK final states, the $N(1650)\frac{1}{2}^-$ and the $N(1710)\frac{1}{2}^+$. Here, equation (4.10) was used directly to obtain values of κ_{N^*p} from experimental information. Similarly, equation (4.9) was employed to estimate the strong $N(1650)\frac{1}{2}^-$ coupling, and the following relation was used to give the $N(1710)\frac{1}{2}^+$ value:

$$\Gamma_{B(\frac{1}{2}^+)\to B'(\frac{1}{2}^+)M(0^-)} = \frac{g^2_{BB'M}}{8\pi}\frac{(m_B - m_{B'})^2 - m_M^2}{m_B^2}Q. \tag{4.11}$$

One type of contribution, which we cannot easily determine, is the coupling to N^* resonances which are below the ΛK threshold. In the kaon photoproduction calculation of Adelseck[31], two values were fit for the coupling constant product $g_{KN(1440)\Lambda}\kappa_{N(1440)p}$. Using our conventions for magnetic couplings, these two values are 4.1 and 5.0.

The signs associated with these various N^* and Y^* amplitudes are not experimentally determined. When numerical results are presented, however, it will become clear that these amplitudes are usually small, and thus do not significantly effect our results.

Table 4.1: Summary of Coupling Constants

Electromagnetic Couplings			
κ_Λ	-0.613	$\kappa_{N(1650)p}$	$+0.320$
κ_p	$+1.793$	$\kappa_{N(1710)p}$	$+0.030$
κ_{Σ^0}	$+0.619$	$\kappa_{\Lambda(1800)\Sigma^0}$	$+0.693$
$\kappa_{\Sigma^0\Lambda}$	$+1.60$	$\kappa_{\Lambda(1670)\Sigma^0}$	$+1.250$
$\kappa_{\Lambda(1800)\Lambda}$	$+0.117$	$\kappa_{\Sigma(1750)\Sigma^0}$	$+0.242$
$\kappa_{\Lambda(1670)\Lambda}$	$+0.094$	κ_{K^*K}	$+1.58$
$\kappa_{\Sigma(1750)\Lambda}$	$+0.102$		

Strong (pseudoscalar) couplings			
$g_{K^-p\Lambda}$	-13.2	$g_{KN(1650)\Lambda}$	0.810
$g_{K^-p\Sigma^0}$	$+6.0$	$g_{KN(1710)\Lambda}$	6.5
$g^V_{K^*p\Lambda}$	-4.5	$g_{KN(1710)\Sigma^0}$	13.0
$g^T_{K^*p\Lambda}$	-16.7	$g_{Kp\Lambda(1670)}$	0.42
$g^V_{K^*p\Sigma^0}$	-2.6	$g_{Kp\Lambda(1800)}$	1.40
$g^T_{K^*p\Sigma^0}$	$+3.2$	$g_{Kp\Sigma(1750)}$	0.72

Chapter 5

NUMERICAL RESULTS FOR $K^-p \rightarrow Y\gamma$

Both PS and PV results are presented in Table 5.1 for $\Lambda\gamma$ and $\Sigma^0\gamma$ final states using the couplings of Table 4.1. Results have been given for various combinations of the amplitudes given in equations (3.2) to (3.7), so as to understand the relative contributions of the various terms.

Consider first the $\Lambda\gamma$ Born graphs of fig. 1a-c and, for PV couplings, 1e which give 3.61×10^{-3} and 2.65×10^{-3} for the PS and PV coupling schemes respectively. It is interesting to note that both coupling schemes give branching ratios in basic agreement with the published[14] experimental range of $(2.8 \pm 0.8) \times 10^{-3}$ for this simplest possible calculation. Addition of the $\Sigma^0 \rightarrow \Lambda$ transition diagram, fig. 1d, moves both the PS and PV results closer to the central experimental value, but produces only a 13% and 4% effect respectively in the two cases. Further addition of the K^* contribution, fig. 2c, lowers both the PS and PV branching ratios by about 10%. The $\Sigma^0 \rightarrow \Lambda$ transition diagram and the K^* diagram contribute primarily through interference with the other diagrams. Thus the alternative choice of sign for $\kappa_{\Sigma\Lambda}$, as was taken in reference 13, or for κ_{K^*K}, where the sign is really not known, would change the sign but not the magnitude of these contributions. The N^* contribution, fig. 2b, which combines the individual contributions of the $N(1650)$ and $N(1710)$ is basically negligible in both coupling schemes. As mentioned in Chapter 4, this N^* contribution neglects the effect

of N^* resonances below the ΛK threshold. The PS $N(1440)$ couplings fit by Adelseck produce a 10% change in our PS branching ratio. Thus, although our estimate of the $N(1440)$ contribution is model-dependent, it appears that this resonance plays a minor role in determining the $\Lambda\gamma$ branching ratio. Likewise, the Y^* contribution, fig. 2a, which combines the individual contributions of the $\Lambda(1670)$, $\Lambda(1800)$ and $\Sigma(1750)$, gives only a few per cent correction to the Born plus $\Sigma^0 \rightarrow \Lambda$ transition graph result. The omission of $J^P = \frac{1}{2}^+$ Y^* resonances should therefore not seriously effect our results. The $\Lambda(1116)\frac{1}{2}^+$ itself gives only a small contribution to the $K^-p \rightarrow \Lambda\gamma$ rate.

In order to determine the $\Lambda(1405)$ contribution, we have added the amplitude in equation (3.4) and have allowed the composite $g_{Kp\Lambda(1405)}\kappa_{\Lambda(1405)\Lambda}$ coupling to vary freely. If we take the value of 3.2 for $g_{Kp\Lambda(1405)}$, as was done in reference 13, the resulting dependence of the $\Lambda\gamma$ branching ratio on $\Lambda(1405)$ is illustrated in fig. 5.1. In fig. 5.1, the PS $\Lambda(1405)$ amplitude has been added separately to the Born plus $\Sigma^0 \rightarrow \Lambda$ transition and the Born plus $\Sigma^0 \rightarrow \Lambda$ transition plus K^* amplitudes. For the latter combination, the $\kappa_{\Lambda(1405)\Lambda}$ values of 0.0 ± 0.1 and -0.8 ± 0.1 are compatible with the published experimental range of branching ratios. The first range of small $\kappa_{\Lambda(1405)\Lambda}$ values should be expected, as the theoretical branching ratio lies within the published experimental bounds without any contribution from the $\Lambda(1405)$. The actual value of $\kappa_{\Lambda(1405)\Lambda}$ here will be sensitive to the choice of diagrams, since in this case the small $\Lambda(1405)$ contribution will be comparable to the small contributions from, for example, the Y^* and N^* diagrams. The $\Lambda(1405) \rightarrow \Lambda\gamma$ radiative width corresponding to this solution is 0 ± 2 keV. The second range of values requires a large cancellation between the $\Lambda(1405)$ and other diagrams. Now the radiative width is 93 ± 25 keV. The value of $\kappa_{\Lambda(1405)\Lambda}$, and thus this width, is relatively insensitive to the other included diagrams as the $\Lambda(1405)$ contribution is dominant.

The above values of $\kappa_{\Lambda(1405)\Lambda}$ and the $\Lambda(1405)$ radiative width depend very directly on the one published experimental branching ratio[14] which is soon to be supplemented

by a new value from the Brookhaven experiment[3]. Fig. 5.1 is thus valuable as it can be used to extract a value for $\kappa_{\Lambda(1405)\Lambda}$, and thus for the contribution of the $\Lambda(1405)$, from any new branching ratio data. For example, the minimum branching ratio obtainable this way is about 1×10^{-3}, which corresponds to $\kappa_{\Lambda(1405)\Lambda} \approx -0.4$ and a $\Lambda(1405)$ radiative width of 23 keV. Any preferred value of $g_{Kp\Lambda(1405)}$ can be accommodated by simply scaling $\kappa_{\Lambda(1405)\Lambda}$.

The above investigation has been repeated for a PV coupling scheme as well. In fig. 5.2, the PV analogue of the $\Lambda(1405)$ amplitude was added separately to the Born plus $\Sigma^0 \to \Lambda$ and Born plus $\Sigma^0 \to \Lambda$ plus K^* amplitudes as in the PS case. For either of the combinations, any given branching ratio gives $\kappa_{\Lambda(1405)\Lambda}$ values and $\Lambda(1405)$ radiative widths which are essentially equivalent to the PS values.

The $\Sigma^0\gamma$ calculation appears to be more sensitive to the addition of diagrams beyond the Born graphs. The $\Lambda \to \Sigma^0$ transition diagram dramatically lowers the PS rate while having a 16% effect on the PV rate. The resulting rate is in the PS case about an order of magnitude below the Born plus $\Sigma^0 \to \Lambda$ result for $\Lambda\gamma$. The large difference between our $\Lambda\gamma$ and $\Sigma^0\gamma$ Born results can be understood simply from equation (3.29) and the ratio of the strong $Kp\Lambda$ and $Kp\Sigma$ couplings we have used. Addition of the K^* amplitude produces an essentially negligible change in the $\Sigma^0\gamma$ rate. The same is true of the $N(1710)$ contribution represented by N^* in Table 5.1. The $N(1650)$ resonance has not been included, as it is below the ΣK threshold, and thus we have no experimental information on the $KN(1650)\Sigma$ coupling. The Y^* contribution, which represents the same set of resonances considered in the $\Lambda\gamma$ case, is appreciable for a $\Sigma^0\gamma$ final state. The addition of this amplitude to the Born plus $\Lambda \to \Sigma^0$ terms increases the PS and PV rates by 44% and 22% respectively. Recall that in Chapter 4 we obtained the Y^* couplings indirectly from the NRQM; thus this last contribution is model-dependent both as to the magnitude and the relative signs of the various contributions. The omitted $J^P = \frac{1}{2}^+$ Y^* resonances could also make a large contribution here. If the $\Sigma^0\gamma$

branching fraction were of the order of 10^{-4}, the Y^* resonances would severely limit our ability to determine the $\Lambda(1405)$ contribution. However, we will see that the $\Sigma^0\gamma$ branching fraction is probably much larger than 10^{-4}.

We can add to our calculation the $\Sigma^0\gamma$ analogue of the $\Lambda(1405)$ amplitude of equation (3.4) within both the PS and PV coupling schemes. Results are given for PS and PV couplings in figs. 5.3 and 5.4 respectively showing the $\Sigma^0\gamma$ branching ratio for a range of $\kappa_{\Lambda(1405)\Sigma}$ values. The $\Lambda(1405)$ amplitude has been added to both the Born plus $\Lambda \to \Sigma^0$ and Born plus $\Lambda \to \Sigma^0$ plus Y^* calculations. The current experimental limit[15] of 4×10^{-3} puts a weak limit on the range of $\kappa_{\Lambda(1405)\Sigma}$ values allowed. Assuming, as before, that $g_{Kp\Lambda(1405)}$ has a value 3.2, we have $\kappa_{\Lambda(1405)\Sigma}$ constrained to be between 1.0 and -0.6 in both coupling schemes. One should note that for $\Sigma^0\gamma$, unlike $\Lambda\gamma$, since the Born and other contributions are relatively small, the $\Lambda(1405)$ dominates over almost all of the allowed range of $\kappa_{\Lambda(1405)\Sigma}$.

It is of interest to consider the ratio of the branching fraction for $\Lambda\gamma$ to that for $\Sigma^0\gamma$, as this ratio is independent of the quantity W_p appearing in equation (2.2), and thus is perhaps better determined than either of the individual branching ratios. Both the NRQM[12] and the CBM[11] make a definite prediction of 1.3 for the $\Lambda\gamma/\ \Sigma^0\gamma$ ratio. In our model, without the $\Lambda(1405)$, the $\Lambda\gamma$ rate is much larger than the $\Sigma^0\gamma$ rate. When the $\Lambda(1405)$ is included, however, the results change dramatically depending on the relative values of $\kappa_{\Lambda(1405)\Lambda}$ and $\kappa_{\Lambda(1405)\Sigma}$ as can be seen directly from figs. 5.1 to 5.4.

In principle, the $\kappa_{\Lambda(1405)\Lambda}$ and $\kappa_{\Lambda(1405)\Sigma}$ transition moments are independent. Given a model for the $\Lambda(1405)$, however, these two constants can be related. The simplest possible approach is to treat the $\Lambda(1405)$ as a pure SU(3) singlet. With this assumption, $\kappa_{\Lambda(1405)\Sigma}$ is a factor of $\sqrt{3}$ larger than $\kappa_{\Lambda(1405)\Lambda}$. Using this relation and the value of $\kappa_{\Lambda(1405)\Lambda} \approx -0.8$, the branching ratio for $\Sigma^0\gamma$ is greater than 10^{-2}. Thus this value of $\kappa_{\Lambda(1405)\Lambda}$ is probably ruled out by the experimental upper limit of 4×10^{-3}. For $\kappa_{\Lambda(1405)\Lambda} \approx -0.4$, corresponding to the minimum $\Lambda\gamma$ branching ratio, the branching ratio

for $\Sigma^0\gamma$ would also be slightly above the experimental upper limit. Although the $\Lambda(1405)$ is mainly a SU(3) singlet in the NRQM, care must be taken in making comparisons. In the NRQM, interference between singlet and octet components is particularly important to the $\Lambda(1405) \rightarrow \Sigma^0\gamma$ transition, so that the factor of $\sqrt{3}$ may not be appropriate.

As indicated in Section 2.2, the value of W_p used in our determination of the $K^-p \rightarrow Y\gamma$ branching fractions has a 25% error. Thus, this factor introduces a 25% error in our branching fraction results. However, since this factor is not present in our $\Lambda\gamma/\Sigma^0\gamma$ branching ratio calculation, the results of these calculations, for a small $\Lambda(1405)$ contribution, should be relatively firm. If the $\Lambda(1405)$ contribution is large, we will require a (model-dependent) relation between the couplings $\kappa_{\Lambda(1405)\Lambda}$ and $\kappa_{\Lambda(1405)\Sigma}$ in order to calculate this ratio.

Another problem is linked to the uncertainty in the $\Lambda(1405)$ full decay width. The full decay width is quoted[23] as 40 ± 10 MeV. If the $\Lambda(1405)$ is the dominant resonance contributing to the $K^-p \rightarrow Y\gamma$ reactions, then the magnitude at the minima of the curves in figs. 5.1 to 5.4 is related to the $\Lambda(1405)$ width. In order to display this effect, fig. 5.5 shows a calculation of the $K^-p \rightarrow \Lambda\gamma$ branching fraction using the Born plus $\Sigma^0 \rightarrow \Lambda$ transition plus $\Lambda(1405)$ amplitudes. Fig. 5.5 illustrates the effect of choosing a width between 30 and 50 MeV. Hemingway[32] has fit a Breit-Wigner form to the $\Sigma\pi$ mass distribution and finds a best value of 32 MeV for the $\Lambda(1405)$ width. Fig. 4 of this reference also illustrates that the CBM and K-matrix methods are more successful than the Breit-Wigner form in fitting this mass distribution.

In principle, one could make the $\Lambda(1405)$ full width energy dependent, evaluating $\Gamma(\sqrt{s})$ at $\sqrt{s} = 1432$ MeV corresponding to the $\Lambda(1405)$ energy[33]. However, as $\Gamma(1432$ MeV) is within the 40 ± 10 MeV range, if one chooses $\Gamma(1405$ MeV) to be 40 MeV, the additional complication of an energy dependent width is not useful.

The preliminary[4] $K^-p \rightarrow Y\gamma$ branching fraction results from Brookhaven appear to indicate a $\Sigma^0\gamma$ branching fraction of the order of 10^{-3} and in excess of the $\Lambda\gamma$ value.

If this is indeed true, the $\Lambda(1405)$ contribution will dominate our $K^- p \to \Sigma^0 \gamma$ branching fraction calculation. In addition, as can be seen from figs. 5.3 and 5.4, the uncertainty induced by the Y^* resonances will have a small effect.

Table 5.1: Branching Fractions for $K^-p \to \Lambda\gamma$ and $K^-p \to \Sigma^0\gamma$

Branching Fractions for $K^-p \to \Lambda\gamma$		
Diagrams Included	*Pseudoscalar*	*Pseudovector*
Born	3.61×10^{-3}	2.65×10^{-3}
Born + $\Sigma^0 \to \Lambda$	3.13×10^{-3}	2.75×10^{-3}
Born + $\Sigma^0 \to \Lambda + K^*$	2.84×10^{-3}	2.48×10^{-3}
Born + $\Sigma^0 \to \Lambda + Y^*$	3.03×10^{-3}	2.70×10^{-3}
Born + $\Sigma^0 \to \Lambda + N^*$	3.09×10^{-3}	2.78×10^{-3}

Branching Fractions for $K^-p \to \Sigma^0\gamma$		
Diagrams Included	*Pseudoscalar*	*Pseudovector*
Born	6.57×10^{-4}	4.14×10^{-4}
Born + $\Lambda \to \Sigma^0$	3.67×10^{-4}	4.79×10^{-4}
Born + $\Lambda \to \Sigma^0 + K^*$	3.65×10^{-4}	4.76×10^{-4}
Born + $\Lambda \to \Sigma^0 + Y^*$	5.29×10^{-4}	5.89×10^{-4}
Born + $\Lambda \to \Sigma^0 + N^*$	3.72×10^{-4}	4.80×10^{-4}

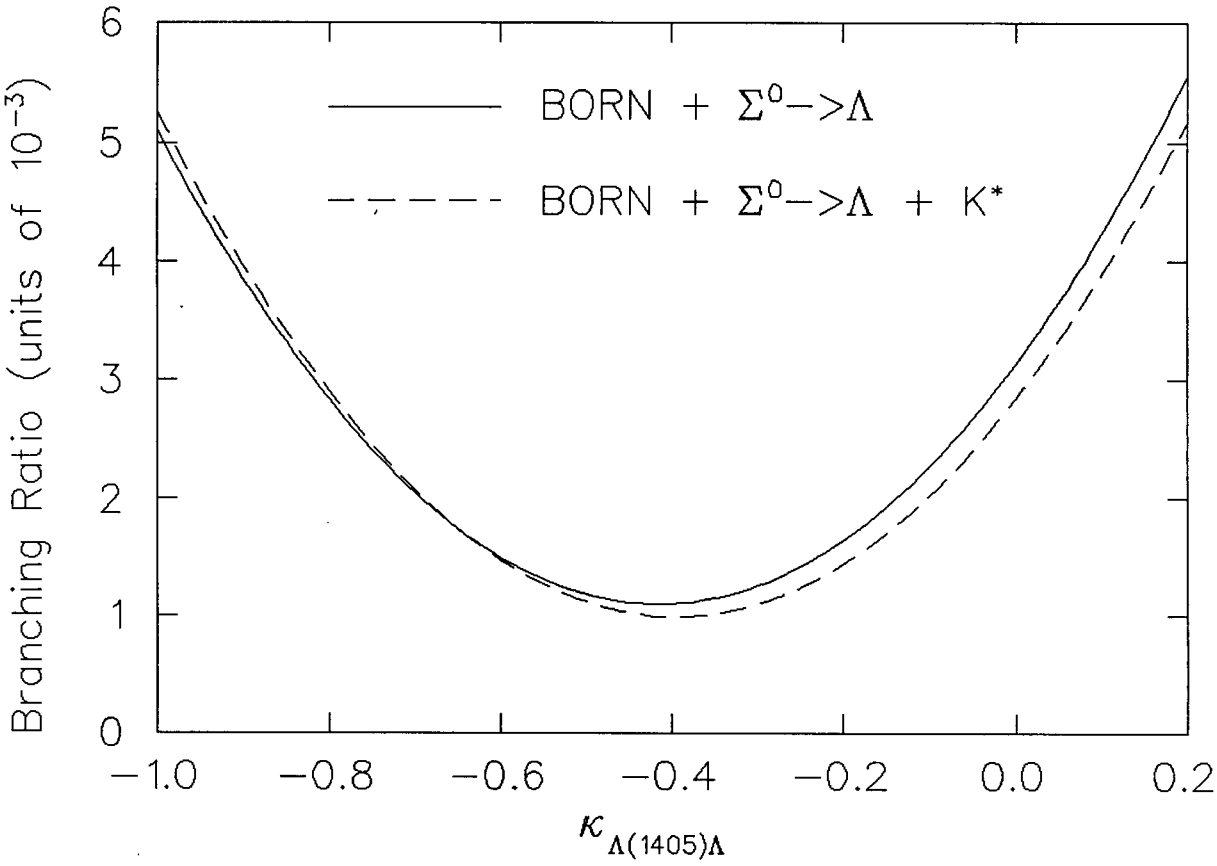

Figure 5.1: PS branching fractions for $K^- p \to \Lambda\gamma$

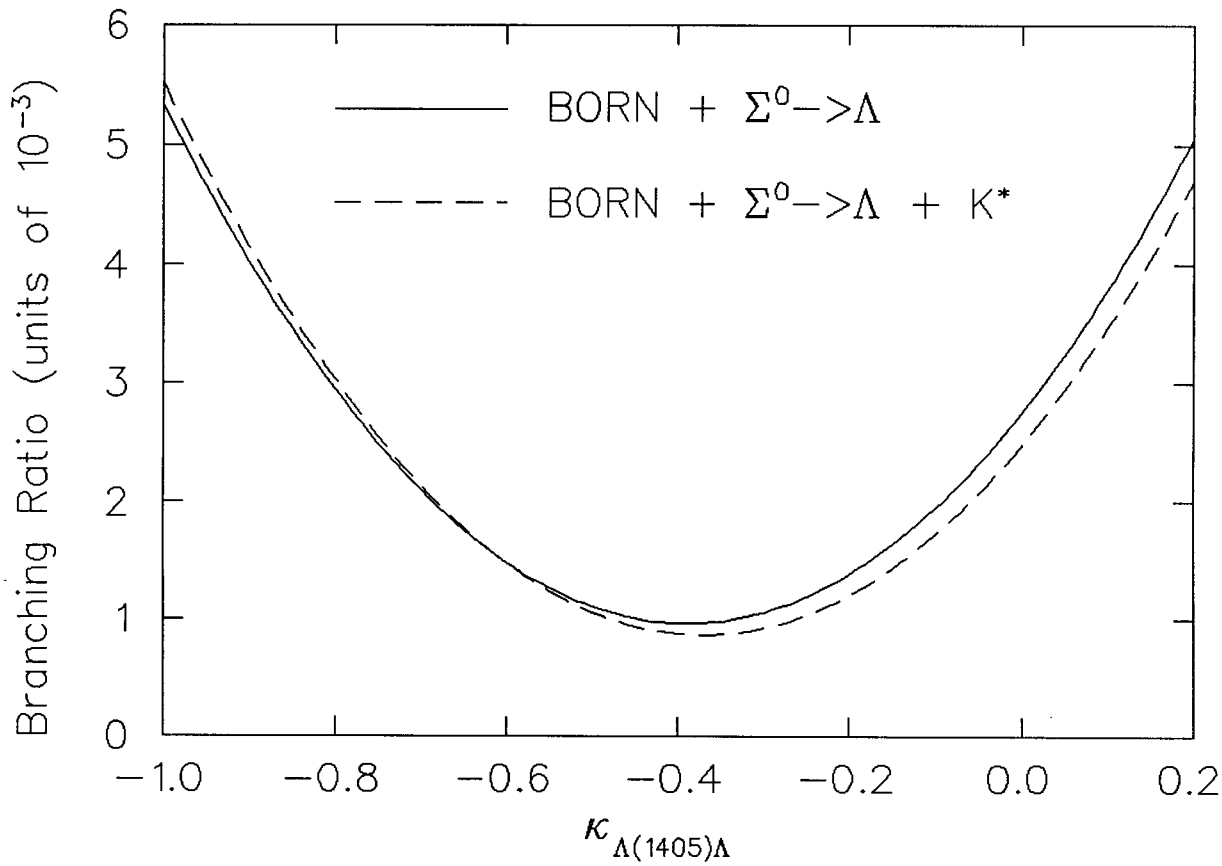

Figure 5.2: PV branching fractions for $K^- p \to \Lambda\gamma$

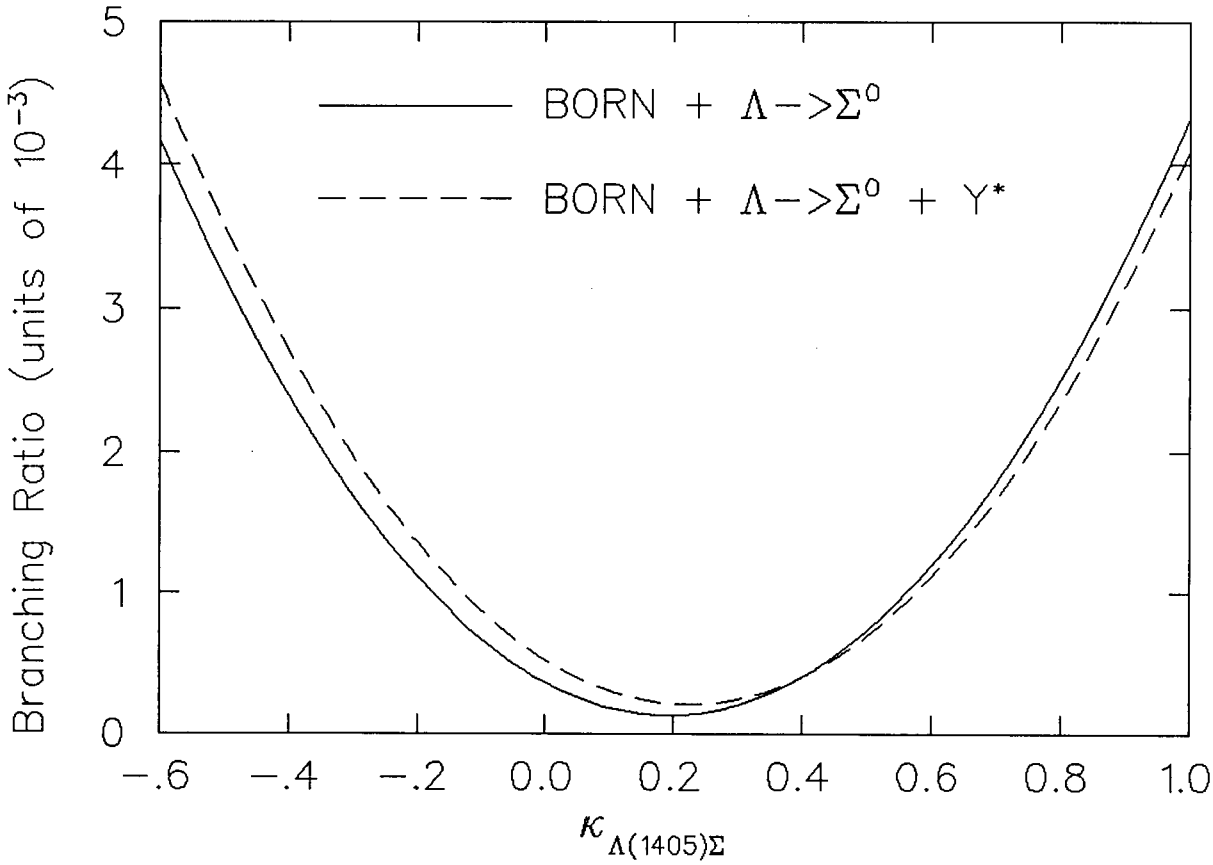

Figure 5.3: PS branching fractions for $K^- p \to \Sigma^0 \gamma$

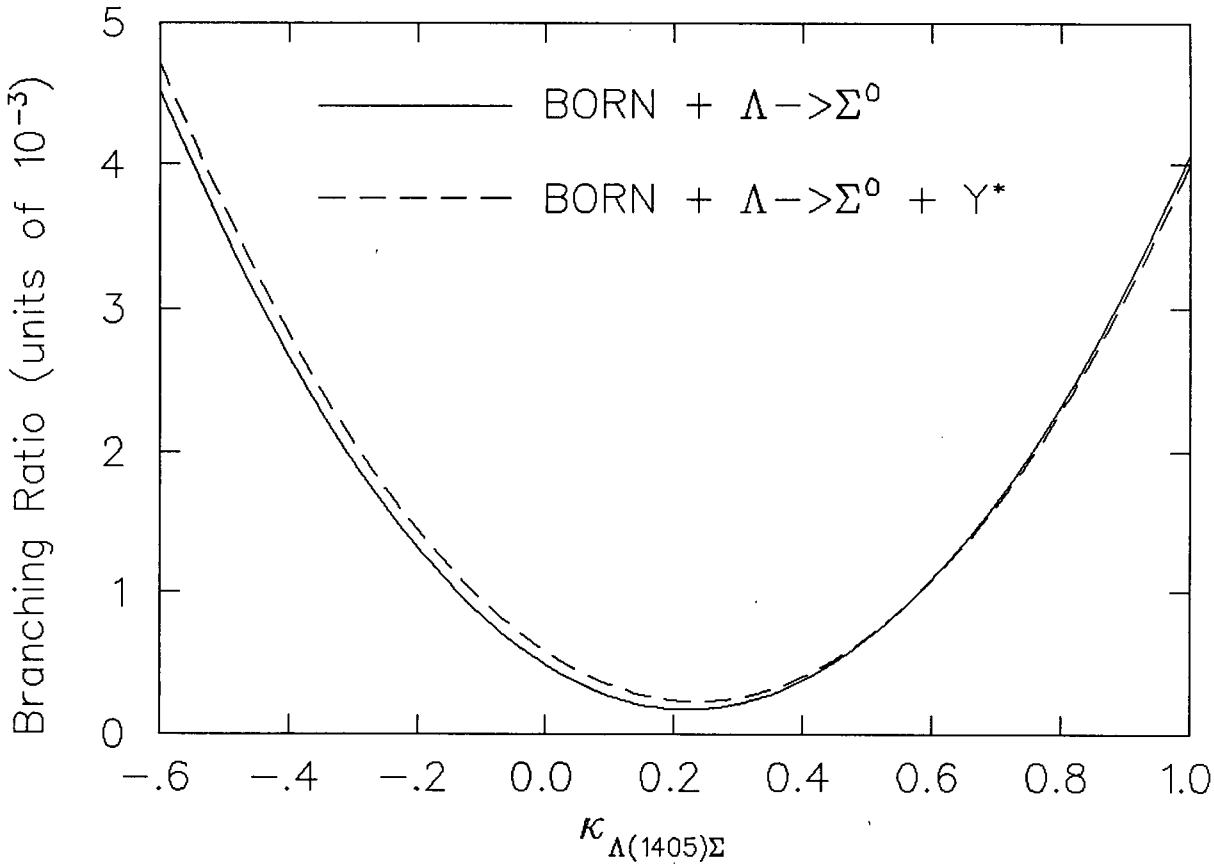

Figure 5.4: PV branching fractions for $K^- p \to \Sigma^0 \gamma$

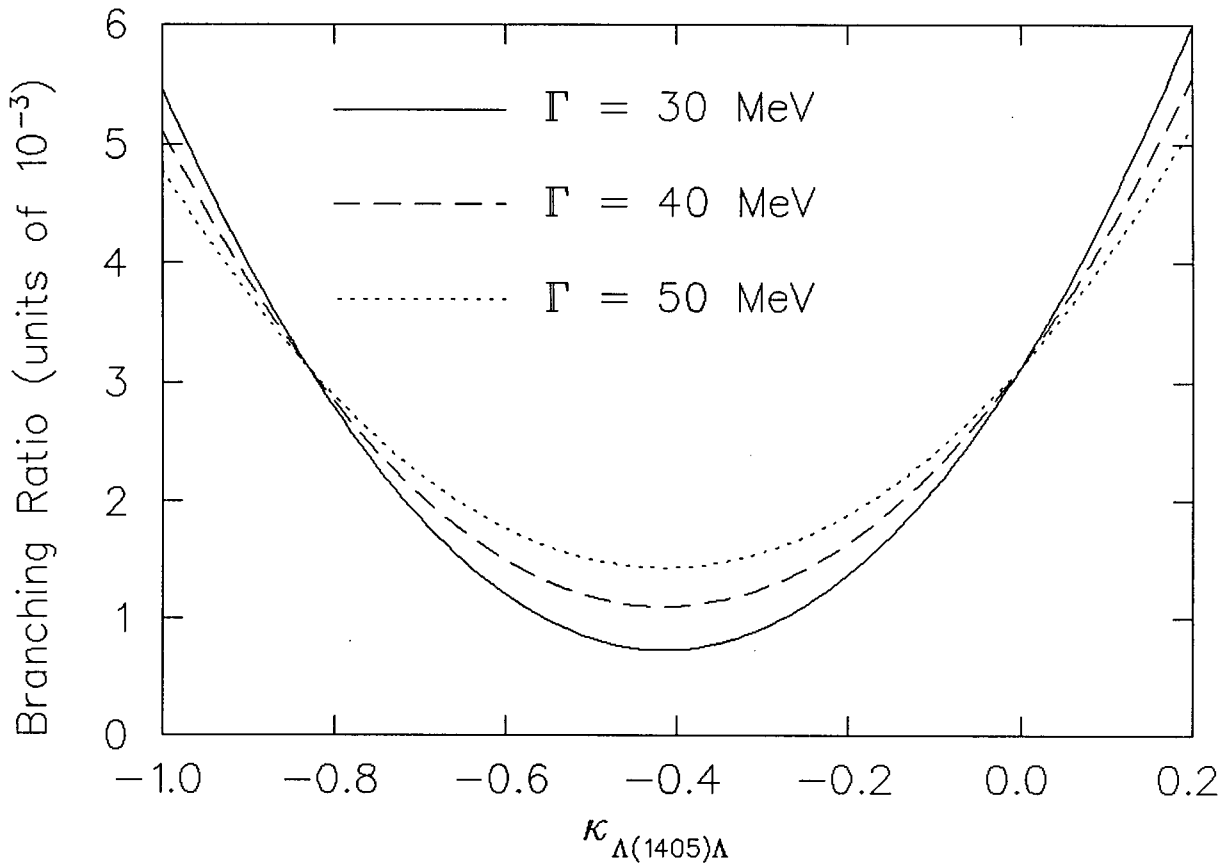

Figure 5.5: $K^- p \to \Lambda\gamma$ dependence on $\Gamma_{\Lambda(1405)}$

Chapter 6

COMPARISONS WITH OTHER MODELS

First consider the calculation of Burkhardt, Lowe and Rosenthal[13]. This is a pole model calculation done in the same spirit as the the one described here. It uses PS couplings only, but contains many of the intermediate resonances we considered. Our calculations do not, however, reproduce their results. The rate relation quoted in reference 13 has an extra, and erroneous, factor of m_K/m_p as compared to that given in equation (2.1) which was obtained from the rules of Bjorken and Drell[19], and which seems to agree with the analogous expressions used in other capture processes, e.g. muon capture. This is apparently a typographical error. The process of comparison was complicated by the fact that explicit definitions of vertex factors or matrix elements analogous to our equation (3.1) were not given in reference 13, so that we could not compare at an analytic level.

Our comparisons were aided by J. Lowe who supplied a copy of the Fortran code used in the calculations of reference 13. The erroneous phase space factor was not contained in this code. From the relations in his code, it appears that the rate calculations of reference 13 utilized two-component amplitudes analogous to our equation (3.22).

The major difference between our calculation and the calculation of reference 13 seems to be a consistent difference of sign for all of the magnetic couplings relative to the proton charge coupling. This sign difference can arise if one is not careful to

distinguish between incoming and outgoing photons. For outgoing photons, the vertex relation in equation 10.88 of reference 19 leads to the vertex factors in equations (3.2) to (3.6). When reduced to a two-component form, as in equation (3.29), the Born terms contain a factor $1 + \kappa_p + \kappa_\Lambda$ which agrees with the standard Blomqvist-Laget[34] operator for radiative pion capture and photoproduction. However, the code supplied by Lowe contains the factor $1 - \kappa_p - \kappa_\Lambda$ with similar sign changes for all of the other magnetic couplings. This conflicts with Blomqvist-Laget[34] and Dressler[20], and is erroneous. If these signs are reversed in Lowe's code and allowances are made for the magnitudes of our couplings, then Lowe's code can reproduce our results, thus giving added confidence in the correctness of the other aspects of both calculations. Unfortunately, the interference between charge and magnetic terms is quite large, and so this sign change produces a large change in the branching fractions. Consequently, the results of reference 13 are quite different from those we have obtained.

In reference 13, the contribution from the $N(1690)$, which is equivalent to our $N(1650)$, and the $N(1710)$ contributions were considered. However, only crude estimates were taken for their couplings. The strong $KN(1650)\Lambda$ and $KN(1710)\Lambda$ couplings were taken to be equal to $g_{Kp\Lambda}$. In addition, the transition moments were approximated by the Dirac static proton magnetic moment scaled by the ratio m_p/m_{N^*}. In comparison, our strong and electromagnetic couplings are much smaller, leading to an essentially negligible contribution from the N^* resonances above the ΛK threshold.

Our calculation validates the neglect of higher Y^* resonances in the $K^-p \to \Lambda\gamma$ calculation of reference 13. However, we find a small but non-negligible contribution from the $K^*(892)$, in contrast to the negligible contribution found in reference 13. The K^* couplings quoted in Table I of reference 13 are denoted *SU(3) values*. As described in Chapter 4, though, SU(3) alone is not enough to determine these couplings.

Two other calculations of the process $K^-p \to Y\gamma$, one in the NRQM[12] and one in the CBM[11], also obtain branching ratios in fair agreement with experiment. As

these involve rather different physics both from each other and from the calculation we have described here, it is of interest to compare and contrast these calculations to try to understand the important features which are responsible for the result in each case.

Consider first the NRQM calculation of reference 12, which is in principle a rather attractive approach. The NRQM involves a number of assumptions but does correlate a large amount of data and does a good job of describing the spectroscopy of a very large number of states. For the present process, one can calculate the vertex functions purely in terms of parameters fixed from the fits to masses and decays. Thus the result for the branching ratio is firmly predicted and can be compared directly to data.

When one looks in detail, however, there is quite a difference between the physics incorporated in this model and that in our calculation. This difference can be traced to a quite different choice of contributing diagrams, which we now discuss.

The NRQM calculation of reference 12 starts from the framework of time-ordered perturbation theory, which effectively separates the Feynman diagrams into separate parts involving positive and negative frequency propagation. The positive frequency parts correspond to the usual non-relativistic theory, whereas the negative frequency parts represent the so-called Z-graphs. In reference 12 all these Z-graphs are neglected, as is the full contribution of the Born graphs, figs. 1(a-c) and the transition term fig. 1d. The entire contribution then comes from the positive frequency parts of diagrams such as fig. 2a involving a $\frac{1}{2}^-$ exchange in the s-channel, plus some rather small quark exchange corrections, which cannot easily by related to any of the diagrams we have used. The major exchange is the $\Lambda(1405)$, but also included are the well established resonances $\Lambda(1670)$, $\Lambda(1800)$, and $\Sigma(1750)$ plus two other resonances, $\Sigma(1620)$ and $\Sigma(1810)$, which have not been seen experimentally with much confidence.

Within the NRQM, the $\Lambda(1405)$ contribution dominates and taken alone gives a branching ratio of 2.9×10^{-3}. In contrast, with the present model based on Feynman graphs, for $\kappa_{\Lambda(1405)\Lambda} = 0.0 \pm 0.1$ the $\Lambda(1405)$ contribution is quite small and the Born

graphs of fig. 1 dominate, whereas for $\kappa_{\Lambda(1405)\Lambda} = -0.8 \pm 0.1$, the $\Lambda(1405)$ contribution is very large and the result is a consequence of a strong destructive interference between the $\Lambda(1405)$ and Born graphs.

The arguments used in reference 12, for neglecting all but the positive frequency part of the $\Lambda(1405)$ and similar exchanges, are several. Parity requires that s-channel resonances be $\frac{1}{2}^-$ when the initial kaon and nucleon are at rest in an s-state. This rules out the positive frequency parts of figs. 1c and 1d which involve Λ and Σ exchange. However, the Feynman graph approach also conserves parity, and one can explicitly show that these positive frequency contributions do vanish in that approach also. Thus the parity argument provides physical insight, but does not distinguish between the two approaches.

The remaining graphs are neglected in reference 12, based on arguments originating in the composite nature of the hadrons in the quark picture. For the negative frequency part or Z-graphs, it is argued that form factors will suppress their contribution. For the other graphs such as figs. 1a and 1b, the claim is that the interaction is short ranged involving overlapping hadrons, and thus that the description of hadrons as point particles in this region is not appropriate.

These arguments have a certain attractiveness in the context of the NRQM. Note, however, that the second argument really does not imply that contributions from the diagrams of figs. 1a and 1b are small and should be neglected, but instead that the calculation would have to be done in some more complicated way.

These arguments however present a number of difficulties. In the first place there is a long history of describing medium energy reactions successfully via a series of Feynman diagrams which include both positive and negative frequency parts. Perhaps the most relevant example is $\pi^- p \to n\gamma$, which is the direct analogue of the process considered here. In this case the Feynman graph approach gives reasonable agreement with data and, at threshold, the Born terms are dominant[34].

The Z-graphs are also known to be important in other contexts, notably in $\gamma d \to pn$, where the importance of such graphs at threshold was a classic manifestation of meson exchange corrections[35], and in a variety of other situations, particularly few body electromagnetic reactions at the higher momentum transfers[36], which are more relevant to the situation here. There has also been at least one explicit calculation in a strong interaction process[37], pion-nucleon scattering, which finds that neglect of the Z-graphs gives incorrect results.

One can also gain insight into this problem by comparing PS and PV couplings as we have done. As is well known, one effect of the PV coupling is to suppress the pair terms. Thus, although we get roughly similar branching ratios with PS and PV couplings, in the PV case a major contribution comes from the contact term necessary for gauge invariance and, unlike the PS case, relatively little from the Z-graphs. Thus, neglect of these negative frequency contributions will give quite different results depending on the choice of basic coupling.

There is a further difficulty arising from the gauge invariance requirement, which enters into the choice of diagrams and the interaction appropriate for each diagram. In the Feynman graph approach, the $\frac{1}{2}^-$ exchanges, such as the $\Lambda(1405)$, involve a magnetic type coupling and thus are gauge invariant by themselves separately for positive and negative frequency components. However, in the NRQM of reference 12 this amplitude is generated by taking the product of matrix elements of single quark operators corresponding to electromagnetic and strong interactions. For a gauge invariant result however, even at the level of free quarks in the intermediate state, one must include the operators which will generate all of the quark level Born graphs, i.e. the quark analog of the Blomqvist-Laget[34] operator for pion-photoproduction, which contains for example extra contact type terms. In addition, for bound quarks, further terms, depending on the binding, will be necessary for full gauge invariance. This latter point is a well known, but not completely solved, problem which arises for example in attempts to define a

conserved current for the two[38] or three[39] nucleon system.

For the Born terms in the Feynman graph approach, if any are included, all must be, as they are not individually gauge invariant. Thus, neglecting the Z-graph parts of the Born terms leads to a non-gauge invariant result. This is in fact consistent with the non-relativistic approach with only positive frequency components, where to get gauge invariance one must add contact terms of the same general type as those which would be generated in a PS theory from the Z-graphs in a two component reduction of the Feynman graphs. It is also consistent with the discussion above of the current operator at the quark level.

Aside from the question of gauge invariance, one would usually expect that the Born graphs should be included, as they are normally important and are graphs which are included in simple non-relativistic calculations. For example, the very successful Bonn nucleon-nucleon potential is based on a sum of the positive frequency parts of such simple graphs[40]. In our calculation, these Born graphs give the dominant contribution, apart from possibly the $\Lambda(1405)$, though the positive frequency pieces are relatively small compared to the negative frequency ones, in the case of PS coupling or to the contact term for PV coupling. In the NRQM, it should, in principle, be possible to calculate these extra Born terms, as has been done for pion photoproduction[41]. The calculation of reference 41 indicates that, for pion photoproduction, the Born terms alone reproduce the data fairly well. It would be very interesting to see a detailed calculation of this contribution in the NRQM.

It is an interesting question whether or not one can distinguish between these two approaches empirically, rather than via arguments as above. As long as there is only one piece of experimental information, the branching ratio, the answer is probably not. The NRQM, together with the particular assumptions of reference 12, makes a specific prediction for $K^- p \to \Lambda\gamma$ and $K^- p \to \Sigma^0\gamma$ branching ratios, which can be tested and in principle ruled out. The approach here, however, depends on the unknown $\Lambda(1405)$

couplings which can be adjusted to fit the data, and so cannot be ruled out without additional experimental information. It might also be possible to distinguish the two sets of assumptions by looking at the in-flight process, as one might expect the momentum dependence of the various diagrams to be different.

Detailed comparisons with the CBM calculation of reference 11 are more difficult, as it is a very different approach to the problem. The most obvious difference is the inclusion of K^-p rescattering and coupling to intermediate $\Sigma\pi$ channels. In this model, the $\Lambda(1405)$ is manifested as a $\overline{K}N$ bound state rather than the three quark state considered in reference 12. The lowest mass $\frac{1}{2}^-$ state is then taken to be the $\Lambda(1630)$ and treated as an SU(3) singlet, as opposed to the more complicated structure suggested in the NRQM calculation. No higher mass Y^* resonances are included.

For the $\Lambda\gamma$ and $\Sigma^0\gamma$ branching ratios, the CBM predicts values of 1.9×10^{-3} and 1.5×10^{-3} respectively. While these branching ratios are lower than the NRQM values, both models predict a $\Lambda\gamma/\Sigma^0\gamma$ ratio near 1.3. In addition, this $\Lambda\gamma/\Sigma^0\gamma$ ratio is shown to be insensitive to reasonable changes in the CBM parameters and is thus a firm prediction of the model. Although the CBM uses a PV strong coupling, a comparison with our PV calculation is complicated by the fact that only the numerical CBM amplitudes are given in reference 11. The ratio of $K^-p \to \Lambda\gamma$ and $K^-p \to \Sigma^0\gamma$ contact term amplitudes in Table 1 of reference 11 is, up to a relative sign, just what one would expect for $K^-p\Lambda$ and $K^-p\Sigma^0$ strong couplings obeying SU(6) symmetry. The ratio of our contact term amplitudes is determined by the $K^-p\Lambda$ and $K^-p\Sigma$ couplings of Martin and Antolin which are not related in magnitude by SU(6) symmetry. As described in Chapter 4, the relative sign of the above couplings was determined by SU(6) symmetry. However, unlike the amplitudes listed in table 1 of reference 11, our contact term amplitudes have a different sign for the $\Lambda\gamma$ and $\Sigma^0\gamma$ reactions. This may, perhaps, be due to a difference in sign conventions. There also appears to be a typographical error in Table 1 of reference 11, as the individual contributions to the imaginary part of the $\Lambda\gamma$ amplitude do not

sum to the total. Thus, some care is required in making a detailed comparison.

It now appears[42] that reference 11 also contains a computational error. The preliminary indication is that the CBM calculation actually predicts a $\Sigma^0\gamma$ branching fraction in excess of the $\Lambda\gamma$ value.

Since only the dominant contact term is retained from the full set of PV Born diagrams, this calculation is clearly not gauge invariant. Since we find that the remaining PV Born terms are not negligible in our calculation, perhaps they should also be estimated within the CBM. This has recently been done in a chiral bag model[43] for the analogous pion photoproduction reaction, in which these terms are much smaller.

Chapter 7

GENERAL FORMALISM FOR $K^-d \to \Lambda n\gamma$

7.1 Introduction

The $K^-d \to \Lambda n\gamma$ reaction is also attracting renewed interest, mainly because of the possibility of deducing a value for the $\Lambda - n$ scattering length from the γ-spectrum. As mentioned in the Introduction, this sensitivity of the γ-spectrum to final state interactions has been exploited in the analogous non-strange reaction, $\pi^-d \to nn\gamma$. There, the $n - n$ scattering length was determined from the high energy end of the γ-spectrum of the $\pi^-d \to nn\gamma$ reaction. As the high energy endpoint of that γ-spectrum corresponds to a geometry in which the two neutrons are emitted anti-parallel to the photon, the $n - n$ final state interaction is enhanced. In addition, as the relative $n - n$ momentum is small near the γ-spectrum endpoint, an effective range approximation is possible, giving a simple relation between the final state wavefunction and scattering length.

It is hoped that similar techniques will apply to the $K^-d \to \Lambda n\gamma$ reaction. Information on the $\Lambda - n$ scattering length is currently due mainly to bubble-chamber and hypernuclear data. Dover and Walker[44] have extensively reviewed the attempts to learn about the ΛN interaction through (K^-, π^-) scattering off nuclei. Clearly this is not an unambiguous procedure as the ΛN interaction takes place in the nuclear medium. Nagels, Rijken and de Swart have carried out a long program[29,45,46] of fitting $\Sigma N \to \Sigma N$, $\Sigma N \to \Lambda N$ and $\Lambda p \to \Lambda p$ bubble-chamber data[47-50] within a

boson-exchange-potential model. Although no $\Lambda n \rightarrow \Lambda n$ bubble-chamber data exists, as both particles are neutral, $\Lambda - n$ scattering information has been obtained indirectly from the boson exchange potential model and the couplings fit to the abovementioned reactions, for which there exist data.

The $K^- d \rightarrow \Lambda n \gamma$ reaction thus promises to provide an independent and relatively direct check on previous determinations of the low energy $\Lambda - n$ scattering parameters. The $K^- d \rightarrow \Lambda n \gamma$ reaction is of particular interest now, due to a recent measurement of its γ-spectrum in a Brookhaven experiment[3]. As this is the first detailed measurement of the $K^- d \rightarrow \Lambda n \gamma$ γ-spectrum, it is important to reconsider the $K^- d \rightarrow \Lambda n \gamma$ calculation.

In this chapter, we will present a general formalism for the $K^- d \rightarrow \Lambda n \gamma$ impulse-approximation calculation. The $K^- d \rightarrow \Lambda n \gamma$ amplitude and differential-rate relations will be given in terms of the $K^- N \rightarrow Y \gamma$ and $Y' N' \rightarrow Y N$ amplitudes. As has been done in the previous[6,9] $K^- d \rightarrow \Lambda n \gamma$ calculations, we will factor the kaon atomic wavefunction from our amplitude.

The assumption of a constant kaonic wavefunction is clearly only an approximation to the true kaonic wavefunction. The effects of a strong $\pi^- - d$ interaction on the pionic wavefunction has been estimated[51] in calculations of the analogous $\pi^- d \rightarrow nn\gamma$ reaction. There it was found to add an uncertainty of approximately 0.2 fm to the $n - n$ scattering length determination. Estimates given in reference 6 suggest that the uncertainty introduced by the strong $K^- - d$ interaction will add an uncertainty of about 0.2 fm to the $\Lambda - n$ scattering length as well.

It should be mentioned that the derivation of a precise kaonic-atom wavefunction is a difficult problem. The difficulty lies in the large number of channels to which $K^- p$ can couple, and is manifested in the notoriously-difficult-to-fit $K^- p$ atom 1s level energy shift. Considerable progress has, however, recently[52] been made toward an understanding of this problem.

The effect of a momentum dependent transition operator will be tested in Chapters 8 and 10, as this contribution has not yet been considered for the $K^-d \rightarrow \Lambda n\gamma$ process. A momentum-dependent operator has been used in a previous $\pi^-d \rightarrow nn\gamma$ rate calculation[53]. However, the effect of momentum dependence on a determination of the $n-n$ scattering length was not discussed.

7.2 The Differential Rate Relation

As described in Section 7.1, in the following we will develop the general formalism for an impulse- approximation calculation of the $K^-d \rightarrow \Lambda n\gamma$ γ-spectrum, using a momentum-independent transition operator. Alterations due to the inclusion of momentum dependence in the transition operator will be considered in the next chapter.

In this section, we will derive the invariant amplitude and the general differential rate relation accounting for $\Lambda n \rightarrow \Lambda n$ final state scattering, as well as contributions from final state $\Sigma N \rightarrow \Lambda n$ conversion processes.

The transition amplitude for $K^-d \rightarrow \Lambda n\gamma$ is given by

$$M = \sum_{j=1}^{3} < \Psi_j^{(f)} \mid \hat{T}_j \mid \Psi^{(i)} >, \tag{7.1}$$

where the subscript j in equation (7.1) labels the three contributing processes illustrated in fig. 7.1. The $j = 1$ label denotes the final state $\Lambda n \rightarrow \Lambda n$ scattering mechanism of fig. 7.1a, while $j = 2, 3$ denote respectively the $\Sigma^0 n \rightarrow \Lambda n$ and $\Sigma^- p \rightarrow \Lambda n$ conversion reactions depicted in figures 7.1b and 7.1c.

The initial state wavefunction, $\Psi^{(i)}$, contains the deuteron wavefunction and an S-state atomic wavefunction for the kaon:

$$\Psi^{(i)} = \phi_K(0)\Phi_d(\vec{r}). \tag{7.2}$$

As mentioned in Section 7.1 , the kaon atomic wavefunction has been approximated as a constant over the range of strong interactions. The deuteron state[54] is represented by

$$\begin{aligned} < \vec{r} \mid \Phi_d > &= \frac{u(r)}{r} Y_{00}(\Omega_r) \mid 1M > \\ &+ \frac{w(r)}{r} \sum_{m\mu} Y_{2m}(\Omega_r) \mid 1\mu >< 2m1\mu \mid 211M >, \end{aligned} \tag{7.3}$$

where $u(r)$ and $w(r)$ are respectively the S- and D-state deuteron radial wavefunctions, $\mid 1\mu >$ is a spin 1 state constructed from the spin 1/2 proton and neutron spinors

$$\mid 1\mu >= \sum_{m_1 m_2} \mid \frac{1}{2}m_1 > \mid \frac{1}{2}m_2 >< \frac{1}{2}m_1 \frac{1}{2}m_2 \mid \frac{1}{2}\frac{1}{2}1\mu >, \tag{7.4}$$

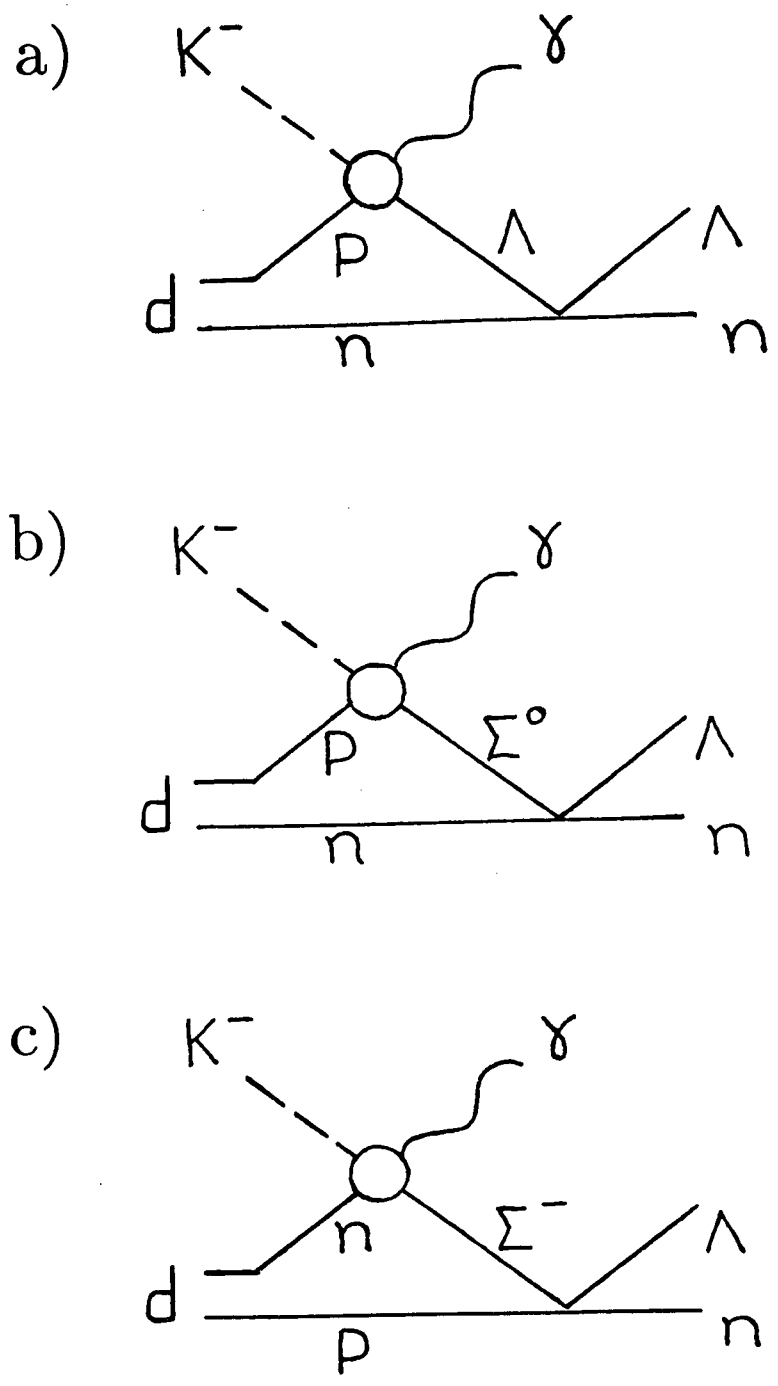

Figure 7.1: Impulse approximation contributions to $K^- d \to \Lambda n \gamma$

and the Y_{lm} functions are spherical harmonics. The variable $\vec{r}$ is the proton - neutron relative coordinate. The center of mass wavefunction is not explicitly included here as our calculation will be performed in the deuteron rest frame.

In equations (7.3) and (7.4), $< s_1 m_1 s_2 m_2 \mid s_1 s_2 SM >$ is a Clebsch-Gordon coefficient coupling the spins s_1 and s_2 to a total spin S. The usual Condon and Shortley sign convention sign convention has been followed in assigning numerical values to the Clebsch-Gordon coefficients.

The transition operators, $\hat{T}_j$, in equation (7.1) are

$$\hat{T}_1 = F_1 e^{-i\vec{k}\cdot\vec{r}_p}\delta(\vec{r}_p - \vec{r}_\Lambda)\delta(\vec{r}_{n_i} - \vec{r}_{n_f})\vec{\sigma}_1 \cdot \vec{\epsilon}, \tag{7.5}$$

$$\hat{T}_2 = F_2 e^{-i\vec{k}\cdot\vec{r}_p}\delta(\vec{r}_p - \vec{r}_\Lambda)\delta(\vec{r}_{n_i} - \vec{r}_{n_f})\vec{\sigma}_1 \cdot \vec{\epsilon}, \tag{7.6}$$

$$\hat{T}_3 = F_3 e^{-i\vec{k}\cdot\vec{r}_{n_i}}\delta(\vec{r}_{n_i} - \vec{r}_\Lambda)\delta(\vec{r}_p - \vec{r}_{n_f})\vec{\sigma}_2 \cdot \vec{\epsilon}, \tag{7.7}$$

where $\vec{\sigma}_1$ ($\vec{\sigma}_2$) is the proton (neutron) spin and n_i (n_f) labels the initial (final) neutron coordinate. The factors F_i can be deduced from the two-component reduction of the $K^- N \to Y\gamma$ amplitudes in Section 3.2 with

$$F_1 \equiv F(K^- p \to \Lambda\gamma), \tag{7.8}$$

$$F_2 \equiv F(K^- p \to \Sigma^0\gamma), \tag{7.9}$$

$$F_3 \equiv F(K^- n \to \Sigma^-\gamma), \tag{7.10}$$

taken as momentum-independent and derived from the at-rest capture reactions.

The final state YN wavefunction is

$$\Psi_j^{(f)} = \frac{1}{(2\pi)^{3/2}} e^{i(\vec{p}_\Lambda + \vec{p}_n)\cdot\vec{R}}\psi_j(\vec{r}). \tag{7.11}$$

In the absence of spin, we have the usual relation for an asymptotic scattering wave-function[55]:

$$\psi_j = \frac{1}{(2\pi)^{3/2}} \left\{ \delta_{j1} e^{i\vec{p}\cdot\vec{r}} + f_j(\cos\theta) \frac{e^{ipr}}{r} \right\}, \tag{7.12}$$

where $\cos\theta = \hat{r}\cdot\hat{p}$, p is the magnitude of $\vec{p}$, and the following separation of relative and center of mass variables is implicit:

$$\vec{R} = \frac{m_\Lambda \vec{r}_\Lambda + m_n \vec{r}_n}{m_\Lambda + m_n}, \tag{7.13}$$

$$\vec{r} = \vec{r}_\Lambda - \vec{r}_n, \tag{7.14}$$

$$\vec{P} = \vec{p}_\Lambda + \vec{p}_n, \tag{7.15}$$

$$\vec{p} = \frac{m_n \vec{p}_\Lambda - m_\Lambda \vec{p}_n}{m_n + m_\Lambda}, \tag{7.16}$$

where the subscript (n) now refers to the final neutron variable. The scattering amplitude f_j is then the amplitude for the j^{th} type of final state interaction

$$f_1 = f_1(\Lambda n \to \Lambda n), \tag{7.17}$$

$$f_2 = f_2(\Sigma^0 n \to \Lambda n), \tag{7.18}$$

$$f_3 = f_3(\Sigma^- p \to \Lambda n). \tag{7.19}$$

Including spin, we have

$$\psi_j(\vec{r}) = \frac{1}{(2\pi)^{3/2}} \left\{ \delta_{j1} e^{i\vec{p}\cdot\vec{r}} \mid Sm > + \left(f_j^s \mid 00 > + f_j^t \mid 1m > \right) \frac{e^{ipr}}{r} \right\}, \tag{7.20}$$

where the superscript s (t) labels a spin singlet (triplet) scattering amplitude.

It is useful to write equation (7.20) in the form

$$\psi_j(\vec{r}) = \left\{ \delta_{j1} e^{i\vec{p}\cdot\vec{r}} + \left(f_j^s \hat{a}_s + f_j^t \hat{a}_t \right) \frac{e^{ipr}}{r} \right\} \chi_1^{(f)} \chi_2^{(f)}, \tag{7.21}$$

where $\chi_1^{(f)}$ and $\chi_2^{(f)}$ are respectively the final state lambda and neutron spinors, and we have used the spin singlet ($\hat{a}_s$) and triplet ($\hat{a}_t$) projection operators[56]

$$\hat{a}_s = \frac{1}{4}(1 - \vec{\sigma}_1 \cdot \vec{\sigma}_2), \tag{7.22}$$

and

$$\hat{a}_t = \frac{1}{4}(3 + \vec{\sigma}_1 \cdot \vec{\sigma}_2), \tag{7.23}$$

in order to project out the desired spin states.

The $K^- d \to \Lambda n \gamma$ amplitude in equation (7.1) can be split into pieces depending on the S- and D-state deuteron wavefunctions

$$M = M_S + M_D. \tag{7.24}$$

The spin part of the S-state amplitude is then

$$M_S = \chi_1^{(f)\dagger} \chi_2^{(f)\dagger} \left\{ A_1 F_1 \vec{\sigma}_1 \cdot \vec{\epsilon} + B_1 \sum_{j=1}^{3} \left(f_j^s \hat{a}_s + f_j^t \hat{a}_t \right)^* F_j (\vec{\sigma} \cdot \vec{\epsilon})_j \right\} \hat{a}_t \chi_1^{(i)} \chi_2^{(i)}, \tag{7.25}$$

where A_1 and B_1 are spin independent factors, and $(\vec{\sigma} \cdot \vec{\epsilon})_j$ is equal to $\vec{\sigma}_1 \cdot \vec{\epsilon}$ for $j = 1, 2$ and is equal to $\vec{\sigma}_2 \cdot \vec{\epsilon}$ for $j = 3$. We have written the deuteron spin wavefunction in the form $\hat{a}_t \chi_1^{(i)} \chi_2^{(i)}$, with $\chi_1^{(i)}$ ($\chi_2^{(i)}$) being the initial state proton (neutron) spinor. Equation (7.25) can be reduced to a more manageable form if one commutes the final state spin projection operators past the transition operator using

$$(\vec{\sigma}_1 \cdot \vec{\sigma}_2)\, \vec{\sigma}_1 \cdot \vec{\epsilon} = -\vec{\sigma}_1 \cdot \epsilon\, (\vec{\sigma}_1 \cdot \vec{\sigma}_2) + 2\vec{\sigma}_2 \cdot \vec{\epsilon}, \tag{7.26}$$

and the properties of projection operators

$$\hat{a}_t \hat{a}_t = \hat{a}_t, \tag{7.27}$$

and

$$\hat{a}_s \hat{a}_t = 0. \tag{7.28}$$

The result is

$$M_S = \chi_1^{(f)\dagger}\chi_2^{(f)\dagger}\left\{A_1F_1\vec{\sigma}_1\cdot\vec{\epsilon}+\frac{1}{2}B_1\left(F_+\vec{\sigma}_1\cdot\vec{\epsilon}-F_-\vec{\sigma}_2\cdot\vec{\epsilon}\right)\right\}\hat{a}_t\chi_1^{(i)}\chi_2^{(i)}, \tag{7.29}$$

where we have defined

$$F_\pm = F_1(f_1^s \pm f_1^t)^* + F_2(f_2^s \pm f_2^t)^* - F_3(f_3^s \mp f_3^t)^*. \tag{7.30}$$

The plane wave factors in M, coming from equations (7.5) to (7.7), (7.11) and (7.12), can be regrouped using the relations in equations (7.13) to (7.16). Writing these products in terms of the relative and center of mass coordinates, we have

$$e^{-i\vec{P}\cdot\vec{R}}\ e^{-i\vec{k}\cdot\vec{r}_\Lambda}\ e^{-i\vec{p}\cdot\vec{r}} = e^{-i(\vec{p}_\Lambda+\vec{p}_n+\vec{k})\cdot\vec{R}}\ e^{i\vec{p}_n\cdot\vec{r}}, \tag{7.31}$$

and

$$e^{-i\vec{P}\cdot\vec{R}}\ e^{-i\vec{k}\cdot\vec{r}_\Lambda}\frac{e^{-ipr}}{r} = e^{-i(\vec{p}_\Lambda+\vec{p}_n+\vec{k})\cdot\vec{R}}\ e^{-i\vec{q}\cdot\vec{r}}\ \frac{e^{-ipr}}{r}, \tag{7.32}$$

where we have defined

$$\vec{q} = \frac{m_n\vec{k}}{(m_n+m_\Lambda)}. \tag{7.33}$$

Integration over the center of mass variable $\vec{R}$ then leads to a $\delta(\vec{p}_\Lambda+\vec{p}_n+\vec{k})$ factor, enforcing momentum conservation. The remaining plane wave functions of $\vec{r}$ are decomposed using[57]

$$e^{i\vec{p}\cdot\vec{r}} = 4\pi\sum_{l=0}^{\infty}\sum_{m=-l}^{l} i^l j_l(pr)Y_{lm}^*(\Omega_p)Y_{lm}(\Omega_r). \tag{7.34}$$

The angular integral corresponding to the amplitude M_S is

$$\int d\Omega_r\ Y_{lm}^*(\Omega_r)Y_{00}(\Omega_r) = \delta_{l0}\delta_{m0}, \tag{7.35}$$

where the Y_{00} factor has come from the S-state deuteron wavefunction. The $\delta_{l0}\delta_{m0}$ factor selects the $l=0$ spherical Bessel function from the sum in equation (7.34) and converts the numerical factor $4\pi i^l Y_{lm}(\Omega_p)$ to $\sqrt{4\pi}$.

We are then left with the radial integrals

$$U_0 = \int_0^\infty dr\ ru(r)j_0(p_nr), \tag{7.36}$$

and

$$V_0 = \int_0^\infty dr\ u(r) j_0(qr) e^{-ipr}, \tag{7.37}$$

which have been evaluated in Appendix B, for common parametrizations of the deuteron wavefunction. Thus, the spin independent factors of equation (7.25) are given by

$$A_1 = \sqrt{4\pi}\phi_K(0) U_0, \tag{7.38}$$

and

$$B_1 = \sqrt{4\pi}\phi_K(0) V_0, \tag{7.39}$$

and the final result for M_S is then

$$M_S = \sqrt{4\pi}\phi_K(0) \chi_1^{(f)\dagger} \chi_2^{(f)\dagger} \left\{ U_0 F_1 \vec{\sigma}_1 \cdot \vec{\epsilon} + \frac{1}{2} V_0 \left(F_+ \vec{\sigma}_1 \cdot \vec{\epsilon} - F_- \vec{\sigma}_2 \cdot \vec{\epsilon} \right) \right\} \hat{a}_t \chi_1^{(i)} \chi_2^{(i)}. \tag{7.40}$$

Next, consider the amplitude M_D due to the D-state component of the deuteron wavefunction. The spin matrix elements can be simplified, as was done for M_S, to yield

$$M_D = < S' m'_S \mid A_2 F_1 \vec{\sigma}_1 \cdot \vec{\epsilon} + \frac{1}{2} B_2 \left(F_+ \vec{\sigma}_1 \cdot \vec{\epsilon} - F_- \vec{\sigma}_2 \cdot \vec{\epsilon} \right) \mid 1\mu >, \tag{7.41}$$

where A_2 and B_2 are spin independent factors.

Once again, the relations in equations (7.31), (7.32) and (7.34) are used to separate the radial and angular integrals. Here the angular integral is

$$\int d\Omega_r\ Y^*_{l'm'}(\Omega_r) Y_{2m}(\Omega_r) = \delta_{l2}\delta_{m'm}, \tag{7.42}$$

which selects the $l = 2$ spherical Bessel function.

The required radial integrals are then

$$W_2 = \int_0^\infty dr\ r w(r) j_2(p_n r), \tag{7.43}$$

and

$$V_2 = \int_0^\infty dr\ w(r) j_2(qr) e^{-ipr}, \tag{7.44}$$

which are evaluated in Appendix B.

The remaining factors, coming from the plane wave decomposition and the Clebsch-Gordon coefficient in equation (7.3), are of the form

$$-4\pi \sum_{m\mu} Y_{2m}(\Omega_p) \mid 1\mu >< 2m1\mu \mid 211M >, \tag{7.45}$$

and can be written as

$$-\sqrt{\frac{\pi}{2}}\hat{S}_{12}(\hat{p}) \mid 1\mu >, \tag{7.46}$$

if we use the relation[54]

$$\hat{S}_{12}(\hat{r})Y_{00}(\Omega_r) \mid 1\mu >= \sqrt{8}\sum_{m\mu} Y_{2m}(\Omega_r) \mid 1\mu >< 2m1\mu \mid 211M >, \tag{7.47}$$

wherein $\hat{S}_{12}(\hat{r})$ is the usual tensor operator[58] defined by

$$\hat{S}_{12}(\hat{r}) = 3\vec{\sigma_1}\cdot\hat{r}\ \vec{\sigma_2}\cdot\hat{r} - \vec{\sigma_1}\cdot\vec{\sigma_2}. \tag{7.48}$$

Using the above relation, the spin independent factors defined in equation (7.41) are

$$A_2 = -\sqrt{\frac{\pi}{2}}\phi_K(0)W_2\hat{S}_{12}(\hat{p}_n), \tag{7.49}$$

and

$$B_2 = -\sqrt{\frac{\pi}{2}}\phi_K(0)V_2\hat{S}_{12}(\hat{q}). \tag{7.50}$$

Combining the above relations with equation (7.39), we have

$$\begin{aligned} M_D &= -\sqrt{\frac{\pi}{2}}\phi_K(0)\chi_1^{(f)\dagger}\chi_2^{(f)\dagger}\left\{W_2F_1\vec{\sigma}_1\cdot\vec{\epsilon}\hat{S}_{12}(\hat{p}_n)\right. \\ &+ \left.\frac{1}{2}V_2\left(F_+\vec{\sigma}_1\cdot\vec{\epsilon} - F_-\vec{\sigma}_2\cdot\vec{\epsilon}\right)\hat{S}_{12}(\hat{q})\right\}\hat{a}_t\chi_1^{(i)}\chi_2^{(i)}. \end{aligned} \tag{7.51}$$

The relations for M_S and M_D in equations (7.40) and (7.51) agree with those quoted in reference 6 thus giving added confidence in these results.

In the calculation of $\overline{\sum} \mid M \mid^2$ we calculate $\overline{\sum} \mid M_S + M_D \mid^2$ in order to isolate the S- and D-state contributions. A representative example of the calculational technique is given by the term

$$M_1 = \chi_1^{(f)\dagger}\chi_2^{(f)\dagger}W_2F_1\vec{\sigma}_1\cdot\vec{\epsilon}\hat{S}_{12}(\hat{p}_n)\hat{a}_t\chi_1^{(i)}\chi_2^{(i)}, \tag{7.52}$$

in the amplitude M_D. The sum over final and average over initial spins leads to

$$\overline{\sum_{spins}} \mid M_1 \mid^2 = \frac{1}{3}\sum_{\lambda} W_2^2 \mid F_1 \mid^2 Tr_1 Tr_2 \left(\vec{\sigma}_1 \cdot \vec{\epsilon}\hat{S}_{12}(\hat{p}_n)\hat{a}_t\hat{S}_{12}(\hat{p}_n)\vec{\sigma}_1 \cdot \vec{\epsilon}\right), \tag{7.53}$$

where Tr_i denotes a trace over σ matrices labeled i. Summing over photon polarizations (λ) and factoring out non-spin factors, we have

$$\begin{aligned}\overline{\sum_{spins}} \mid M_1 \mid^2 &= \frac{2}{3}W_2^2 \mid F_1 \mid^2 Tr_1 Tr_2 \left(\sigma_1^{(j)}\sigma_2^{(k)}\hat{a}_t\sigma_1^{(l)}\sigma_2^{(m)}\right) \\ &\cdot \quad [3(\hat{p}_n)_j(\hat{p}_n)_k - \delta_{jk}][3(\hat{p}_n)_l(\hat{p}_n)_m - \delta_{lm}].\end{aligned} \tag{7.54}$$

Through use of the relation

$$\sigma^{(l)}\sigma^{(m)} = \delta^{lm} + i\epsilon^{lmn}\sigma^{(n)}, \tag{7.55}$$

we can eliminate the σ factors in equation (7.54), utilizing the fact that the trace of a single σ-matrix is equal to zero. The final result, after some algebra, is then

$$\overline{\sum_{spins}} \mid M_1 \mid^2 = 12W_2^2 \mid F_1 \mid^2 . \tag{7.56}$$

For the total amplitude we have

$$\overline{\sum_{spins}} \mid M_S + M_D \mid^2 = \overline{\sum_{spins}} \mid M_S \mid^2 + 2Re\overline{\sum_{spins}} M_S M_D^* + \overline{\sum_{spins}} \mid M_D \mid^2, \tag{7.57}$$

where

$$\begin{aligned}\overline{\sum_{spins}} \mid M_S \mid^2 &= \frac{8}{3}\pi\phi_K^2(0)\left\{3U_0^2 \mid F_1 \mid^2 + U_0 Re[V_0 F_1^*(3F_+ - F_-)]\right. \\ &+ \left.\frac{1}{4} \mid V_0 \mid^2 (3 \mid F_+ \mid^2 - 2Re(F_+F_-^*) + 3 \mid F_- \mid^2)\right\},\end{aligned} \tag{7.58}$$

$$\begin{aligned}2Re\overline{\sum_{spins}} M_S M_D^* &= -2\sqrt{2}\pi\phi_K^2(0)Re\left\{\left(U_0V_2 + \frac{1}{2}W_2V_0(3(\hat{p}_n \cdot \hat{k})^2 - 1)\right)F_1^*F_-\right. \\ &+ \left. V_0V_2^*(F_+F_-^*)\right\},\end{aligned} \tag{7.59}$$

$$\begin{aligned}\overline{\sum_{spins}} \mid M_D \mid^2 &= 2\pi\phi_K^2(0)\left\{3W_2^2 \mid F_1 \mid^2 + \frac{1}{2}W_2(3(\hat{p}_n \cdot \hat{k})^2 - 1)ReV_2F_1^*(3F_+ - 2F_-)\right. \\ &+ \left.\frac{1}{4} \mid V_2 \mid^2 (3 \mid F_+ \mid^2 - 4Re(F_+F_-^*) + 3 \mid F_- \mid^2)\right\}.\end{aligned} \tag{7.60}$$

In order to calculate the differential-rate relation, we start with the general relation[59]

$$d\Gamma = \frac{1}{2(m_K + m_D)} \overline{\sum_{spin}} \mid M \mid^2 \frac{d^3\vec{p}_\Lambda}{(2\pi)^3} \frac{d^3\vec{p}_n}{(2\pi)^3} \frac{d^3\vec{k}}{(2\pi)^3} \frac{m_n m_\Lambda}{2E_n E_\Lambda k} (2\pi)^4 \delta^4(p_K + p_D - p_\Lambda - p_n - k). \tag{7.61}$$

Integrating over $d^3\vec{p}_n$ we have

$$\frac{d\Gamma}{dk\ dE_\Lambda} = \overline{\sum_{spins}} \mid M \mid^2 \frac{m_n m_\Lambda}{2(2\pi)^3(m_K + m_D)}. \tag{7.62}$$

The γ-spectrum is then found by integrating the result in equation (7.62)

$$\frac{d\Gamma}{dk} = \frac{m_\Lambda m_n}{2(2\pi)^3(m_K + m_D)} \int_{E_\Lambda(min)}^{E_\Lambda(max)} dE_\Lambda \overline{\sum_{spin}} \mid M \mid^2, \tag{7.63}$$

over the allowed range of E_Λ values

$$E_\Lambda \binom{max}{min} = \frac{(m_K + m_D - k)(E_{max} - k) \pm \Delta}{m_K + m_D - 2k}, \tag{7.64}$$

with

$$E_{max} = \frac{(m_K + m_D)^2 + m_\Lambda^2 - m_n^2}{2(m_K + m_D)}, \tag{7.65}$$

and

$$\Delta = k\sqrt{(E_{max} - k)^2 - \frac{m_\Lambda^2}{(m_K + m_D)}(m_K + m_D - 2k)}. \tag{7.66}$$

It is $d\Gamma/dk$ which we will plot versus the photon energy in Chapter 10, using the wavefunctions and scattering parameter sets of Chapter 9. In the next chapter, however, we will first indicate what changes are required in order to accommodate a momentum dependent transition operator.

Chapter 8

THE MOMENTUM DEPENDENT TRANSITION OPERATOR

8.1 Introduction

In this chapter, we will evaluate the required matrix elements of our $K^- p \to \Lambda\gamma$ transition operator, given in equation (3.51), in order to account for proton momentum within the deuteron. As we will soon find that $\Sigma N \to \Lambda n$ conversion effects are very small near the γ-spectrum endpoint, it is sufficient to consider momentum dependence in only the above transition operator.

As the momentum-dependent terms are of $O(p_p/m)$ and O(k/m), relative to the leading $O(1)$ momentum-independent term in equation (3.51), we do not expect a large deviation from the results derived in Chapter 7. This expectation will be verified when numerical results are presented in Chapter 10. Clearly, as the factor $k/2m_\Lambda$ in equation (3.51) changes by only 3% over the 285 MeV to 293 MeV energy range, such O(k/m) terms would normally be considered negligible. However, if there is a large cancellation between the $O(k/m)$ $\Lambda(1405)$ contribution and the O(1) terms in $\hat{T}$, as occurs for the $\kappa_{\Lambda(1405)\Lambda}$ value of -0.8 considered in Chapter 5, O(k/m) terms can have a larger effect on the γ-spectrum shape. The possible effect of $O(p_p/m)$ terms is less obvious from the form of $\hat{T}$, but will become more apparent in the next section.

Matrix elements of the proton momentum operator will mix in new angular momentum states and require some additional radial integrals to be evaluated. The required

radial integrals can, however, be evaluated analytically and thus introduce no additional computational difficulties.

8.2 Matrix Elements of $\hat{T}$

From the form of our transition operator, given in Section 3.3, we require matrix elements of the photon and proton momentum operators. As the photon is represented by a plane wavefunction, an eigenfunction of the momentum operator, terms involving the photon momentum present no additional difficulty. The photon momentum operator can simply be replaced by the photon momentum. The $\vec{p}_p$-operator can be written as

$$\vec{p}_p = \vec{p}_d + \frac{\vec{P}_d}{2} \tag{8.1}$$

where $\vec{P}_d$ is the deuteron center of mass momentum and $\vec{p}_d$ is the constituent proton-neutron relative momentum. Since we are in the deuteron rest frame, $\vec{P}_d$ gives zero contribution so that $\vec{p}_p$ is, in coordinate space, replaced by $-i\vec{\nabla}_r$ where $\vec{r}$ is the deuteron relative coordinate. Matrix elements of the gradient operator corresponding to the proton momentum are not as trivial as those described for the photon momentum since the deuteron wavefunction is not a momentum eigenstate. The proton momentum operator couples initial states with orbital angular momentum l to final states with orbital angular momentum $l \pm 1$. From the form of our transition operator, given in equation (3.51), we must evaluate matrix elements of the operators $\vec{p}_p \cdot \hat{k}$ and $\vec{p}_p \cdot \vec{\epsilon}$, in order to include the effects of the constituent proton momentum.

We will first examine the contributions from these operators to the amplitude M_S which, as in Chapter 7, is the amplitude involving the deuteron S-state wavefunction. Consider first the matrix elements of the operator $\vec{p}_p \cdot \hat{k}$. It is convenient to write the scalar product $\vec{p}_p \cdot \hat{k}$ in the following way[60]:

$$\vec{p}_p \cdot \hat{k} = \sum_{\mu} (-1)^{\mu} (\vec{p}_p)_{\mu} (\hat{k})_{-\mu}, \tag{8.2}$$

where we have represented the vectors in terms of spherical coordinates. In this system, a Cartesian vector, $\vec{V}$, written in spherical coordinates, has components[61]

$$V_{\pm} = \mp \frac{1}{\sqrt{2}} (V_x \pm i V_y) \quad , \quad V_0 = V_z. \tag{8.3}$$

Making the replacement $\vec{p}_p \rightarrow -i\vec{\nabla}_r$ in equation (8.2), the matrix element of this term will have an angular integral of the form

$$\sum_{lm} \int d\Omega_r Y^*_{lm}(\Omega_r) \left(-i\vec{\nabla}_r\right)_\mu Y_{00}(\Omega_r), \tag{8.4}$$

which is analogous to the integral in equation (7.35). As in equation (7.35), the $Y_{00}(\Omega_r)$ factor comes from the deuteron S-state wavefunction and $Y_{lm}(\Omega_r)$ is one term in the plane wave decomposition given in equation (7.34). Only the $l = 1$ term in equation (8.4) is non-zero and we have[62]

$$\sum_m \int d\Omega_r Y^*_{1m}(\Omega_r) \left(\vec{\nabla}_r\right)_\mu Y_{00}(\Omega_r) = \sum_m (-1)^{m+1} < 1, -m, 1, \mu \mid 1, 1, 0, 0 > \frac{\partial}{\partial r}, \tag{8.5}$$

with the derivative acting on the S-state deuteron radial wavefunction. The resulting radial integral, corresponding to the plane wave factor in equation (7.31) and analogous to U_0 in equation (7.36), is given below:

$$U_1 = \int_0^\infty dr\ r^2 j_1(p_n r) \frac{\partial}{\partial r} \left(\frac{u(r)}{r}\right), \tag{8.6}$$

and evaluated in Appendix B. The remaining terms in equations (7.34), (8.2) and (8.5) combine to give an overall factor

$$C_1 = 4\pi \sum_{m\mu} (-1)^{m+\mu+1} < 1, -m, 1, \mu \mid 1100 > (\hat{k})_{-\mu} Y_{1m}(\Omega_{p_n}). \tag{8.7}$$

This factor can be simplified through the use of equation (8.2) and the relations

$$Y_{10}(\hat{p}) = \frac{1}{2}\sqrt{\frac{3}{\pi}} (\hat{p})_0\,, \tag{8.8}$$

and

$$Y_{1\pm1}(\hat{p}) = \frac{1}{2}\sqrt{\frac{3}{\pi}} (\hat{p})_\pm\,, \tag{8.9}$$

to obtain

$$C_1 = \sqrt{4\pi}\hat{p}_n \cdot \hat{k}. \tag{8.10}$$

Similarly, the radial integral corresponding to the plane wave factor in equation (7.32), and analogous to V_0 in equation (7.37), is given by

$$V_1 = \int_0^\infty dr\ r j_1(qr) \frac{\partial}{\partial r} \left(\frac{u(r)}{r}\right) e^{-ipr}, \tag{8.11}$$

In addition, in Chapter 10 we will also find that the D-state contributions are quite small and, therefore, the $O(p_p/m)$ corrections to our D-state contribution will produce an entirely negligible change in our γ-spectrum. These correction terms have therefore been dropped.

with the overall factor

$$C_2 = -\sqrt{4\pi}\hat{q} \cdot \hat{k}. \tag{8.12}$$

Again, V_1 has been evaluated in Appendix B, for common parametrizations of the deuteron S-state wavefunction.

For the momentum dependent transition operator terms proportional to $\vec{p}_p \cdot \vec{\epsilon}$, we obtain the same radial integrals as given in equations (8.6) and (8.11). However, the overall factors analogous to C_1 and C_2 are in this case equal to $\sqrt{4\pi}\ \hat{p}_n \cdot \vec{\epsilon}$ and $-\sqrt{4\pi}\ \hat{q} \cdot \vec{\epsilon}$ respectively. Note that, since $\vec{q}$ is proportional to $\vec{k}$, the second factor gives zero contribution in the transverse gauge. The first factor is also suppressed in the region of interest, as $\vec{p}_n$ and $\vec{k}$ are anti-parallel at the high-energy endpoint of the photon spectrum.

For contributions to the D-state amplitude, M_D, we have an angular integral of the form

$$\sum_{l'm'} \int d\Omega_r Y^*_{l'm'}(\Omega_r) \left(\vec{\nabla}_r\right)_\mu Y_{2m}(\Omega_r). \tag{8.13}$$

Here, the $\vec{\nabla}_r$ operator couples both the $l = 1$ and $l = 3$ states to the deuteron D-state and we require the angular integrals

$$\int d\Omega_r Y^*_{3m'} \left(\vec{\nabla}_r\right)_\mu Y_{2m}(\Omega_r)$$

$$= (-1)^{m+m'+1}\sqrt{\frac{1}{5}} < 3, -m', 1, \mu \mid 3, 1, 2, m > \left(\frac{\partial}{\partial r} - \frac{2}{r}\right), \tag{8.14}$$

and

$$\int d\Omega_r Y^*_{1m'} \left(\vec{\nabla}_r\right)_\mu Y_{2m}(\Omega_r)$$

$$= (-1)^{m+m'}\sqrt{\frac{2}{5}} < 1, -m', 1, \mu \mid 1, 1, 2, m > \left(\frac{\partial}{\partial r} + \frac{3}{r}\right), \tag{8.15}$$

where the derivative acts on the D-state deuteron radial wavefunction.

The D-state matrix elements of our momentum dependent transition operator can be evaluated as described above for the S-state. We will see in Chapter 10, however, that these $O(p_p/m)$ corrections to the S-state calculation alter the γ-spectrum only slightly.

Chapter 9

THE REQUIRED WAVEFUNCTIONS AND AMPLITUDES

9.1 Introduction

In Chapters 7 and 8, we have given expressions for the $K^-d \to \Lambda n\gamma$ amplitude and differential rate in terms of several transition amplitudes and integrals over the deuteron S- and D-state wavefunctions. Here, the required amplitudes and wavefunctions will be discussed in more detail.

In Section 9.2, we will briefly indicate our choice of deuteron wavefunctions. Section 9.3 will deal with the momentum independent $K^-N \to Y\gamma$ transition amplitudes. Finally, in Section 9.4, we will consider the $Y'N' \to YN$ scattering and conversion amplitudes, indicate why conversion effects will be small near the endpoint of the $K^-d \to \Lambda n\gamma$ γ-spectrum, and give the relations connecting the $\Lambda - n$ scattering parameters to our final state wavefunctions.

9.2 The Deuteron Wavefunctions

In order to calculate the initial-state wavefunction in equation (7.2), we must choose a deuteron wavefunction. Several such wavefunctions have been plotted in figs. 9.1 and 9.2. Both the S- and D-state radial wavefunctions show a reasonable agreement between the various models beyond 2 fm. The variation between models, as one would expect, is greatest near $r = 0$.

The various S-state wavefunctions plotted in fig. 9.1 show, in general, closer agreement than the D-state wavefunctions. The Hulthen S-state wavefunction is an exception;

$$u(r)_{HULTHEN} = \sqrt{\frac{2\alpha\beta(\alpha+\beta)}{(\alpha-\beta)^2}}\left(e^{-\alpha r} - e^{-\beta r}\right), \tag{9.1}$$

constructed from only two exponential terms, one of which is fixed by the required asymptotic behavior. The S-state wavefunctions of McGee[63] and the Bonn group[40] are fitted to five and eleven terms respectively.

The most widely used modern $N - N$ potentials are those of the Paris[64] and Bonn[40] groups. These potentials have similar on-shell and off-shell behavior. In addition, the Paris and Bonn S-state deuteron wavefunctions show agreement, at the 10% level, down to 0.7 fm. We have chosen to use the Bonn deuteron, as a convenient parametrized form has recently been given[40] for the radial wavefunctions.

The two Bonn D-state wavefunctions in fig. 9.2 are fits to the full and one-boson exchange potential(OBEP) deuterons which we shall refer to as BONN1 and BONN2 respectively. Both agree reasonably well down to about 1 fm. The older wavefunction of McGee, by comparison, is quite different. The behavior of this wavefunction near $r = 0$ is due to a fault in McGee's parametrization, which gives an analytic D-state that is formally divergent at the origin.

As tables of parameters sometimes contain errors, we have tested the deuteron parametrizations of reference 40 by checking the normalization

$$\int_0^\infty dr\left\{u(r)^2 + w(r)^2\right\} = 1, \tag{9.2}$$

and the deuteron radius value

$$r_D^2 = \frac{1}{4}\int_0^\infty dr\ r^2 \left\{u(r)^2 + w(r)^2\right\}. \tag{9.3}$$

Both tests are satisfied by the parametrizations, with the exception that the version of equation (9.3), given in reference 40, is missing the factor of $\frac{1}{4}$. The value of r_D quoted in Table 6 of reference 40 requires this factor, which appears in the standard definition of r_D[65].

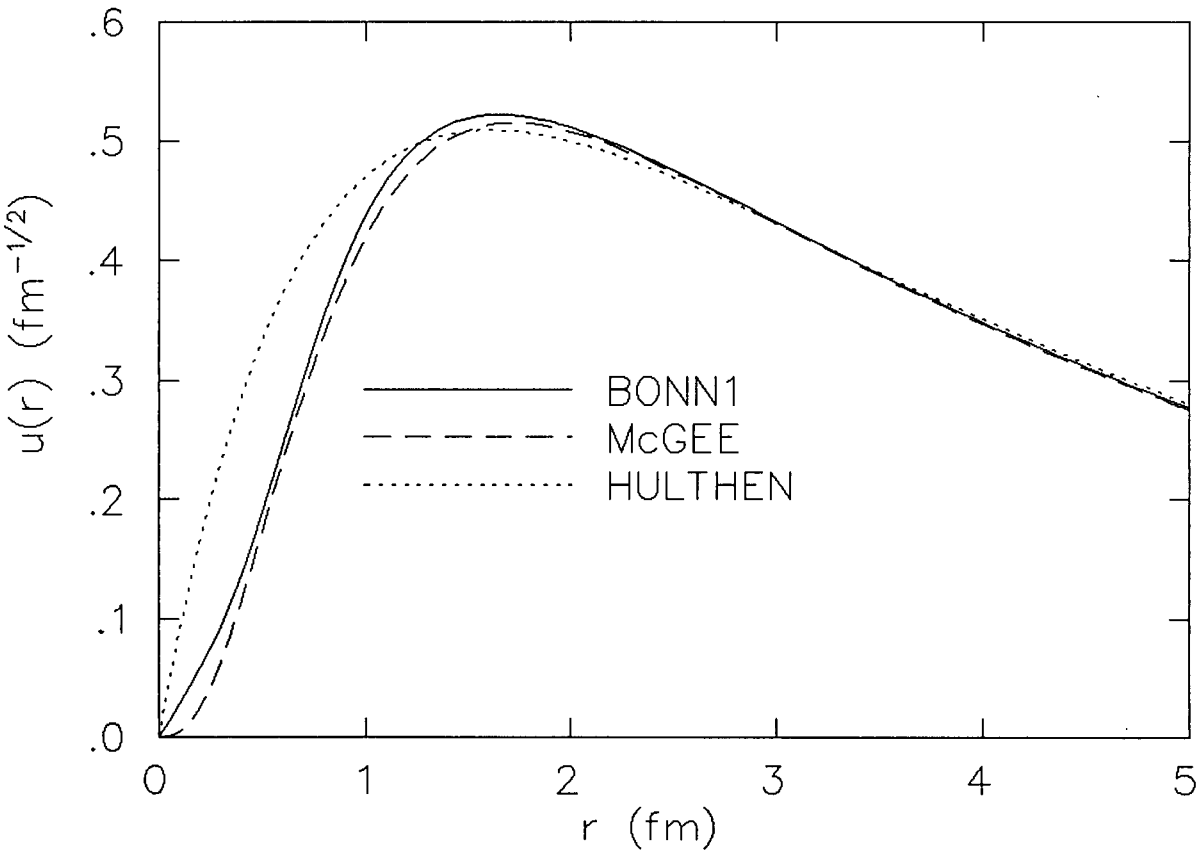

Figure 9.1: Deuteron S-state wavefunctions

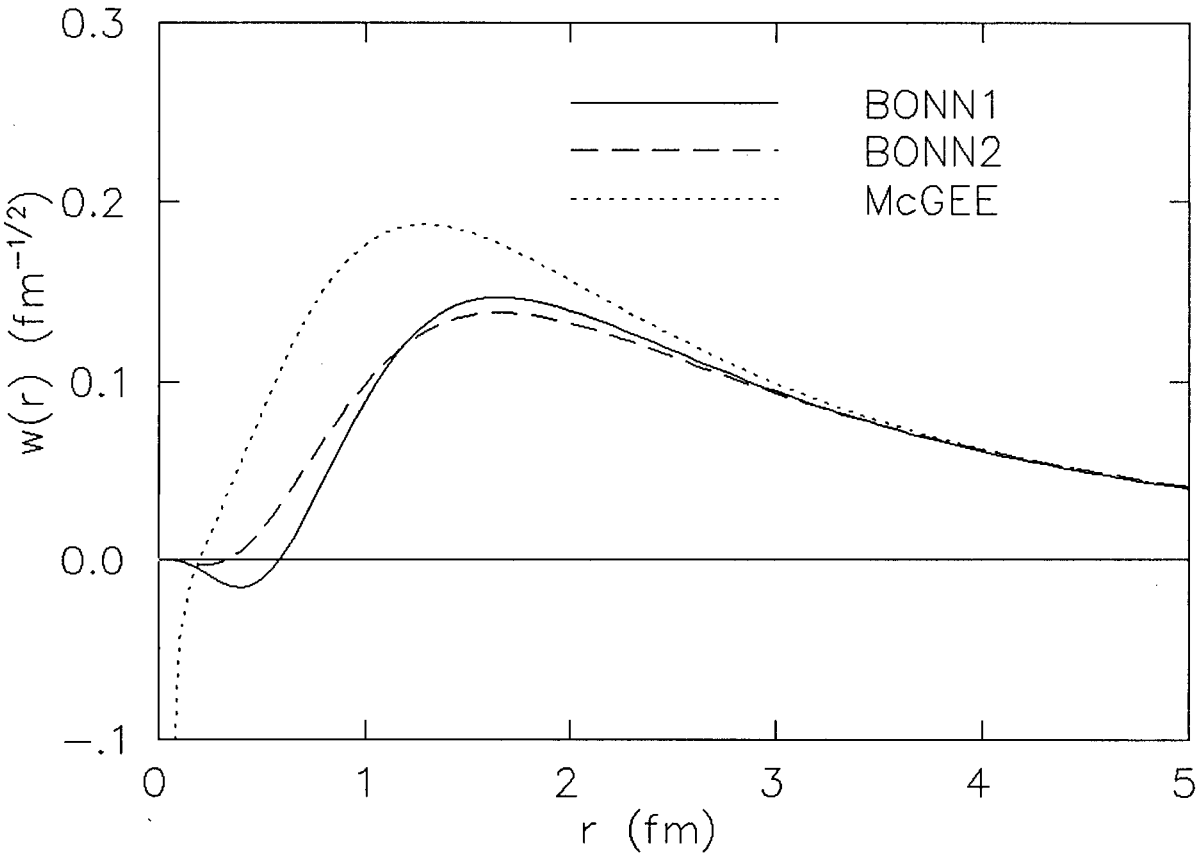

Figure 9.2: Deuteron D-state wavefunctions

9.3 The $K^-N \to Y\gamma$ Transition Amplitudes

The momentum dependent factors, F_i^{PS}, in our two-component $K^-N \to Y\gamma$ transition operators of Section 3.2 are given in Table 9.1. Recall that, from the form of equation (3.22), the factors $\tilde{F}_i^{PS}$ are dimensionless and are to first order just equal to g_{KNY} if one neglects O(k/m) terms. The expressions for $\tilde{F}_i^{PS}$ obtained in Section 3.2 have been multiplied by $e/2m_p$, in order to obtain the F_i^{PS} values appearing in the table. As only PS values have been considered, the PS superscript has been dropped.

Values of the F_i have been given for factors derived from the Born, Born plus $\Sigma^0 \to \Lambda$ and, Born plus $\Sigma^0 \to \Lambda$ plus $\Lambda(1405)$ amplitudes. Notice the very different character of the Born plus $\Sigma^0 \to \Lambda$ plus $\Lambda(1405)$ results for $F_1(K^-p \to \Lambda\gamma)$ and $F_2(K^-p \to \Sigma^0\gamma)$. In the calculation of F_1 we have taken the value $\kappa_{\Lambda(1405)\Lambda} = -0.8$. The $\Lambda(1405)$ amplitude corresponding to this choice of $\kappa_{\Lambda(1405)\Lambda}$ results in a contribution of $(-0.617 + i0.458)$ fm to F_1. This destructively interferes with the Born plus $\Sigma^0 \to \Lambda$ contribution, leaving a predominantly imaginary result. The choice of $\kappa_{\Lambda(1405)\Lambda} \approx -0.4$, corresponding to the minimum $\Lambda\gamma$ branching fraction, is intermediate to the Born plus $\Sigma^0 \to \Lambda$ and Born plus $\Sigma^0 \to \Lambda$ plus $\Lambda(1405)$ results listed in Table 9.1.

Recall, from the discussion of Chapter 5, that $\kappa_{\Lambda(1405)\Sigma}$ is only weakly constrained by the current experimental upper limit to the $\Sigma^0\gamma$ branching fraction. The value of 0.8 for $\kappa_{\Lambda(1405)\Sigma}$ was chosen in the calculation of F_2, as this coupling produces a $K^-p \to \Sigma^0\gamma$ branching fraction near to the experimental upper limit, as well as the current experimental value for the $K^-p \to \Lambda\gamma$ branching fraction. In this case there is less cancellation and the amplitude is mainly due to the $\Lambda(1405)$ contribution.

The corresponding factors $\mathcal{F}_i$ used in the calculation of Akhiezer et al.[9] have also been included in Table 9.1. These transition amplitudes were extracted from the $K^-N \to Y\gamma$ calculation of reference 10, which used SU(3) relations to relate the couplings in their Born plus $\Sigma^0 \leftrightarrow \Lambda$ plus $\Lambda(1405)$ pole-model calculation. Here the $\Lambda(1405)$ decay width to $\Sigma\pi$ final states was used to determine the $\Lambda(1405)\Sigma\pi$ coupling and SU(3)

symmetry, assuming a singlet $\Lambda(1405)$, was used to determine a $K^- p \Lambda(1405)$ coupling. The $\Lambda(1405) Y \gamma$ coupling was taken from dispersion relations[66]. Unfortunately, the factors $\mathcal{F}_i$ used in reference 9 have not been taken directly from the calculation of reference 10, but rather have been modified in some unstated manner. A quantitative comparison between the transition amplitudes of reference 9 and our results has not been made due to the fact that a choice of units and conventions has not been clearly stated in references 9 and 10.

Table 9.1: PS Transition Amplitudes for $K^-N \to Y\gamma$

Transition Amplitudes			(fm)
Diagrams Included	F_1	F_2	F_3
Born	$+0.535$	-0.228	-0.119
Born + $\Sigma^0 \leftrightarrow \Lambda$	$+0.497$	-0.170	–
Born + $\Sigma^0 \leftrightarrow \Lambda$ + $\Lambda(1405)$	$-0.120 + i0.458$	$+0.297 - i0.347$	–

Akhiezer's Transition Amplitudes			
F/(F+D) Ratio	$\mathcal{F}_1$	$\mathcal{F}_2$	$\mathcal{F}_3$
1/4	$0.99 - i2.47$	$-7.03 - i3.33$	-1.82
2/5	$4.07 - i1.10$	$-2.52 - i1.49$	-0.73

9.4 The $Y'N' \rightarrow YN$ Transition Amplitudes

The effect of final state $Y'N' \rightarrow YN$ interactions on the $K^-d \rightarrow \Lambda n\gamma$ amplitude is contained in the final state wavefunction defined in equation (7.12). More specifically, it is the scattering amplitude, $f_j(\cos\theta)$, which contains this information. There exist three distinct regions of the γ-spectrum for the reaction $K^-d \rightarrow \Lambda n\gamma$, each of which requires special consideration in the calculation of $Y'N' \rightarrow YN$ scattering amplitudes. Although we require knowledge of only that part of the spectrum near the high-energy endpoint, we will discuss the general behavior of the scattering amplitudes over the entire photon energy range.

For photon energies below 222 MeV, there exists sufficient energy in the K^-d interaction to produce both $\Sigma^0 n\gamma$ and $\Sigma^- p\gamma$ final states as well as the $\Lambda n\gamma$ final state. The amplitudes for $\Lambda n \rightarrow \Lambda n$ scattering and $\Sigma N \rightarrow \Lambda n$ conversion can be described by a two-channel S-matrix

$$S^{(\frac{1}{2})} = \begin{pmatrix} \eta e^{2iRe\delta_1} & , & i\sqrt{1-\eta^2}e^{iRe(\delta_1+\delta_2)} \\ i\sqrt{1-\eta^2}e^{iRe(\delta_1+\delta_2)} & , & \eta e^{2iRe\delta_2} \end{pmatrix},$$

where

$$\eta = e^{-2Im\delta_1} = e^{-2Im\delta_2}. \tag{9.4}$$

The form of equation (9.4) follows[67] from unitarity and time-reversal invariance. The phase shifts δ_1 and δ_2 in equation (9.4) describe the isospin $\frac{1}{2}$ $\Lambda n \rightarrow \Lambda n$ and $\Sigma N \rightarrow \Sigma N$ interactions respectively. The corresponding T-matrices are[68]

$$T^{(\frac{1}{2})}_{\Lambda n \rightarrow \Lambda n} = \frac{1}{2ip}\left(\eta e^{2iRe\delta_1} - 1\right), \tag{9.5}$$

$$T^{(\frac{1}{2})}_{\Sigma N \rightarrow \Sigma N} = \frac{1}{2ip'}\left(\eta e^{2iRe\delta_2} - 1\right), \tag{9.6}$$

and

$$T^{(\frac{1}{2})}_{\Sigma N \rightarrow \Lambda n} = \frac{1}{2}\sqrt{\frac{1-\eta^2}{pp'}}e^{iRe(\delta_1+\delta_2)}, \tag{9.7}$$

where p and p' are the YN relative momenta in the $\Lambda n \rightarrow \Lambda n$ and $\Sigma N \rightarrow \Sigma N$ channels respectively.

The isospin space relations in equations (9.5) to (9.7) can be transformed into a particle basis through the relations

$$\mid \Sigma^- p >= \frac{1}{\sqrt{3}} \mid 3/2, -1/2 > -\sqrt{\frac{2}{3}} \mid 1/2, -1/2 >, \tag{9.8}$$

$$\mid \Sigma^0 n >= \sqrt{\frac{2}{3}} \mid 3/2, -1/2 > +\frac{1}{\sqrt{3}} \mid 1/2, -1/2 >, \tag{9.9}$$

$$\mid \Lambda n >= \mid 1/2, -1/2 >, \tag{9.10}$$

in which $\mid I, I_3 >$ is an isospin state. The scattering amplitudes required in equation (7.12) are then

$$f_1(\Lambda n \rightarrow \Lambda n) = T^{(\frac{1}{2})}_{\Lambda n \rightarrow \Lambda n}, \tag{9.11}$$

$$f_2(\Sigma^0 n \rightarrow \Lambda n) = \frac{1}{\sqrt{3}} T^{(\frac{1}{2})}_{\Sigma N \rightarrow \Lambda n}, \tag{9.12}$$

$$f_3(\Sigma^- p \rightarrow \Lambda n) = -\sqrt{\frac{2}{3}} T^{(\frac{1}{2})}_{\Sigma N \rightarrow \Lambda n}. \tag{9.13}$$

One should also note[69] that p' is the relative momentum in the isospin 1/2 channel. Using equations (9.8) and (9.9) we have

$$p' = \frac{2}{3} p_{\Sigma^0 n \rightarrow \Sigma^0 n} + \frac{1}{3} p_{\Sigma^- p \rightarrow \Sigma^- p}, \tag{9.14}$$

a relation between the isospin channel momentum and the particle momenta.

Relations similar to those in equations (9.11) to (9.13) have been given in reference 9 for the scattering amplitudes required in a calculation of the $K^- d \rightarrow \Sigma^- p \gamma$ reaction. It should be noted that the above approach is valid over the whole γ-spectrum of the reaction $K^- d \rightarrow \Sigma^- p \gamma$. In the $K^- D \rightarrow \Lambda n \gamma$ calculation, however, there are additional difficulties near the 222-MeV to 225-MeV photon-energy range. Since the threshold photon energies for $\Sigma^- p$ and $\Sigma^0 n$ production are at 222 MeV and 225 MeV respectively, there are corresponding threshold cusps in the γ-spectrum at these energies.

Luckily these cusps are far from the endpoint of the γ-spectrum for the reaction $K^-d \rightarrow \Lambda n\gamma$. In the $K^-d \rightarrow \Sigma^0 n\gamma$ reaction, however, there is a cusp very near the γ-spectrum endpoint and thus, even in the absence of the existing very large background of extraneous photons, this reaction is less suited to an accurate determination of the $\Sigma^0 n$ scattering length.

Dalitz[70] has shown that the T-matrix of equation (9.7) may be expressed in terms of the $\Lambda n \rightarrow \Lambda n$ scattering length in the following way:

$$\mid T^{(\frac{1}{2})}_{\Sigma N \rightarrow \Lambda n} \mid^2 = \frac{b}{p' \mid 1 + ipA \mid^2}, \tag{9.15}$$

where $A = a + ib$ is a complex Λn scattering length. The imaginary part of A thus determines the strength of transitions between the ΣN and Λn channels. For energies slightly below the ΣN threshold, a naive calculation of p' yields a complex value, as the corresponding energy is negative. Dalitz has further shown[71] that equation (9.15) can be extended below threshold, assuming that the corresponding K-matrix elements are approximately constant, by simply replacing p' with $i \mid p' \mid$. Clearly this is not a valid extrapolation near the γ-spectrum endpoint, where $\mid p' \mid$ is about 280 MeV and our Λn scattering length is real.

An analogous situation occurs in the $K^-d \rightarrow \Lambda p\pi^-$ reaction[72]. Fig. 5 of reference 72 illustrates the separation of regions in which $\Lambda p \rightarrow \Lambda p$ and $\Sigma N \rightarrow \Lambda p$ are important[73].

Thus, near the γ-spectrum endpoint, we require only $f_1(\Lambda n \rightarrow \Lambda n)$ given in equation (9.11). In addition, the above simplification removes the need for the transition amplitudes $F_2^{PS}(K^-p \rightarrow \Sigma^0\gamma)$ and $F_3^{PS}(K^-n \rightarrow \Sigma^-\gamma)$. In this case, for a momentum independent transition operator, $F_1^{PS}(K^-p \rightarrow \Lambda\gamma)$ becomes an overall constant and may be factored out of the amplitude, leaving no dependence on the $K^-N \rightarrow Y\gamma$ amplitude other than its $\vec{\sigma} \cdot \vec{\epsilon}$ form.

As our numerical calculations will concentrate on the high-energy end of the photon

spectrum, the effective range approximation[74] should be valid:

$$p \cot \delta = -\frac{1}{a} + \frac{1}{2} r p^2, \tag{9.16}$$

since p, the relative $\Lambda - n$ momentum, is small near the γ-spectrum endpoint. In equation (9.16), a and r are the usual s-wave scattering length and effective range. Using the relation

$$\frac{e^{2i\delta} - 1}{2i} = \frac{1}{\cot \delta - i}, \tag{9.17}$$

we can write the scattering amplitude in the form

$$f_1 = \frac{-a}{(1 - \frac{1}{2} a r p^2) + iap}. \tag{9.18}$$

Notice that for small values of p, equation (9.18) is basically dependent on only the scattering length and, in the limit of zero $\Lambda - n$ relative momentum, the scattering amplitude is simply equal to $-a$.

We can estimate the effect of higher partial waves by expanding the scattering amplitude of equation (7.12) using

$$f_1(\cos\theta) = \frac{1}{p} \sum_{l=0}^{\infty} (2l+1) P_l(\cos\theta) e^{i\delta_l} \sin \delta_l, \tag{9.19}$$

where $P_l(\cos\theta)$ is a Legendre polynomial. Using the zero range relation[74]

$$p^{2l+1} \cot \delta_l = -\frac{1}{a_l}, \tag{9.20}$$

the $l = 1$ contribution to our scattering amplitude is then

$$f_1(l=1) = -\frac{a_1 p^2}{1 + i a_1 p^3} (3 \cos\theta), \tag{9.21}$$

where a_1 is the p-wave $\Lambda - n$ scattering volume. The p-wave contribution is suppressed here for two reasons, the most obvious being that this amplitude is proportional to p^2 and thus goes to zero for small values of p. In addition to this, the p-wave scattering volume is quite small. Nagels[29] has determined that the s-wave $\Lambda - n$ scattering length is

approximately -2 fm, while the values[29] determined for the p-wave scattering lengths are all less than 0.2 fm^3 in magnitude.

We have chosen 5 sets of s-wave scattering lengths and effective ranges for use in these calculations. These have been listed in table 9.2. Set 1 is that which corresponds to no final state scattering. Sets 2, 3 and 4 are those fitted by Nagels, Rijken and de Swart in their potential model calculations of references 45, 29 and 46 respectively. Set 5 consists of scattering lengths, which are much larger in magnitude than those of sets 1 to 4 but are within the one standard deviation bounds of reference 47. Thus, set 5 produces, for comparison purposes, a final state scattering enhancement in excess of that which is expected, based on the potential model results.

If charge independence holds for the ΛN interaction, we should also be able to estimate the ΛN scattering parameters from Λp values. The recently reviewed[75] Λp scattering parameters appear to justify a choice of Λn scattering lengths near -2 fm and effective ranges near 3 fm.

In the next chapter we will examine the effect of variations in the Λn scattering parameters on the γ-spectrum shape. We will also consider the sensitivity of the resulting γ-spectra to differences in the deuteron wavefunctions and momentum dependence in the $K^- p \rightarrow \Lambda\gamma$ transition operator. These results will then be compared to those of references 6 and 9.

Table 9.2: Λn Scattering Parameter Sets

Λn Scattering Lengths and Effective Ranges - Singlet and Triplet		
Set	Scattering Length (fm)	Effective Range (fm)
1	$a_s = 0$ $a_t = 0$	$r_s = 0$ $r_t = 0$
2	$a_s = -2.67 \pm 0.35$ $a_t = -1.02 \pm 0.05$	$r_s = 2.04 \pm 0.1$ $r_t = 2.55 \pm 0.1$
3	$a_s = -2.03 \pm 0.32$ $a_t = -1.84 \pm 0.1$	$r_s = 3.66 \pm 0.32$ $r_t = 3.32 \pm 0.11$
4	$a_s = -2.40$ $a_t = -1.84$	$r_s = 3.15$ $r_t = 3.37$
5	$a_s = -5.0$ $a_t = -3.0$	$r_s = 3.5$ $r_t = 3.5$

Chapter 10

NUMERICAL RESULTS FOR $K^- d \to \Lambda n \gamma$

Figs. 10.1 to 10.8 are the results of our numerical calculations, illustrating the sensitivities and insensitivities of our γ-spectra to various modifications of the calculation.

Fig. 10.1 shows the possible variations of our γ-spectrum shape, using the BONN1 S-state deuteron and the scattering parameter sets of Table 9.2. This figure also illustrates the insensitivity of the γ-spectrum peak position to reasonable changes in the final state scattering parameters. All three spectra peak near 280 MeV in photon energy. Clearly a $\Lambda - n$ scattering length near the $n - n$ scattering length value would shift the spectrum peak towards the high-energy endpoint. However, for scattering length values near to the prediction of reference 46, the peak position and region most sensitive to final state interactions are disconnected.

The spectra displayed in fig. 10.1 have been normalized to equal area between 265 MeV and 293 MeV in photon energy. Recall that, as in our $K^- p \to Y\gamma$ calculation, an absolute rate calculation would require knowledge of the distribution of atomic states from which the kaon is captured. Thus, as we are only exploring the γ-spectrum shape and each curve is normalized to equal area, our $d\Gamma/dk$ values are given in arbitrary units.

Fig. 10.2 displays the region between 280 MeV and 293 MeV and illustrates more clearly the difference in γ-spectrum shapes nearer to the high-energy endpoint. As in

fig. 10.1, and henceforth, the γ-spectra have been normalized to equal area over the displayed energy range.

Fig. 10.3 focuses on the sensitive region between 285 MeV and 293 MeV, where final state effects are most prominent. Here γ-spectra have been calculated from the three parameter sets of Nagels et al. using the BONN1 S-state deuteron. Note that the γ-spectrum derived from the earliest parameter set (Set 2) is separated from sets 3 and 4, which give very similar results.

The result of variations in the effective range is shown in fig. 10.4, using the parameters of set 4. Fig. 10.4 demonstrates that the spectrum shape will be insensitive to the errors quoted in Table 9.2 for the effective ranges determined by Nagels et al. In fact, a change of 1 fm in the effective ranges has a negligible effect on the γ-spectrum in the range 292 MeV to 293 MeV.

In fig. 10.5 we have plotted the γ-spectra arising from the scattering parameters of set 4 and three different S-state deuteron wavefunctions. While the BONN1 and BONN2 S-state wavefunctions produce very similar results over most of the range 285 MeV to 293 MeV, the Hulthen S-state wavefunction deviates only slightly from the two Bonn results over much of this range.

Fig. 10.6 reveals that D-state contributions alter the γ-spectrum shape very little near its endpoint. Variations among the different D-state wavefunctions can then be expected to have a negligible effect on our results.

The effect of momentum dependence in our $K^-p \rightarrow \Lambda\gamma$ transition operator is demonstrated in figs. 10.7 and 10.8. Fig. 10.7 indicates the effect of $O(k/m)$ terms, where k is the photon momentum. The solid curve in fig. 10.7 gives, for comparison purposes, the γ-spectrum resulting from a momentum-independent transition operator. The curve corresponding to a $\kappa_{\Lambda(1405)\Lambda}$ value of zero gives the γ-spectrum due to a transition operator derived from the Born and $\Sigma^0 \rightarrow \Lambda$ contributions alone. The curve resulting from a choice of -0.8 for $\kappa_{\Lambda(1405)\Lambda}$ displays the effect of a large cancellation between O(1)

and O(k/m) terms in the transition operator. Clearly, in the case of a small $\Lambda(1405)$ contribution, the O(k/m) terms are negligible, as $k/2m_\Lambda$ varies only slightly over the displayed photon energy range. Fig. 10.8 indicates that $O(p_p/m)$ terms are very small as well. Thus our expansion of $\hat{T}$ to first order in p_p/m and k/m was justified.

Clearly, although we are relatively insensitive to errors in the effective range, differences in the deuteron wavefunction, and momentum dependence in our transition operator, it will be difficult to differentiate between the scattering parameter sets of Nagels et al.[29,45,46]. Unfortunately, statistics will limit a measurement of the γ-spectrum in the last few MeV, where final state interactions are most important. Figs. 10.2 and 10.3, however, indicate that, for reasonable choices of the Λn scattering parameters, the γ-spectrum is nearly linear over most of the region between the peak and high-energy endpoint. A measurement over this region is probably feasible since, for each photon in the range 265 MeV to 293 MeV, about 18% will have energies in the range 285 MeV to 293 MeV, given that the singlet and triplet Λn scattering lengths are near -2 MeV. Twice that number will have energies in excess of 280 MeV.

A determination of the γ-spectrum slope in this region could easily be compared to the results in fig. 10.3. Fig. 10.2 also suggests the possibility of comparing the number of counts near the γ-spectrum peak and endpoint. This method, however, would be more limited by statistics at the high-energy endpoint.

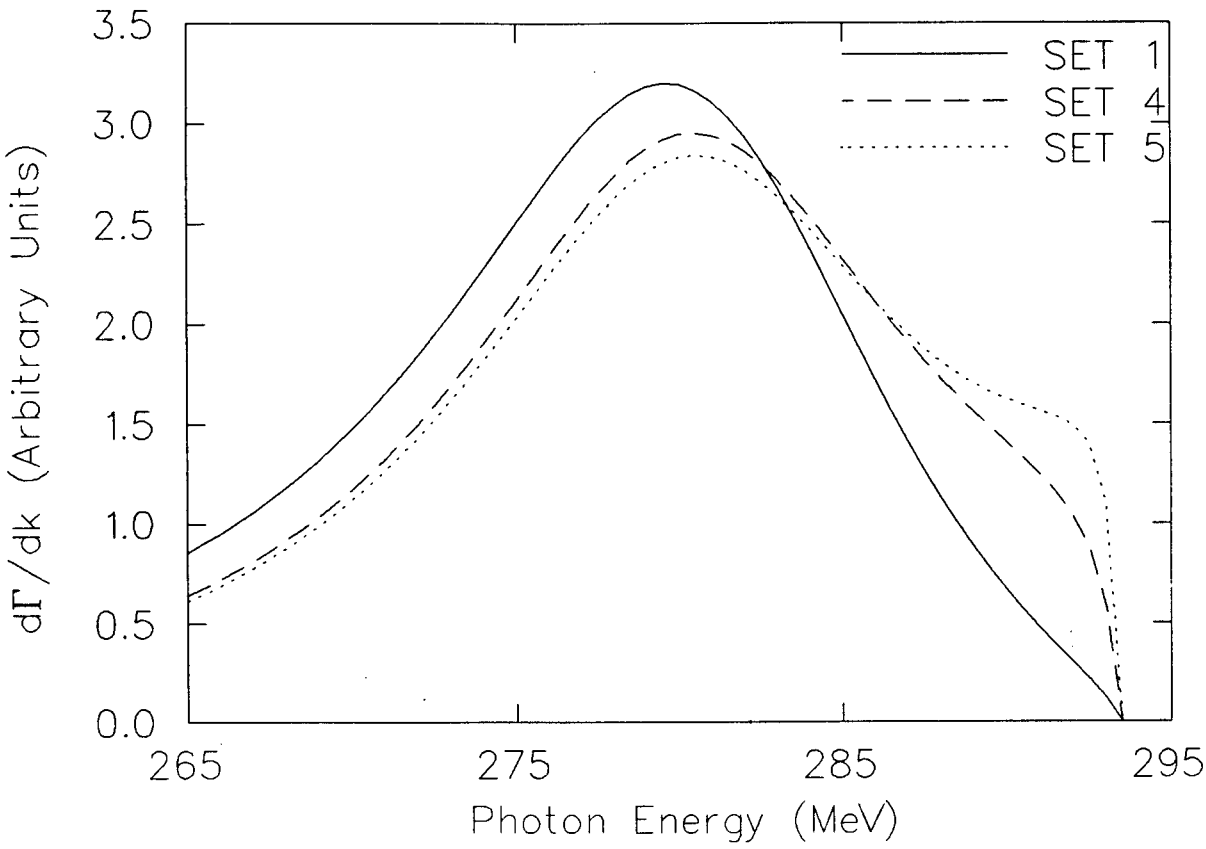

Figure 10.1: γ-spectrum peak for the reaction $K^- d \to \Lambda n \gamma$

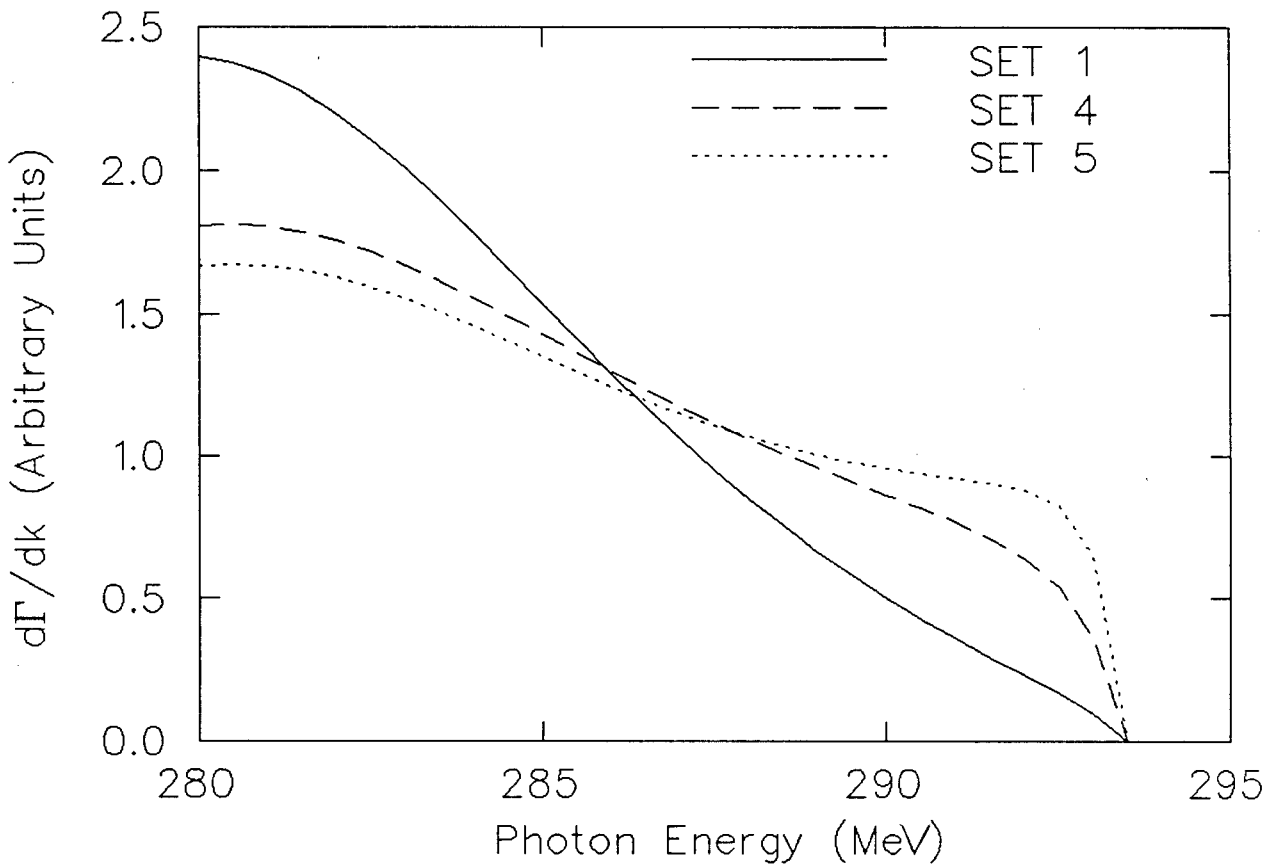

Figure 10.2: γ-spectrum dependence on $\Lambda - n$ scattering parameters

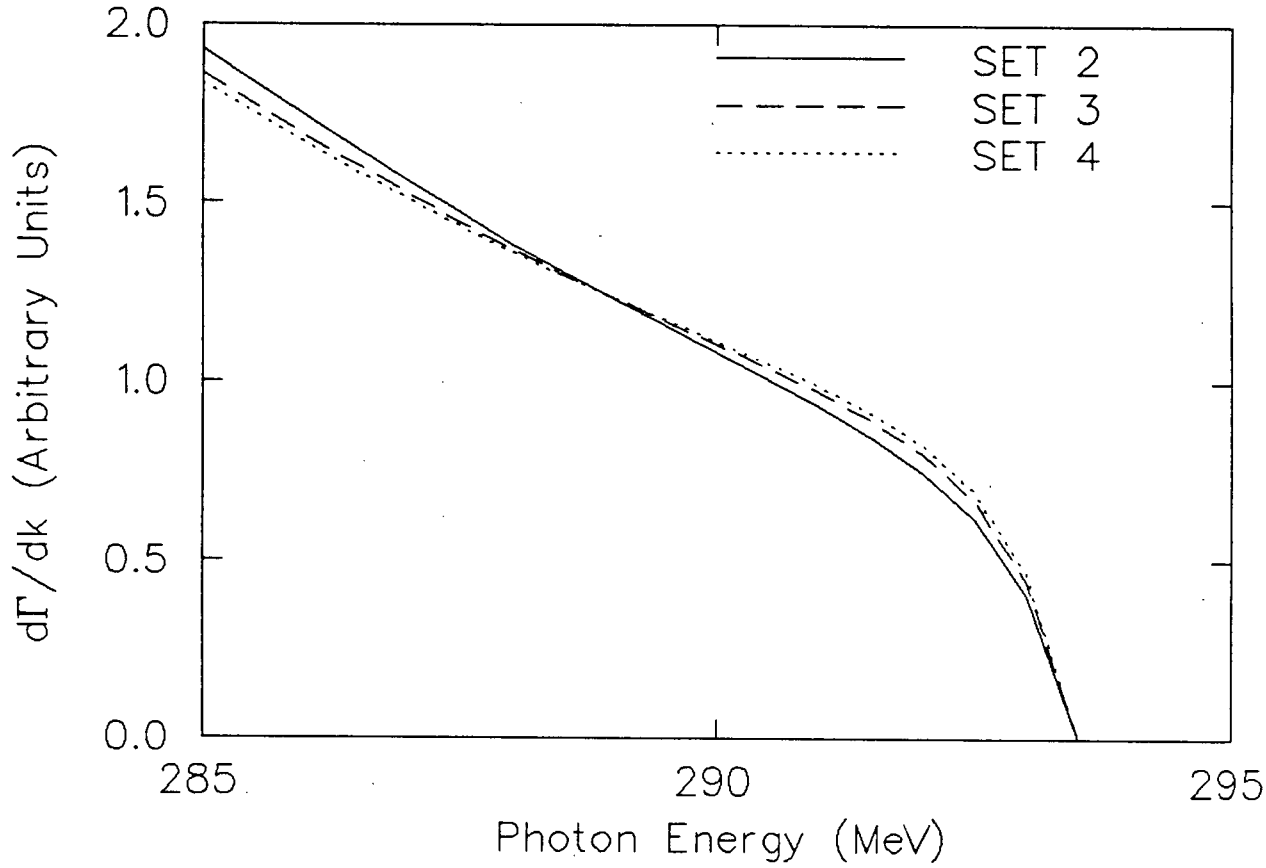

Figure 10.3: γ-spectrum sensitivity to the parameter sets of Nagels et al.

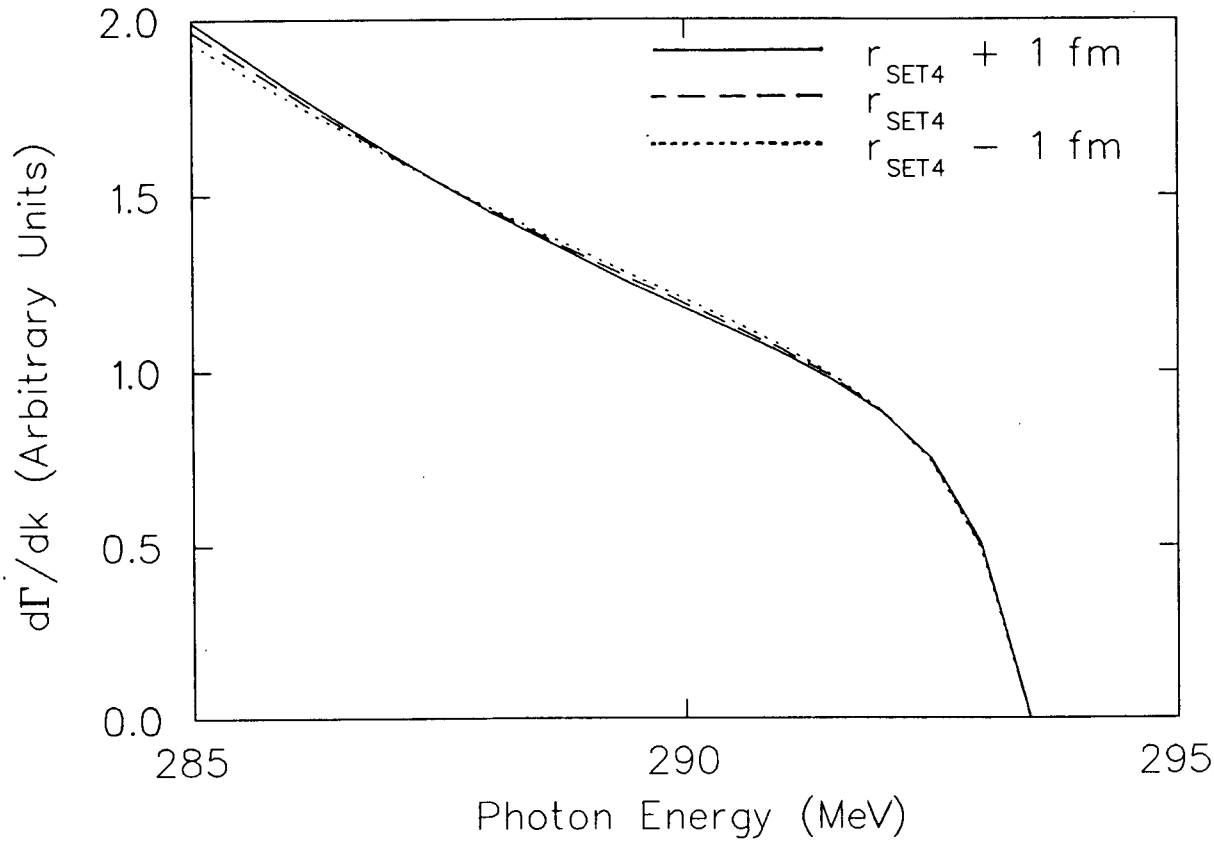

Figure 10.4: γ-spectrum sensitivity to the $\Lambda - n$ effective range

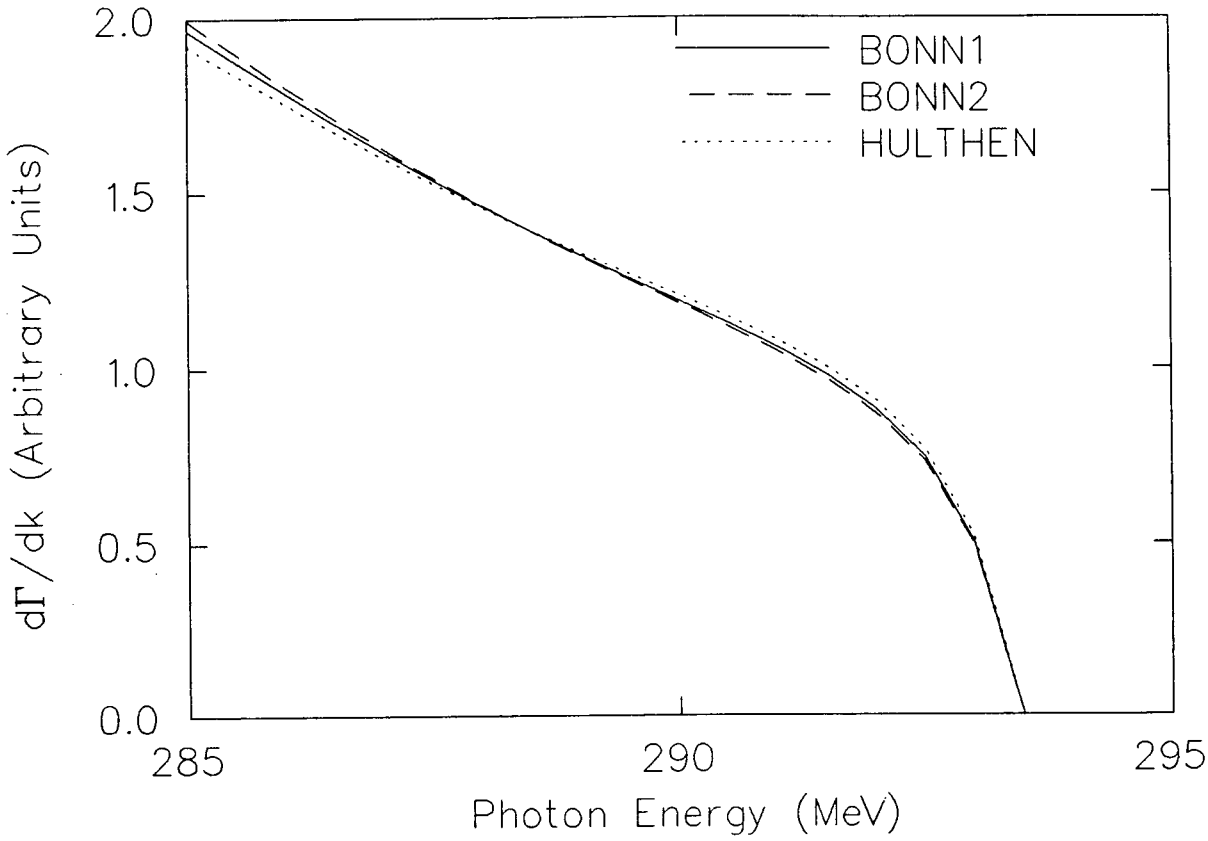

Figure 10.5: γ-spectrum sensitivity to the S-state deuteron wavefunction

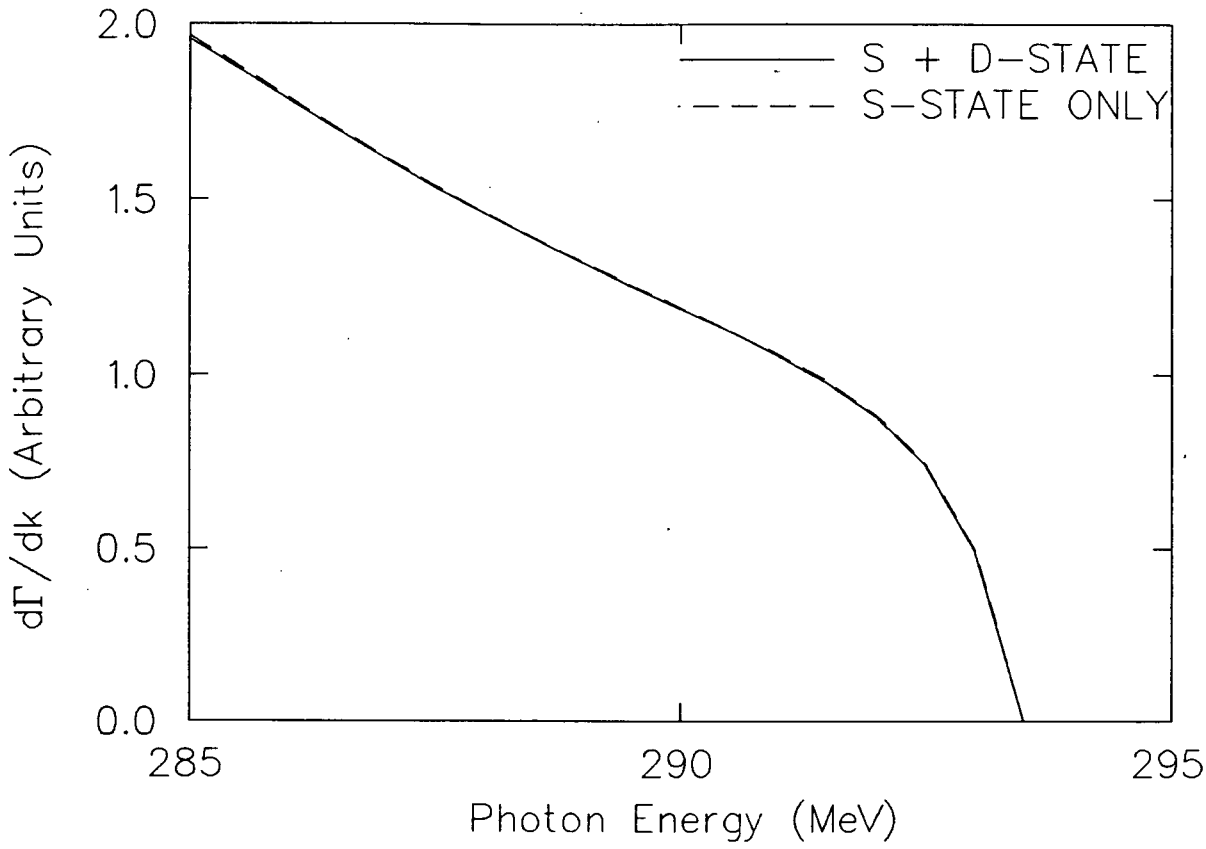

Figure 10.6: γ-spectrum contributions from the deuteron D-state

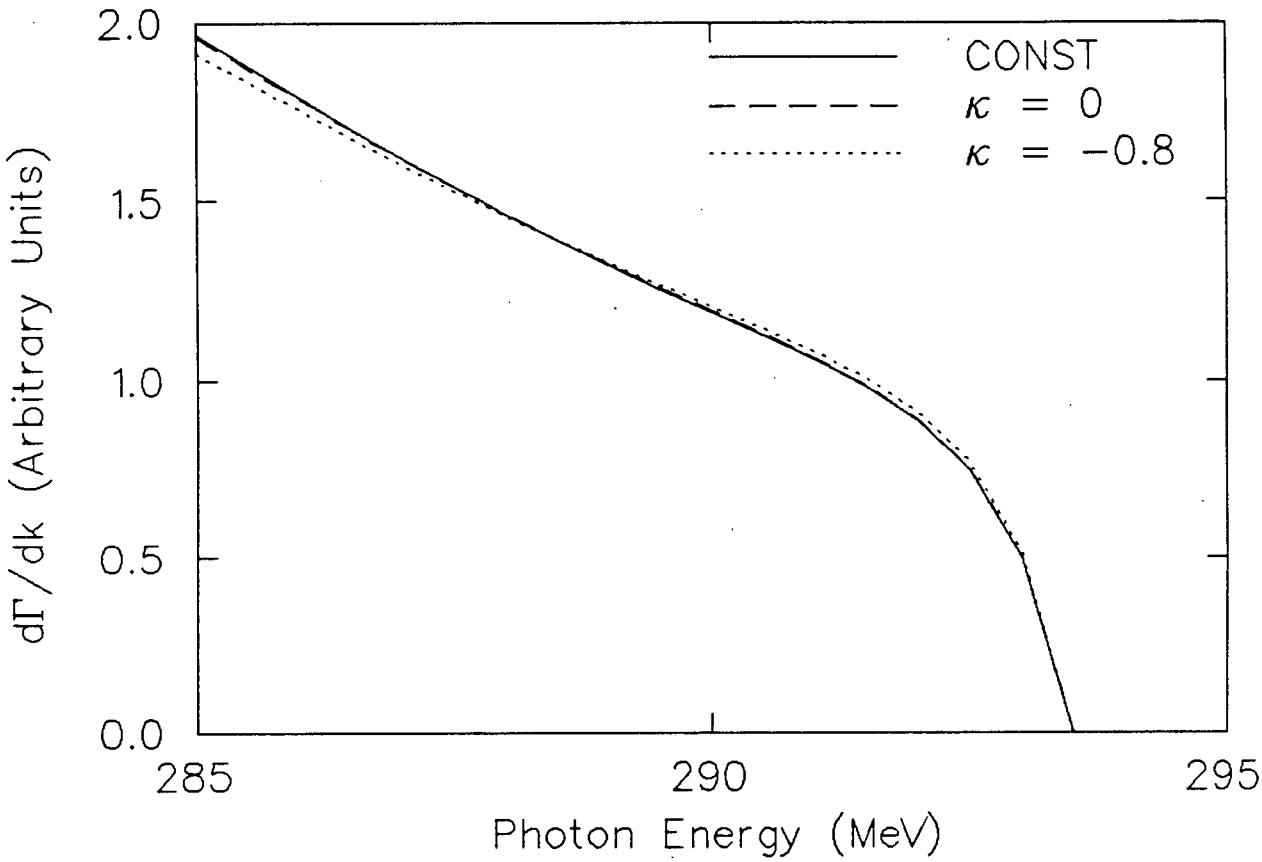

Figure 10.7: γ-spectrum sensitivity to O(k/m) terms

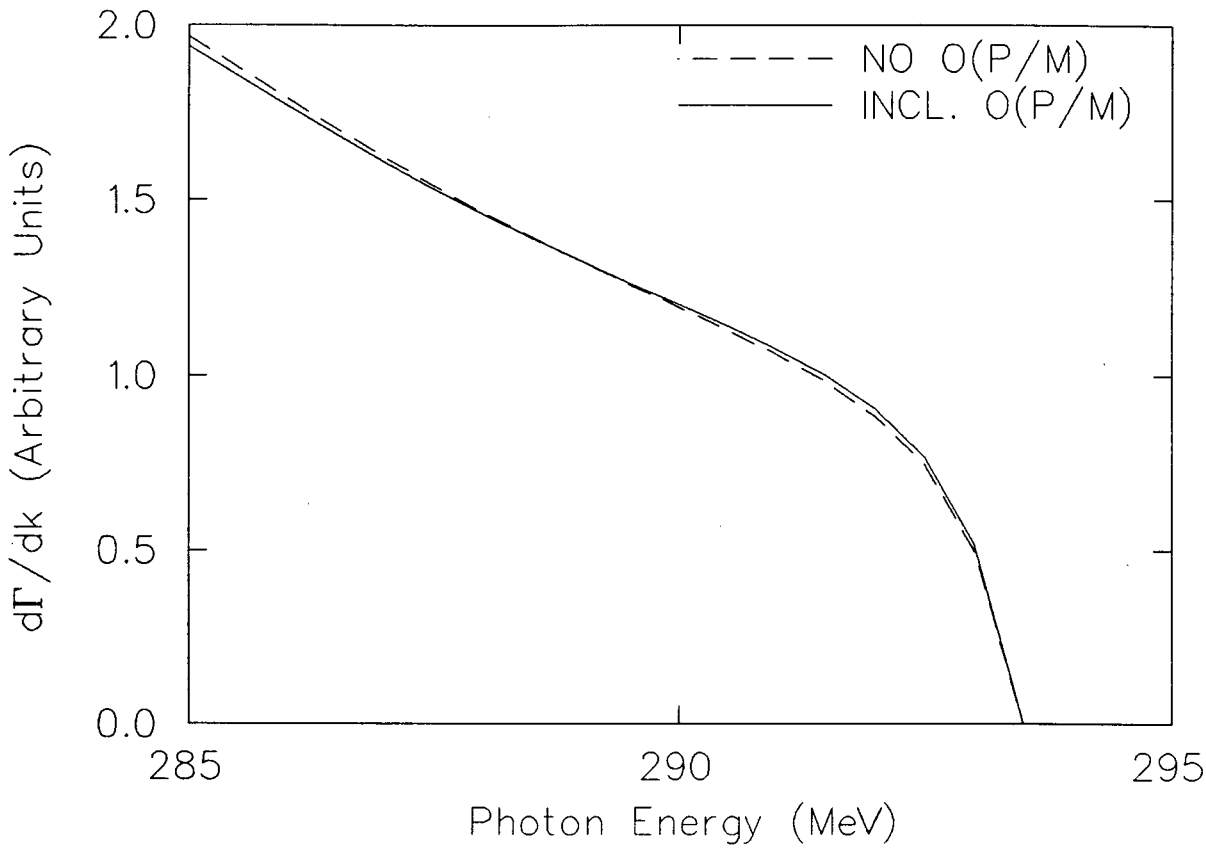

Figure 10.8: γ-spectrum sensitivity to $O(p_p/m)$ terms

Chapter 11

COMPARISONS WITH PREVIOUS CALCULATIONS

The calculation of Gibson et al.[6] is also an impulse-approximation calculation of the γ-spectrum for the reaction $K^-d \rightarrow \Lambda n\gamma$. The initial state is constructed from a Reid soft-core deuteron wavefunction and a kaon atomic wavefunction. A momentum-independent transition operator is used and $\Sigma N \rightarrow \Lambda n$ conversion is neglected. As in our calculation, the kaon wavefunction is taken to be approximately equal to constant and is factored from the amplitude.

The final-state Λn radial wavefunction is constructed from a zero-range wavefunction for values of r greater than 1.4 fm, and a fifth-order polynomial in r is used for values of r from the origin out to the 1.4 fm matching radius. The polynomial and its first two derivatives are matched at $r_0 = 1.4$ fm and set equal to zero at the origin. This polynomial model is due to Picker, Redish and Stephenson[8] and has been utilized in the $\pi^-d \rightarrow nn\gamma$ calculation of Gibbs et al.[7] as well.

The resulting γ-spectra of reference 6 have been normalized to equal area, as have the spectra of Section 10.1. The qualitative behavior displayed in these spectra is also in basic agreement with the findings of Section 10.1. For scattering lengths near -2 fm, the spectra rise rapidly in the photon-energy range between 293 MeV and 290 MeV, and are then nearly linear between 290 MeV and 285 MeV.

Although we have verified that momentum dependence is unimportant in the $K^-p \rightarrow$

$\Lambda\gamma$ transition operator, except possibly for $\kappa_{\Lambda(1405)\Lambda}$ values near -0.8, the reasoning put forth for its neglect in reference 6 is faulty. In reference 6, it is stated that the momentum-independent term dominates the transition operator. Clearly, from our two-component reductions of Chapter 3, this is not necessarily true. The O(k/m) terms have only a small effect on the spectrum shape, due mainly to the fact that the overall factor $k/2m_\Lambda$ changes by only 3% over the 285 MeV to 293 MeV energy range.

The addition of a polynomial dependence in the final-state radial wavefunction of reference 6 is intended to account for short-range suppression in the $\Lambda - n$ interaction. In the corresponding $\pi^- d \rightarrow nn\gamma$ calculation of reference 7, the matching radius was also taken to be 1.4 fm, the pion Compton wavelength. Outside this radius, a Reid soft-core potential was used to generate the $n - n$ wavefunction to be matched at $r_0 = 1.4$ fm. The exterior wavefunction was found to be essentially independent of the potential used, as only the 1π exchange tail is important for large r values. Note, however, that in the $\Lambda - n$ interaction the 2π exchange gives the longest range contribution to the $\Lambda - n$ potential. Thus, a matching radius of 1.4 fm may not be appropriate.

Since the radial integrals in equations (7.36) and (7.37) depend on an overlap of deuteron and final-state wavefunctions, the proper choice of r_0 is important. The effect of altering this matching radius has not been addressed in references 6 and 7. Clearly, a value of r_0 less than 1 fm would greatly reduce the effect of this polynomial extrapolation, as the S-state deuteron wavefunction drops off very steeply below 1 fm. A more appropriate method of evaluating the effect of short-range suppression would involve matching to an external wavefunction generated, for example, from the long-range tail of a $\Lambda - n$ boson-exchange potential.

We have used an asymptotic Λn wavefunction for two reasons. The effects of short-range variations, introduced into the Λn wavefunction in reference 6, are suppressed by the sharp decline of the deuteron S-state wavefunction below 1 fm. This short-range variation thus has a small effect[6,7] of the scattering length determination. In addition,

as we are evaluating overlap integrals with the deuteron wavefunction, an inappropriate choice of r_0 could itself introduce error into the scattering length determination.

Although explicit matrix elements are not given in reference 6, it is stated that the γ-spectra can be parametrized in terms of a single effective scattering length equal to $(2a_t + a_s)/3$. The γ-spectra presented in this reference are then labelled by this constant and an effective range, which is presumably some combination of the singlet and triplet effective ranges.

The amplitudes given in equations (7.58) and (7.60) and in reference 9, however, indicate that the γ-spectrum of the reaction $K^-d \rightarrow \Lambda n\gamma$ depends on the singlet and triplet scattering parameters independently and cannot be expressed in terms of the above scattering length combination.

Next consider the calculation of Akhiezer et al.[9], which allows for $\Sigma N \rightarrow \Lambda n$ conversion effects and follows the formalism outlined in Chapter 7. A momentum-independent transition operator of the form $F_i(K^-N \rightarrow Y\gamma)\vec{\sigma} \cdot \vec{\epsilon}$ is also used here with the factors F_i as discussed in Section 9.3. Unfortunately, it appears that many important features of the $K^-d \rightarrow \Lambda n\gamma$ reaction have been ignored in this calculation.

Akhiezer et al. claim to have calculated total rates for the $K^-d \rightarrow \Lambda n\gamma$ and $K^-d \rightarrow \Sigma^- p\gamma$ reactions. The calculation of a total rate, however, requires knowledge of the distribution of atomic states from which the kaon is captured. The calculation of Akhiezer et al. has been performed only for a 1s atomic capture. In addition, the $\pi^-d \rightarrow nn\gamma$ results of reference 16 appear to indicate that the assumption of a constant kaonic wavefunction and the neglect of the deuteron D-state will add a large error to the total rate calculation.

As mentioned earlier, the γ-spectra presented in reference 9 have not been normalized and concentrate on the rather insensitive γ-spectrum peak, instead of the sensitive region near the γ-spectrum endpoint. Thus reference 9 reveals very little about the one region of the γ-spectrum which is sensitive to the Λn scattering parameters.

Relations for the photon and hyperon polarization calculations have also been given in Akhiezer et al., though no numerical values have been calculated. As it may be possible[4] to measure the Λ polarization in the $K^- d \to \Lambda n \gamma$ reaction, this would place an additional constraint on the $\Lambda n \to \Lambda n$ and $K^- p \to \Lambda \gamma$ amplitudes.

Chapter 12

CONCLUSIONS

In the following, we will summarize what has been learned through our calculations of the at-rest capture $K^-p \to \Lambda\gamma$, $K^-p \to \Sigma^0\gamma$ and $K^-d \to \Lambda n\gamma$ reactions.

Our detailed findings from the $K^-p \to \Lambda\gamma$ and $K^-p \to \Sigma^0\gamma$ branching-fraction calculations are presented in Table 5.1 and figs. 5.1 to 5.5. Although conclusions concerning the $\Lambda(1405)$ contribution to these reactions will depend upon the precise branching-fraction results expected from Brookhaven[3], several comments can now be made.

The published[14] $\Lambda\gamma$ branching fraction of $(2.8 \pm 0.8) \times 10^{-3}$ results in two allowed ranges of $\kappa_{\Lambda(1405)\Lambda}$ values, 0.0 ± 0.1 and -0.8 ± 0.1, corresponding to a choice of 3.2 for $g_{K^-p\Lambda(1405)}$. The second range of $\kappa_{\Lambda(1405)\Lambda}$ values requires a large cancellation between the Born and $\Lambda(1405)$ contributions. If, however, the preliminary[4] indications of a $\Lambda\gamma$ branching fraction close to 1×10^{-3} are correct, $\kappa_{\Lambda(1405)\Lambda}$ is actually near -0.4 and definitely negative. If the preliminary[4] value of $(2 - 3) \times 10^{-3}$ holds for the $\Sigma^0\gamma$ branching fraction, the $\Lambda(1405)$ contribution is dominant in this reaction. Our calculations of the $\Sigma^0\gamma$ branching fractions yield values an order of magnitude lower if the $\Lambda(1405)$ contribution is neglected. In contrast with the calculations of references 11 and 12, we are able to obtain a $\Sigma^0\gamma$ branching fraction in excess of the branching fraction for $\Lambda\gamma$

As no data are yet available, such quantitative conclusions are not yet possible in our γ-spectrum calculations for the reaction $K^-d \to \Lambda n\gamma$. However, as indicated in

Chapter 10, we have found our calculations to be relatively insensitive to changes in the effective range, differences in the deuteron wavefunction, and momentum dependence in the transition operator. Thus, an experiment with very good photon-energy resolution and a large number of counts in the peak region of the γ-spectrum could test the predictions of Chapter 10.

It appears[4], however, that sufficient data is currently difficult to obtain. It is useful to compare with the $\pi^- d \rightarrow nn\gamma$ experiment of reference 1. In that experiment, 2500 events were obtained per 50 keV photon energy bin near the γ-spectrum peak. Preliminary[4] data from Brookhaven[3] indicates that, for the present $K^- d \rightarrow \Lambda n\gamma$ experiment, there will be two orders of magnitude less data in the peak region. Thus, this experiment may require a Kaon Factory in order to extract quantitative information on the $\Lambda - n$ interaction.

Throughout this thesis, necessarily crude estimates have been used for the kaonic wavefunctions. However, as there has recently been considerable progress[52] in the study of kaonic atoms, realistic kaonic wavefunctions may soon be available. The possibility of using a Λn wavefunction constructed from the model of Picker, Redish and Stephenson[8] is also being considered.

In conclusion, several important results have come from this work. The influence of the $\Lambda(1405)$ on the $K^- p \rightarrow Y\gamma$ reactions has been constrained. The structure of this resonance, however, has yet to be determined. The low energy, in-flight $K^- p \rightarrow Y\gamma$ reaction may help to narrow our choices. In addition, the γ-spectrum for the $K^- d \rightarrow \Lambda n\gamma$ reaction has been calculated in order to allow the extraction of information on the $\Lambda - n$ final state interaction. As has been mentioned, though, there is not yet sufficient data from this reaction to improve our knowledge of the $\Lambda - n$ scattering length.

REFERENCES

1. B.Gabioud, J.-C. Alder, C. Joseph, J.-F. Loude, N. Morel, A. Perrenoud, J.-P. Perroud, W. Dahme, H. Panke, D. Renker, C. Zupancic, G. Strassner & P. Truol, Phys. Rev. Lett. **42**, 1508 (1979).

2. K.M. Watson & R.N. Stuart, Phys. Rev. **82**, 738 (1951); M. Bander, Physical Review **134**, B1052 (1964).

3. E.C. Booth, K.P. Gall, E.K. McIntyre, J.P. Miller, B.L. Roberts, D. Whitehouse, J. Lowe, F. Entezami, M.D. Hasinoff, D.F. Measday, S. Stanislaus, C. Waltham, D. Horvath & M. Salomon, *Brookhaven National Lab Experimental Proposal*, 1985 (B.L. Roberts, spokesman).

4. D.F. Measday, private communication.

5. F.M. Renard & Y. Renard, Phys. Lett. **24B**, 159 (1967); Nucl. Phys. **B1**, 389 (1967); Il. Nuo. Cim. **55A**, 631 (1968).

6. B.F. Gibson, G.J. Stephenson, V.R. Brown & M.S. Weise, *Proc. of Summer Study on Nucl. and Hypernucl. Phys.*, Brookhaven National Lab, 1973, ed. H. Palevsky, p.296.

7. W.R. Gibbs, B.F. Gibson & G.J. Stephenson, Phys. Rev. **C11**, 90 (1975).

8. H.S. Picker, E.F. Redish & G.J. Stephenson, Phys. Rev. **C8**, 2495 (1973).

9. A.I. Akhiezer, G.I. Gakh, A.P. Rekalo & M.P. Rekalo, Sov. J. Nucl. Phys. **27**, 115 (1978).

10. I.V. Krive & Yu. V. Kulish, Ukr. Fiz. Zhu. **18**, 416 (1973); The author gratefully acknowledges the assistance of Dr. E. Truhlik in translating this paper.

11. Y.S. Zhong, A.W. Thomas, B.K. Jennings & R.C. Barrett, Phys. Lett. **B171**, 471 (1986).

12. J.W. Darewych, R. Koniuk & N. Isgur, Phys. Rev. **D32**, 1765 (1985).

13. H. Burkhardt, J. Lowe & A.S. Rosenthal, Nucl. Phys. **A440**, 653 (1985).

14. J. Lowe, S.H. Chew, J.M. Nelson, C.E. Waltham, G.J. Pyle, G.T.A. Squier, S. Baird, C.J. Batty, P. Sharman, P. Bird, A.S. Clough & K.R. Parker, Nucl. Phys. **B209**, 16 (1982).

15. J.D. Davies, J. Lowe, G.J. Pyle, G.T.A. Squier, C.E. Waltham, C.J. Batty, S.F. Biagi, S.D. Hoath, P.S. Sharman & A.S. Clough, Nucl. Phys. **B160**, 492 (1979).

16. W.R. Gibbs, B.F. Gibson & G.J. Stephenson, Phys. Rev. **C16**, 322 (1977).

17. M. Leon & H.A. Bethe, Phys. Rev. **127**, 636 (1962); W.A. Bardeen & E.W. Torigoe, Phys. Rev. **C3**, 1785 (1971).

18. H.A. Bethe & E.E. Salpeter, *Quantum Mechanics of One- and Two-electron Atoms*, (Plenum, New York, 1977).

19. J.D. Bjorken & S.D. Drell, *Relativistic Quantum Mechanics*, (McGraw-Hill, New York, 1964).

20. For a clear exposition see E. Dressler, *NBS Technical Note* **957**, 1977.

21. See for example the derivation in P. Carruthers, *Unitary Symmetry*, (J. Wiley, New York, 1966).

22. P.C. Petersen, A. Beretvas, T. Devlin, K.B. Luk, G.B. Thomson, R. Whitman, R. Handler, B. Lundberg, L. Pondrom, M. Sheaff, C. Wilkinson, P. Border, J. Dworkin, O.E. Overseth, R. Rameika, G. Valenti, K. Heller & C. James, Phys. Rev. Lett. **57**, 949 (1986).

23. M. Aguilar-Benitez, F.C. Porter, J.J. Hernandez, L. Montanet, R.L. Crawford, K.R. Schubert, M. Roos, N.A. Tornqvist, G. Hohler, R.M. Barnett, I. Hinchliffe, G.R. Lynch, A. Rittenberg, T.G. Trippe, C.G. Wohl, G.P. Yost, B. Armstrong, G.S.

Wagman, D.M. Manley, T. Shimada, J. Primack, K.G. Hayes, R.H. Schindler, R.E. Shrock, R.A. Eichler, R. Frosch, L.D. Roper & W.P. Trower, Phys. Lett. **170B**, 1 (1986).

24. A.D. Martin, Nucl. Phys. **B179**, 33 (1981).

25. J. Antolin, Phys. Rev. **D35**, 122 (1987).

26. J.J. de Swart, Rev. Mod. Phys. **35**, 916 (1963).

27. O. Dumbrajs, R. Koch, H. Pilkuhn, G.C. Oades, H. Behrens, J.J. de Swart, P. Kroll, Nucl. Phys. **B216**, 277 (1983).

28. A. Pais, Rev. Mod. Phys. **38**, 215 (1966).

29. M.M. Nagels, T.A. Rijken & J.J. de Swart, Phys. Rev. **D15**, 2547 (1977).

30. J.W. Darewych, M. Horbatsch & R. Koniuk, Phys. Rev. **D28**, 1125 (1983); R. Koniuk & N. Isgur, Phys. Rev. **D21**, 1868 (1980).

31. R.A. Adelseck, C. Bennhold & L.E. Wright, Phys. Rev. **C32**, 1681 (1985).

32. R.J. Hemingway, Nucl. Phys. **B253**, 742 (1985).

33. See for example the energy dependent widths used by O.V. Maxwell, Nucl. Phys. **A423**, 445 (1984).

34. I. Blomqvist & J.M. Laget, Nucl. Phys. **A280**, 405 (1977).

35. D.O. Riska & G.E. Brown, Phys. Lett. **38B**, 193 (1972).

36. H. Arenhovel, Nucl. Phys. **A374**, 521 (1982); P.U. Sauer, Prog. Part. Nucl. Phys. **16**, 35 (1986).

37. R.J. McLeod & D.J. Ernst, Phys. Rev. **C23**, 1660 (1981).

38. A. Buchmann, W. Leidemann & H. Arenhovel, Nucl. Phys. **A443**, 726 (1985);

D.O. Riska, Phys. Scripta **32**, 581 (1985); **31**, 471 (1985); **31**, 107 (1985).

39. J.M. Lina & B. Goulard, Phys. Rev. **C34**, 714 (1986).

40. R. Machleidt, K. Holinde & Ch. Elster, Phys. Repts. **149**, 1 (1987).

41. D. Drechsel & L. Tiator, Phys. Lett. **148B**, 413 (1984).

42. B. Jennings, private communication.

43. S. Scherer, D. Drechsel & L. Tiator, Phys. Lett. **193B**, 1 (1987).

44. C.B. Dover & G.E. Walker, Phys. Repts. **89**, 1 (1982).

45. M.M. Nagels, T.A. Rijken & J.J. de Swart, Ann. Phys. **79**, 338 (1973).

46. M.M. Nagels, T.A. Rijken & J.J. de Swart, Phys. Rev. **D20**, 1633 (1979).

47. R. Engelmann, H. Filthuth, V. Hepp & E. Kluge, Phys. Lett. **21**, 587 (1966).

48. G. Alexander, U. Karshon, A. Shapira, G. Yekutieli, R. Engelmann, H. Filthuth & W. Lughofer, Phys. Rev. **173**, 1452 (1968).

49. B. Sechi-Zorn, B. Kehoe, J. Twitty & R.A. Burnstein, Phys. Rev. **175**, 1735 (1968).

50. F. Eisele, H. Filthuth, W. Fohlisch, V. Hepp, E. Leitner & G. Zech, Phys. Lett. **B37**, 204 (1971).

51. W.R. Gibbs, B.F. Gibson & G.J. Stephenson, Phys. Rev. **C11**, 90 (1975).

52. J. Schnick & R.H. Landau, Phys. Rev. Lett. **58**, 1719 (1987); J. Law, M.S. Turner & R.C. Barrett, Phys. Rev. **C35**, 305 (1987).

53. W.R. Gibbs, B.F. Gibson & G.J. Stephenson, Phys. Rev. **C16**, 327 (1977).

54. A. Messiah, *Quantum Mechanics*, (J. Wiley, New York, 1967), Vol.II, p.565.

55. M.L. Goldberger & K.M. Watson, *Collision Theory*, (J. Wiley, New York, 1964), p.236.

56. Messiah, Vol.II, p.558.

57. Messiah, Vol.I, p.497.

58. Messiah, Vol.II, p.554.

59. Bjorken & Drell, p.285.

60. A.R. Edmonds, *Angular Momentum in Quantum Mechanics*, (Princeton University Press, Princeton, 1957), p.72.

61. Edmonds, p.69.

62. Edmonds, p.79.

63. I.J. McGee, Phys. Rev. **151**, 772 (1966).

64. M. Lacombe, B. Loiseau, J.M. Richard & R.V. Mau, Phys. Rev. **C21**, 861 (1980).

65. T.E.O. Ericson, Nucl. Phys. **A416**, 281c (1984).

66. J.G. Aznauryan & L.D. Solov'ev, Sov. J. Nucl. Phys. **8**, 73 (1969).

67. R.H. Dalitz, *Strange Particles and Strong Interactions*, (Oxford University Press, Bombay, 1962), p.67.

68. R. Levi Setti & T. Lasinski, *Strongly Interacting Particles*, (University of Chicago Press, Chicago, 1973), p.146.

69. Dalitz, p.129.

70. Dalitz, p.59, 115.

71. Dalitz, p.122.

72. G. Toker, A. Gal & J.M. Eisenberg, Nucl. Phys. **A362**, 405 (1981).

73. Thanks are due to A. Gal for pointing out this calculation and its connection to the $K^- d \to \Lambda n \gamma$ reaction.

74. M.L. Goldberger & K.M. Watson, p.289.

75. J.K. Mohapatra & S. Mohanty, Phys. Rev. **D33**, 699 (1986).

76. J. Dreitlein & H. Primakoff, Phys. Rev. **125**, 1671 (1962).

77. A.J.G. Hey & R.L. Kelly, Phys. Rep. **96**, 71 (1983).

78. S.K. Gupta & S.B. Khadkikar, Phys. Rev. **36**, 307 (1987).

79. D.B. Lichtenberg, *Unitary Symmetry and Elementary Particles*, (Academic Press, New York, 1978).

80. G.E. Baird & L.C. Biedenharn, J. Math. Phys. **4**, 1449 (1963).

81. B. Loiseau, *Ph.D. Thesis*, Universite Pierre et Marie Curie, Paris, 1974.

82. I. Gradshteyn & I. Ryzhik, *Table of Integrals, Series and Products*, (Academic Press, Toronto, 1980).

BIBLIOGRAPHY

Adelseck, R.A., C. Bennhold & L.E. Wright. Physical Review **C32** (1985).

Aguilar-Benitez, M., F.C. Porter, J.J. Hernandez, L. Montanet, R.L. Crawford, K.R. Schubert, M. Roos, N.A. Tornqvist, G. Hohler, R.M. Barnett, I. Hinchliffe, G.R. Lynch, A. Rittenberg, T.G. Trippe, C.G. Wohl, G.P. Yost, B. Armstrong, G.S. Wagman, D.M. Manley, T. Shimada, J. Primack, K.G. Hayes, R.H. Schindler, R.E. Shrock, R.A. Eichler, R. Frosch, L.D. Roper & W.P. Trower. Physics Letters **170B**, 1 (1986).

Akhiezer, A.I., G.I. Gakh, A.P. Rekalo & M.P. Rekalo. Soviet Journal of Nuclear Physics **27**, 115 (1978).

Alexander, G., Y. Gell & I. Stumer. Physical Review **D6**, 2405 (1972).

Alexander, G., U. Karshon, A. Shapira, G. Yekutieli, R. Engelmann, H. Filthuth & W. Lughofer. Physical Review **173**, 1452 (1968).

Antolin, J., Physical Review **D35**, 122 (1987).

Aznauryan, J.G. & L.D. Solov'ev, Soviet Journal of Nuclear Physics **8**, 73 (1969).

Baird, G.E. & L.C. Biedenharn, Journal of Mathematical Physics **4**, 1449 (1963).

Bander, M. Physical Review **134**, B1052 (1964).

Bardeen, W.A., & E.W. Torigoe. Physical Review **C3**, 1785 (1971).

Bethe, H.A., & E.E. Salpeter. *Quantum Mechanics of One- and Two-electron Atoms*, (Plenum, New York, 1977).

Bjorken, J.D. & S.D. Drell. *Relativistic Quantum Mechanics.* New York: McGraw-Hill, 1964.

Blomqvist, I. & J.M. Laget, Nuclear Physics **A280**, 405 (1977).

Burkhardt, H., J. Lowe & A.S. Rosenthal. Nuclear Physics **A440**, 653 (1985).

Carruthers, P. *Unitary Symmetry*, (J. Wiley, New York, 1966).

Darewych, J.W., R. Koniuk & N. Isgur. Physical Review **D32**, 1765 (1985).

Davies, J.D., J. Lowe, G.J. Pyle, G.T.A. Squier, C.E. Waltham, C.J. Batty, S.F. Biagi, S.D. Hoath, P.S. Sharman & A.S. Clough. Nuclear Physics **B160**, 492 (1979).

Dombey, N. & B.J. Read. Nuclear Physics **B60**, 65 (1973).

Dover, C.B. & G.E. Walker. Physics Reports **89**, 1 (1982).

Drechsel, D. & L. Tiator. Physics Letters **148B**, 413 (1984).

Dreitlein, J. & H. Primakoff. Physical Review **125**, 1671 (1962).

Dressler, E.T. *National Bureau of Standards Technical Note* NBS TN-957, 1977.

Dumbrajs, O., R. Koch, H. Pilkuhn, G.C. Oades, H. Behrens, J.J. de Swart & P. Kroll. Nuclear Physics **B216**, 277 (1983).

Edmonds, A.R. *Angular Momentum in Quantum Mechanics.* Princeton: Princeton University Press, 1968.

Eeg, J.O. & H. Pilkuhn. Il Nuovo Cimento **32A**, 44 (1976).

Engelmann, R., H. Filthuth, V. Hepp & E. Kluge. Physics Letters **21**, 587 (1966).

Ericson, T.E.O. Nuclear Physics **A416**, 281c (1984).

Gabioud, B., J.-C. Alder, C. Joseph, J.-F. Loude, N. Morel, A. Perrenoud, J.-P. Perroud, W. Dahme, H. Panke, D. Renker, C. Zupanic, G. Strassner & P. Troul. Physical Review Letters **42**, 1508 (1979).

Gell, Y., G. Alexander & I. Stumer. Nuclear Physics **B22**, 583 (1970).

Gibbs, W.R., B.F. Gibson & G.J. Stephenson. Physical Review **C11**, 90 (1975).

Gibbs, W.R., B.F. Gibson & G.J. Stephenson. Physical Review **C16**, 322 (1977).

Gibbs, W.R., B.F. Gibson & G.J. Stephenson. Physical Review **C16**, 327 (1977).

Gibson, B.F., G.J. Stephenson, V.R. Brown & M.S. Weise. *Proc. of Summer Study on Nuclear and Hypernuclear Physics.* Brookhaven National Lab, ed. H. Palevsky, p.296.

Goldberger, M.L., & K.M. Watson. *Collision Theory.* New York: J. Wiley, 1964.

Gradshteyn, I. & I. Ryzhik. *Table of Integrals, Series and Products.* Toronto: Academic Press, 1980.

Gupta, S.K. & S.B. Khadkikar. Physical Review **36**, 307 (1987).

Hey, A.J.G. & R.L. Kelly. Physics Reports **96**, 71 (1983).

Karplus, R. & L.S. Rodberg. Physical Review **115**, 1058 (1959).

Koniuk, R. & N. Isgur, Physical Review **D21**, 1868 (1980).

Korenman, G.Ya. & V.P. Popov. Physics Letters **40B**, 628 (1972).

Krive, I.V. & Yu.V. Kulish. Ukrainskii Fizicheskii Zhumal **18**, 416 (1972).

Krive, I.V. Soviet Journal of Nuclear Physics **22**, 184 (1976).

Law, J., M.S. Turner & R.C. Barrett. Physical Review **C35**, 305 (1987).

Leon, M. & H.A. Bethe. Physical Review **127**, 636 (1962).

Lichtenberg, D.B. *Unitary Symmetry and Elementary Particles.* New York: Academic Press, 1978.

Lina, J.M. & B. Goulard, Physical Review **C34**, 714 (1986).

Loiseau, B. *Ph.D. Thesis*, Universite Pierre et Marie Curie, Paris, 1974.

Lowe, J., S.H. Chew, J.M. Nelson, C.E. Waltham, G.J. Pyle, G.T.A. Squier, S. Baird, C.J. Batty, P. Sharman, P. Bird, A.S. Clough & K.R. Parker. Nuclear Physics **B209**, 16 (1982).

Mach, R. Nuclear Physics **A205**, 56 (1973).

Machleidt, R., K. Holinde & Ch. Elster. Physics Reports **149**, 1 (1987).

Martin,A.D., Nuclear Physics **B179**, 33 (1981).

Maxwell, O.V. Nuclear Physics **A423**, 445 (1984).

McGee, I.J. Physical Review **151**, 772 (1966).

McLeod, R.J. & D.J. Ernst, Physical Review **C23**, 1660 (1981).

Messiah, A. *Quantum Mechanics.* New York: J. Wiley, 1967, Vol. I,II.

Nagels, M.M., T.A. Rijken & J.J. de Swart. Annals of Physics **79**, 338 (1973).

Nagels, M.M., T.A. Rijken & J.J. de Swart. Physical Review **15**, 2547 (1977).

Nagels, M.M., T.A. Rijken & J.J. de Swart. Physical Review **D20**, 1633 (1979).

Nagels, M.M., T.A. Rijken, J.J. de Swart, G.C. Oades, J.L. Peterson, A.C. Irving, C. Jarlkog, W. Pfeil, H. Pilkuhn & H.P. Jacob. Nuclear Physics **B147**, 189 (1979).

Pais, A. Review of Modern Physics **38**, 215 (1966).

Petersen, P.C., A. Beretvas, T. Devlin, K.B. Luk, G.B. Thomson, R. Whitman, R.

Handler, B. Lundberg, L. Pondrom, M. Sheaff, C. Wilkinson, P. Border, J. Dworkin, O.E. Overseth, R. Rameika, G. Valenti, K. Heller & C. James. Physical Review Letters **57**, 949 (1986).

Picker, H.S., E.F. Redish & G.J. Stephenson. Physical Review **C8**, 2495 (1973).

Renard, F.M. & Y. Renard. Physics Letters **24B**, 159 (1967).

Renard, F.M. & Y. Renard. Nuclear Physics **B1**, 389 (1967).

Renard, F.M. & Y. Renard. Il Nuovo Cimento **55A**, 631 (1968).

Renard, Y. Nuclear Physics **B40**, 499 (1972).

Riska, D.O., Physics Scripta **32**, 581 (1985); **31**, 471 (1985); **31**, 107 (1985).

Ross, M.H. & G.I. Shaw. Annals of Physics **9**, 391 (1960).

Ross, M.H. & G.I. Shaw. Annals of Physics **13**, 147 (1961).

Schnick, J. & R.H. Landau, Phys. Rev. Lett. **58**, 1719 (1987)

Sotona, M. & E. Truhlik. Nuclear Physics **A262**, 400 (1976).

de Swart, J.J. Reviews of Modern Physics **35**, 916 (1963).

de Teramond, G.F. Physical Review **C16**, 1976 (1977).

de Teramond, G.F., J. Paez & C.W. Soto Vargas. Physical Review **C21**, 2542 (1980).

Watson, K.M. & R.N. Stuart. Physical Review **82**, 738 (1951).

Zhong, Y.S., A.W. Thomas, B.K. Jennings & R.C. Barrett. Physics Letters **B171**, 471 (1986).

Appendix A

The $\Sigma^0 \rightarrow \Lambda$ Transition Moment

The magnitude of the $\Sigma^0 \rightarrow \Lambda$ transition moment can, in principle, be derived from the Σ^0 lifetime, since the Σ^0 decays essentially 100% of the time to $\Lambda\gamma$. However, the Σ^0 lifetime is very short[23], about 10^{-20} sec., and thus this is not presently experimentally feasible. In practice, the Primakoff effect[76] is used to determine $\kappa_{\Sigma\Lambda}$. In this process, a beam of Λ particles is converted to Σ^0 particles through its interaction with a nuclear coulomb field. Here too, though, it is only the magnitude of $\kappa_{\Sigma\Lambda}$ which is determined.

In Chapter 4, we have chosen the sign of $\kappa_{\Sigma\Lambda}$ using the SU(3) prediction

$$\kappa_{\Sigma\Lambda} = -\frac{\sqrt{3}}{2}\mu_n, \tag{A.1}$$

relating $\kappa_{\Sigma\Lambda}$ to the neutron magnetic moment. In the calculation of reference 13, however, the opposite sign was chosen for $\kappa_{\Sigma\Lambda}$. There the naive quark model prediction[77]

$$\kappa_{\Sigma\Lambda} = \frac{1}{\sqrt{3}}\left(\mu_d - \mu_u\right), \tag{A.2}$$

was used to determine a sign. In the above, μ_u and μ_d are respectively the up and down quark magnetic moments. Recent values for the up and down quark magnetic moments are[78] 1.85 and -0.972 nuclear magnetons respectively.

Both of the above relations give a $\kappa_{\Sigma\Lambda}$ magnitude near the experimental value of 1.60 quoted in Table 4.1. However, equation (A.2) gives a sign which is opposite to the one we have used. If one reviews the compilations of quark wavefunctions, the reason for this sign difference becomes apparent. Depending on the choice of quark wavefunctions, either sign is obtainable for $\kappa_{\Sigma\Lambda}$. It is thus important to use a set of quark wavefunctions which is consistent with the same SU(3) conventions as were used in the determination of our other couplings. Since we have used the SU(3) relations of de Swart[26], we will calculate $\kappa_{\Sigma\Lambda}$ using the quark wavefunctions of Koniuk and Isgur[30], as these wavefunctions have also been constructed to conform with the SU(3) conventions of de Swart.

The $Y = \Lambda, \Sigma^0$ flavor and spin wavefunctions are then given by

$$\mid Y >= \frac{1}{\sqrt{2}} \left(\phi_Y^\rho \chi_+^\rho + \phi_Y^\lambda \chi_+^\lambda \right), \tag{A.3}$$

where ϕ_Y is the Λ or Σ^0 flavor wavefunction and χ_+ is a spin 1/2 wavefunction constructed from the three quark spins. The superscript λ (ρ) indicates that the baryon wavefunction is symmetric (anti-symmetric) in the first two quark wavefunctions. The spin wavefunctions are given by

$$\chi_+^\rho = \frac{1}{\sqrt{2}}(\alpha\beta\alpha - \beta\alpha\alpha), \tag{A.4}$$

and

$$\chi_+^\lambda = \frac{1}{\sqrt{6}}(2\alpha\alpha\beta - \alpha\beta\alpha - \beta\alpha\alpha), \tag{A.5}$$

where the α (β) quark spin wavefunction has a spin projection value of 1/2 ($-1/2$). The Λ and Σ^0 flavor wavefunctions are given by

$$\phi_\Lambda^\lambda = \frac{1}{2}(usd + sud - dsu - sdu), \tag{A.6}$$

$$\phi_\Lambda^\rho = \frac{1}{\sqrt{12}}(2uds - 2dus + usd - dsu - sud + sdu), \tag{A.7}$$

and

$$\phi^{\lambda}_{\Sigma^0} = \frac{1}{\sqrt{12}}(sdu + sud + dsu + usd - 2uds - 2dus), \tag{A.8}$$

$$\phi^{\rho}_{\Sigma^0} = \frac{1}{2}(sdu - dsu + sud - usd), \tag{A.9}$$

where u, d and s are the up, down and strange quark wavefunctions.

In the quark model, the stable baryon magnetic moments are given by a vector sum of the constituent quark magnetic moments. The baryon magnetic moment operator is then the sum of magnetic moment operators for the constituent quarks

$$\vec{\mu} = \sum_{i=1}^{3} \mu_q(i)\vec{\sigma}(i), \tag{A.10}$$

where $\vec{\sigma}(i)$ is a Pauli spin operator for the i^{th} quark and $\mu_q(i)$ is the i^{th} quark magnetic moment defined by the relations[79]

$$\mu_q u = \mu_u u, \tag{A.11}$$

$$\mu_q d = \mu_d d, \tag{A.12}$$

$$\mu_q s = \mu_s s. \tag{A.13}$$

The baryon magnetic and transition moments are then given by the matrix elements of μ_z for baryon wavefunctions, which are maximally polarized along the z-axis:

$$\mu_{B'B} = < B' \mid \sum_{i=1}^{3} \mu_q(i)\sigma_3(i) \mid B > . \tag{A.14}$$

Using the above relation for $\mu_{B'B}$ and the quark wavefunctions in equations (A.4) to (A.9), we have

$$\kappa_{\Sigma\Lambda} = \frac{1}{\sqrt{3}}(\mu_u - \mu_d), \tag{A.15}$$

which has the opposite sign to equation (A.2) and agrees with equation (A.1).

If one were to use the wavefunction of Lichtenberg[79], the result in equation (A.2) would have been obtained. The wavefunctions given by Lichtenberg conform to the

conventions of Baird and Biedenharn[80] rather than those of de Swart. Unfortunately, however, the choice of conventions is not always clearly stated. Thus, the utilization of couplings from different compilations tends to be a perilous procedure.

Appendix B

Some Useful Integrals

Analytic relations can be obtained for the integrals U_0, V_0, W_2 and V_2 introduced in Chapter 7 and required in the $K^- d \to \Lambda n\gamma$ calculation. This is possible if simple analytic forms are used for the deuteron S- and D-state wave functions. Many N-N potentials, including the Bonn[40] potential, have associated with them deuteron wave functions of the form

$$u(r) = \sum_{j=1}^{n} A_j e^{-\alpha_j r}, \tag{B.1}$$

for the S-state radial wave function, and

$$w(r) = \sum_{j=1}^{n} B_j \left\{ 1 + \frac{3}{\alpha_j r} + \frac{3}{(\alpha_j r)^2} \right\} e^{-\alpha_j r}, \tag{B.2}$$

for the D-state radial wave function. The integrals U_0 and V_0 are easily evaluated:

$$U_0 = \int_0^\infty dr\ r u(r) j_0(p_n r), \tag{B.3}$$

$$V_0 = \int_0^\infty dr\ e^{-ipr} u(r) j_0(qr), \tag{B.4}$$

and one may readily verify the relations

$$U_0 = \sum_{j=1}^{n} \frac{A_j}{p_n^2 + \alpha_j^2}, \tag{B.5}$$

$$V_0 = \sum_{j=1}^{n} \frac{A_j}{2iq} (\ln \lambda_2 - \ln \lambda_1), \tag{B.6}$$

where

$$\lambda_1 = \alpha_j + (p-q)i \qquad \lambda_2 = \alpha_j + (p+q)i. \tag{B.7}$$

Recall that $\vec{p}$ is the relative $\Lambda - n$ momentum, $\vec{q}$ is the photon momentum multiplied by $m_n/(m_n + m_\Lambda)$ and, $\vec{p}_n$ is the outgoing neutron momentum.

In order to calculate numerically V_0, the result in equation (B.6) is split into its real and imaginary parts using

$$\ln Z = \ln R + i\theta \quad , \quad Z = Re^{i\theta}, \tag{B.8}$$

to find

$$ReV_0 = \sum_{j=1}^{n} \frac{A_j}{2q} \left\{ \tan^{-1}\left(\frac{q-p}{\alpha_j}\right) + \tan^{-1}\left(\frac{q+p}{\alpha_j}\right) \right\}, \tag{B.9}$$

$$ImV_0 = \sum_{j=1}^{n} \frac{A_j}{4q} \ln\left\{ \frac{\alpha_j^2 + (q-p)^2}{\alpha_j^2 + (q+p)^2} \right\}. \tag{B.10}$$

Somewhat more involved is the integral

$$W_2 = \int_0^\infty dr\ rw(r) j_2(p_n r). \tag{B.11}$$

Consider just one term of the sum in equation (B.2). Then we have

$$\begin{aligned} W_2^j(r) = \int_0^\infty dr\ r \left\{ 1 + \frac{3}{\alpha_j r} + \frac{3}{(\alpha_j r)^2} \right\} e^{-\alpha_j r} \\ \cdot \left\{ \left(\frac{3}{(p_n r)^3} - \frac{1}{p_n r} \right) \sin p_n r - \frac{3}{(p_n r)^2} \cos p_n r \right\}. \end{aligned} \tag{B.12}$$

Term by term integration is difficult here as some of the individual terms diverge at $r = 0$. The infinities do, however, cancel to give a finite result. The following method[71] is useful in handling these problems. First define

$$I_\lambda^n(r_0) = \int_{r_0}^\infty dr \frac{e^{-\lambda r}}{r^n}, \tag{B.13}$$

and

$$I_\lambda^n = \lim_{r_0 \to 0} I_\lambda^n(r_0) = \lim_{r_0 \to 0} \frac{E_n(\lambda r_0)}{r_0^{n-1}}, \tag{B.14}$$

where $E_n(\lambda r_0)$ is defined by the expression

$$E_n(\lambda r_0) = \int_1^\infty dt \; \frac{e^{-\lambda r_0 t}}{t^n}. \tag{B.15}$$

The integral $E_n(\lambda r_0)$ is well known and has the value[72]

$$E_n(\lambda r_0) = \frac{(-\lambda r_0)^{n-1}}{(n-1)!}(-\ln\lambda - \ln r_0 + \Psi(n)) + \sum_{\substack{m=0 \\ m \neq n-1}} \frac{(-\lambda r_0)^m}{(m-n+1)m!}, \tag{B.16}$$

where $\Psi(n)$ has the value $\Psi(1) = -\gamma$ and

$$\Psi(n) = -\gamma + \sum_{m=1}^{n-1} \frac{1}{m} \quad , \quad (n > 1), \tag{B.17}$$

and γ is Euler's constant. It is clear that the integrals in equation (B.14) would diverge if applied term by term to the integrand of equation (B.12). Note, however, that $j_2(qr)$ is of order r^2 near $r = 0$ so that the overall result in equation (B.12) is finite. Decomposing equation (B.12) into a sum of integrals of the form in equation (B.14), all terms proportional to r_0 cancel - a useful check on the final result - and, after some algebra, one has the result

$$W_2^j = \left(\frac{p_n}{\alpha_j}\right)^2 \frac{B_j}{p_n^2 + \alpha_j^2}. \tag{B.18}$$

Finally, we must calculate

$$V_2 = \int_0^\infty dr \; w(r) j_2(qr) e^{-ipr}. \tag{B.19}$$

In terms of the integral in equation (B.14) and for a single term in $w(r)$, this may be written as

$$B_j^{-1} V_2^j = \frac{3}{2iq^3}\left(I_{\lambda_2}^3 - I_{\lambda_1}^3\right) - \frac{1}{2iq}\left(I_{\lambda_2}^1 - I_{\lambda_1}^1\right)$$

$$
\begin{aligned}
&+ \frac{9}{2i\alpha q^3}\left(I^4_{\lambda_2} - I^4_{\lambda_1}\right) - \frac{3}{2i\alpha q}\left(I^2_{\lambda_2} - I^2_{\lambda_1}\right) \\
&+ \frac{9}{2i\alpha^2 q^3}\left(I^5_{\lambda_2} - I^5_{\lambda_1}\right) - \frac{3}{2i\alpha^2 q}\left(I^3_{\lambda_2} - I^3_{\lambda_1}\right) \\
&- \frac{3}{2q^2}\left(I^2_{\lambda_2} + I^2_{\lambda_1}\right) + \frac{9}{2\alpha q^2}\left(I^3_{\lambda_2} + I^3_{\lambda_1}\right) + \frac{9}{2\alpha^2 q^2}\left(I^4_{\lambda_2} + I^4_{\lambda_1}\right), \qquad \text{(B.20)}
\end{aligned}
$$

wherein,

$$
\lambda_1 = \alpha_j + (p+q)i \quad , \quad \lambda_2 = \alpha_j + (p-q)i. \qquad \text{(B.21)}
$$

Once again the divergences cancel leaving a finite but very unwieldy answer

$$
\begin{aligned}
B_j^{-1}V_2^j &= \frac{3}{2iq^3}\left(\frac{\lambda_1^2}{2}L_1 - \frac{\lambda_2^2}{2}L_2 + \frac{\lambda_2^2-\lambda_1^2}{2}\cdot\frac{3}{2}\right) \\
&- \frac{1}{2iq}\left(L_1 - L_2\right) \\
&+ \frac{9}{2i\alpha q^3}\left(\frac{\lambda_2^3}{6}L_2 - \frac{\lambda_1^3}{6}L_1 + \frac{\lambda_1^2-\lambda_2^2}{6}\cdot\frac{11}{6}\right) \\
&- \frac{3}{2i\alpha q}\left(\lambda_2 L_2 - \lambda_1 L_1 + \lambda_2 - \lambda_1\right) \\
&+ \frac{9}{2i\alpha^2 q^3}\left(\frac{\lambda_1^4}{24}L_1 - \frac{\lambda_2^4}{24}L_2 + \frac{\lambda_2^4-\lambda_1^4}{24}\cdot\frac{50}{24}\right) \\
&- \frac{3}{2i\alpha^2 q}\left(\frac{\lambda_1^2}{2}L_1 - \frac{\lambda_2^2}{2}L_2 + \frac{\lambda_2^2-\lambda_1^2}{2}\cdot\frac{3}{2}\right) \\
&- \frac{3}{2q^2}\left(\lambda_2(L_2+1) + \lambda_1(L_1+1)\right) \\
&- \frac{9}{2\alpha q^2}\left(\frac{\lambda_2^2}{2}L_2 + \frac{\lambda_1^2}{2} - \frac{\lambda_2^2+\lambda_1^2}{2}\cdot\frac{3}{2}\right) \\
&- \frac{9}{2\alpha^2 q^2}\left(\frac{\lambda_2^3}{6}L_2 + \frac{\lambda_1^3}{6} - \frac{\lambda_2^3-\lambda_1^3}{6}\cdot\frac{11}{6}\right), \qquad \text{(B.22)}
\end{aligned}
$$

where we have used the abbreviations

$$
L_1 = \ln\lambda_1 \quad , \quad L_2 = \ln\lambda_2. \qquad \text{(B.23)}
$$

In order to calculate the matrix elements of our momentum dependent transition operator in Chapter 8, we must evaluate

$$
\int_0^\infty dr\ r^2 j_1(p_n r)\frac{\partial}{\partial r}\left(\frac{u(r)}{r}\right). \qquad \text{(B.24)}
$$

The term involving a radial derivative of the deuteron S-state wavefunction

$$\frac{\partial}{\partial r}\left(\frac{u(r)}{r}\right) = \frac{1}{r}\frac{\partial u(r)}{\partial r} - \frac{1}{r^2}u(r), \tag{B.25}$$

is separated into the above two terms where, for the usual parametrization of $u(r)$ given in equation (B.1),

$$\frac{1}{r}\frac{\partial u(r)}{\partial r} = \sum_{i=1}^{n}(-\alpha_i A_i)\frac{e^{-\alpha_i r}}{r}, \tag{B.26}$$

we must evaluate integrals of the form

$$I_1 = \int_0^\infty dr\ re^{-\alpha r} j_1(p_n r), \tag{B.27}$$

and

$$I_2 = \int_0^\infty dr\ e^{-\alpha r} j_1(p_n r). \tag{B.28}$$

Using the above described methods, we have

$$I_1 = \frac{1}{p_n^2}\tan^{-1}\left(\frac{p_n}{\alpha}\right) - \left(\frac{\alpha}{p_n}\right)\frac{1}{p_n^2+\alpha^2}, \tag{B.29}$$

and

$$I_2 = \frac{1}{p_n}\left\{1 - \frac{\alpha}{p_n}\tan^{-1}\left(\frac{p_n}{\alpha}\right)\right\}. \tag{B.30}$$

We must also evaluate those integrals containing the e^{ipr}/r term of equation (7.32). The results are

$$\int_0^\infty dr\ j_1(qr)e^{-\alpha r}e^{-ipr} =$$

$$\frac{1}{2q}\left(\ln\lambda_2 + \ln\lambda_1 + 2\right) + \frac{1}{2iq}\left(\lambda_2\ln\lambda_2 - \lambda_1\ln\lambda_1\right), \tag{B.31}$$

and

$$\int_0^\infty dr\ j_1(qr)e^{-\alpha r}\frac{e^{-ipr}}{r} =$$

$$\frac{1}{4iq^2}\left\{\lambda_1^2(\ln\lambda_1 - \frac{3}{2}) - \lambda_2^2(\ln\lambda_2 - \frac{3}{2})\right\} - \frac{1}{2q}\left\{\lambda_2(\ln\lambda_2 - 1) + \lambda_1(\ln\lambda_1 - 1)\right\}, \tag{B.32}$$

with λ_1 and λ_2 again given in equation (B.21).